# Marine shallow water systems as natural sources of mercury to local systems

**Dissertation**

zur Erlangung des akademischen Grades

Doktor der Naturwissenschaften

(Dr. rer. nat.)

Am Fachbereich Geowissenschaften

der Universität Bremen

vorgelegt von

Hannah Roberts

Bremen, 17.06.2023

**Gutachter**


Prof. Dr. Wolfgang Bach

Fachbereich Geowissenschaften

Universität Bremen


Prof. Dr. Andrea Koschinsky-Frische

Fachbereich School of Science: Physics and Earth Sciences

Constructor University

Tag des Promotionskolloquiums: February 9, 2024

Name / Name: Hannah Roberts                    Date / Date: 17.06.2023

Anschrift / Address:          Klagenfurter Str. 4, 28359 Bremen

E r k l ä r u n g / A f f i r m a t i o n

Ich versichere, dass / I affirm that

1. die Dissertation ohne unerlaubte fremde Hilfe angefertigt wurde / I wrote the present thesis independently and without illicit assistance from third parties,

2. keine anderen als die von mir angegebenen Quellen und Hilfsmittel benutzt wurden und / I used no sources other than those indicated nor aids other than those permissible,

3. die den benutzten Werken wörtlich oder inhaltlich entnommenen Stellen als solche kenntlich gemacht wurden. / I appropriately referenced any text or content from other sources

_____, den / on this day _____

_____

(Unterschrift / Signature)

# Summary

Hydrothermal systems transfer heat and mass through circulating water in a permeable geological formation. The circulating water (hydrothermal fluid) undergoes multiple subsurface processes, gaining and losing constituents dependent upon physical, geological, and chemical factors. According to Beaulieu and Szafranski (2020), a total of 184 systems are confirmed active across the globe. Of these, 43 are considered MSWHS (above 200 m depth). Areas of emission are characterized by diffuse fluid or gas emission (diffuse), or distinct localized points of emission (point sources). Both types of emission can be sedimented or unsedimented dependent upon local conditions.

The goal of the doctoral project was to provide a fundamental understanding of Hg prevalence in MSWHS from three systems (Milos, Greece; Vulcano, Italy; Panarea, Italy). Each system presented unique environmental conditions where Hg was known to be present. The study area on Milos contained multiple areas of diffuse emission and point sources at depths of less than 5 m. Emission was a mixture of fluids, gases, and brines, with extensive microbial white mat activity. The study area on Vulcano dominantly emitted gases at depths of less than 5 m with limited white mat activity. The study areas on Panarea were at greater depth (5 to 30 m), were a mixture of gas and fluid, with greater biodiversity present than the other sites. White mat activity on Panarea was limited. Primary indicators of Hg emission were evaluated and the effect of MSWHS on local environments were investigated as both direct (e.g., through mercury rich gases to the atmosphere) and indirect (e.g., transport and dissolution of precipitated mercury particles). Each study location represented a unique MSWHS, where environmental conditions greatly affected Hg concentrations in emitted fluids and gases. Additionally, the relationship between Hg and the local environment revealed further information on the subsurface environment of the MSWHS.

Samples were collected from diffuse and point sources at approximately 10 cm depth where possible (e.g., sedimented) through PTFE tubes. Gases were collected in Tedlar© bags at the sediment-water interface. Analysis was completed through CV-AFS (THg, $Hg_{diss}$, $Hg^0$, DMHg, $Hg_{gas}$, THg in sediments), and gas chromatography (MMHg).

Organic species of Hg were not present above detection limits within the hydrothermal fluids sampled at any site. Fluid samples were generally comprised of Hg bound to colloids and particles greater than 0.45 µm (THg). Concentrations of THg within sampled hydrothermal fluids ranged from below local background seawater values (0.5 to 5 pM) to 249 nM. Bound and unbound Hg in filtered (0.45 µm) samples ($Hg_{diss}$) generally represented a small portion of THg (BDL to 273 pM). Additionally, $Hg^0$ was not generally a significant portion of THg (BDL to 5.3 pM). Therefore, the greatest Hg specie in hydrothermal fluid was $Hg^{2+}$, the vast majority bound to colloids and particles > 0.45 µm. Within hydrothermal gases, total Hg ($Hg_{gas}$) ranged from below detection limits to 2,792 nmol / $m^3$.

The greatest indicators of high Hg concentrations within gases and fluids were associated with the rate of flow and the presence of sedimentation. Higher rates of flow, particularly when paired with high temperatures, generally indicated high Hg concentrations within the fluid or gas. However, the presence of sedimentation overlying the hydrothermal source greatly decreased the concentration. Higher rates of flow limited the temporal exposure of hydrothermal fluids and gases to surrounding material, were associated with higher temperatures, and tended to prevent sedimentation at the orifice of the hydrothermal source. However, where sedimentation was present at the orifice, high flow rates were not associated with high Hg concentrations.

The effect of MSWHS on local environments was evident through sediment and seawater samples collected at each location. Background sediment samples collected at each site were within normal values. Accumulations of Hg within sediments associated with hydrothermal sources was observed (0.3 to 49.5 nmol / g). However, these accumulations were limited to direct interaction with the point source. Samples taken centimeters away from hydrothermal sources did not show significant Hg accumulation compared to background samples (0.3 to 0.5 nmol / g). The effect of MSWHS on overlying seawater was most dramatically observed in Panarea and Vulcano. In Baia di Levante on the island of Vulcano, the combination of a high density of MSWHS activity coupled with shallow water (< 1 m), resulted in accumulations up to 186 pM THg. Off the coast of Panarea, at La Calcara, a vertical profile directly above the main point source maintained elevated THg (< 1.1 pM) over 20 m of depth.

It can be concluded that MSWHS contribute Hg to the local environment. The extent of impact is largely controlled by environmental factors (e.g., flow rate and sedimentation). However, immediate removal to sediments after emission to overlying seawater is not supported. Rather, Hg is transported away from point sources and areas of diffuse emission. Therefore, the impact of MSWHS on Hg cycling may extend beyond the immediate local area.

## Kurzfassung

Hydrothermale Systeme übertragen Wärme und Masse durch zirkulierendes Wasser in einer durchlässigen geologischen Formation. Das zirkulierende Wasser (hydrothermale Flüssigkeit) durchläuft mehrere unterirdische Prozesse, wobei es in Abhängigkeit von physikalischen, geologischen und chemischen Faktoren Bestandteile gewinnt und verliert. Nach Beaulieu und Szafranski (2020) sind weltweit insgesamt 184 Systeme als aktiv bestätigt. Von diesen gelten 43 als MSWHS (über 200 m Tiefe). Die Emissionsgebiete zeichnen sich durch diffuse Flüssigkeits- oder Gasemissionen (diffus) oder durch deutliche, lokalisierte Emissionspunkte (Punktquellen) aus. Beide Arten von Emissionen können je nach den örtlichen Gegebenheiten sedimentiert oder nicht sedimentiert sein.

Ziel des Promotionsprojekts war es, ein grundlegendes Verständnis der Hg-Prävalenz in MSWHS aus drei Systemen (Milos, Griechenland; Vulcano, Italien; Panarea, Italien) zu gewinnen. Jedes System bot einzigartige Umweltbedingungen, in denen Hg bekanntermaßen vorkommt. Das Untersuchungsgebiet auf Milos enthielt mehrere Bereiche mit diffusen Emissionen und Punktquellen in Tiefen von weniger als 5 m. Die Emissionen waren eine Mischung aus Flüssigkeiten, Gasen und Solen mit einer umfangreichen mikrobiellen Aktivität der weißen Matte. Das Untersuchungsgebiet auf Vulkan emittierte vor allem Gase in Tiefen von weniger als 5 m mit begrenzter Weißmattenaktivität. Die Untersuchungsgebiete auf Panarea lagen in größerer Tiefe (5 bis 30 m), waren eine Mischung aus Gas und Flüssigkeit und wiesen eine größere Artenvielfalt auf als die anderen Standorte. Die Aktivität der weißen Matten auf Panarea war begrenzt. Es wurden primäre Indikatoren für Hg-Emissionen ausgewertet und die Auswirkungen von MSWHS auf die lokale Umwelt sowohl direkt (z. B. durch quecksilberhaltige Gase in der Atmosphäre) als auch indirekt (z. B. durch den Transport und die Auflösung von ausgefällten Quecksilberpartikeln) untersucht. Jeder Untersuchungsort stellte eine einzigartige MSWHS dar, bei der die Umweltbedingungen die Hg-Konzentrationen in den emittierten Flüssigkeiten und Gasen stark beeinflussten. Darüber hinaus lieferte die Beziehung zwischen Hg und der lokalen Umwelt weitere Informationen über die unterirdische Umbgebung der MSWHS. Proben wurden von diffusen und punktuellen Quellen in einer Tiefe von etwa 10 cm entnommen, sofern dies möglich war (z. B. durch Sedimentation). Die Gase wurden in Tedlar©-Beuteln an der Sediment-Wasser-Grenzfläche gesammelt. Die Analyse erfolgte mittels CV-AFS (THg, $Hg_{diss}$, $Hg^0$, DMHg, $Hg_{gas}$, THg in Sedimenten) und Gaschromatographie (MMHg).

Organische Hg-Spezies waren an keinem der beprobten Standorte in den hydrothermalen Fluiden über der Nachweisgrenze vorhanden. Die Flüssigkeitsproben enthielten im Allgemeinen an Kolloide und Partikel größer als 0,45 µm gebundenes Hg (THg). Die THg-Konzentrationen in den beprobten hydrothermalen Fluiden reichten von Werten unterhalb der lokalen Hintergrundwerte im Meerwasser (0,5 bis 5 pM) bis zu 249 nM. Gebundenes und ungebundenes Hg in gefilterten (0,45 µm) Proben (Hgdiss) stellte im Allgemeinen einen kleinen Teil des THg dar (BDL bis 273 pM). Außerdem war $Hg^0$ im Allgemeinen kein signifikanter Anteil des THg (BDL bis 5,3 pM). Die größte Hg-Spezies in der hydrothermalen Flüssigkeit war daher $Hg^{2+}$, das zum größten Teil an Kolloide und Partikel > 0,45 µm gebunden war. In den

hydrothermalen Gasen reichte das Gesamt-Hg ($Hg_{gas}$) von unterhalb der Nachweisgrenze bis zu 2.792 nmol / m3.

Die stärksten Anzeichen für hohe Hg-Konzentrationen in Gasen und Flüssigkeiten waren mit der Fließgeschwindigkeit und dem Vorhandensein von Sedimentation verbunden. Höhere Fließgeschwindigkeiten, insbesondere in Verbindung mit hohen Temperaturen, wiesen im Allgemeinen auf hohe Hg-Konzentrationen in der Flüssigkeit oder dem Gas hin. Das Vorhandensein von Sedimentation über der hydrothermalen Quelle verringerte die Konzentration jedoch erheblich. Höhere Fließgeschwindigkeiten schränken die zeitliche Exposition der hydrothermalen Fluiden und Gase gegenüber dem umgebenden Material ein, gehen mit höheren Temperaturen einher und verhindern tendenziell die Sedimentation an der Mündung der hydrothermalen Quelle. Dort, wo es an der Öffnung zu Ablagerungen kam, waren hohe Durchflussraten jedoch nicht mit hohen Hg-Konzentrationen verbunden.

Die Auswirkungen von MSWHS auf die lokale Umwelt wurden anhand der an jedem Standort entnommenen Sediment- und Meerwasserproben deutlich. Die an jedem Standort entnommenen Hintergrundsedimentproben lagen innerhalb der normalen Werte. Es wurde eine Anreicherung von Hg in Sedimenten beobachtet, die mit hydrothermalen Quellen in Verbindung stehen (0,3 bis 49,5 nmol/g). Diese Anreicherungen waren jedoch auf die direkte Interaktion mit der Punktquelle beschränkt. Proben, die in einem Abstand von einigen Zentimetern von hydrothermalen Quellen entnommen wurden, wiesen im Vergleich zu den Hintergrundproben keine signifikante Hg-Anreicherung auf (0,3 bis 0,5 nmol / g). Die Auswirkungen von MSWHS auf das darüber liegende Meerwasser wurden am deutlichsten in Panarea und Vulcano beobachtet. In Baia di Levante auf der Insel Vulcano führte die Kombination einer hohen Dichte an MSWHS-Aktivitäten in Verbindung mit flachem Wasser (< 1 m) zu Anreicherungen von bis zu 186 pM THg. Vor der Küste von Panarea, in La Calcara, hielt ein vertikales Profil direkt über der Hauptpunktquelle erhöhte THg-Werte (< 1,1 pM) in 20 m Tiefe aufrecht.

Daraus lässt sich schließen, dass MSWHS Hg in die lokale Umgebung einbringen. Das Ausmaß der Auswirkungen wird weitgehend durch Umweltfaktoren (z. B. Fließgeschwindigkeit und Sedimentation) gesteuert. Ein sofortiger Abbau in den Sedimenten nach der Emission in das darüber liegende Meerwasser wird jedoch nicht bestätigt. Vielmehr wird Hg von Punktquellen und Gebieten mit diffusen Emissionen weg transportiert. Daher können die Auswirkungen von MSWHS auf den Hg-Kreislauf über den unmittelbaren lokalen Bereich hinausgehen.

# Table of Contents

## Contents

# List of figures

xi

## List of tables

# List of abbreviations

As .......................................................................................................... arsenic

BDL ......................................................................................... below detection limit

Br.............................................................................................................. bromine

BrCl ...................................................................................... bromine chloride

Ca........................................................................................................... calcium

Cl .......................................................................................................... chloride

CV-AFS .................................................... cold vapor atomic fluorescence spectroscopy

DMHg ................................................................................. dimethyl mercury

e.g. .................................................................................. exempli grata (for example)

eH.................................................................................................. redox potential

EPA ................................................................................ environmental protection agency

Fe .............................................................................................................. iron

$H_2S$ (liq) .................................................................................. hydrogen sulfide in fluid

$H_2S$ (gas) .................................................................................. hydrogen sulfide in gas

Hg.............................................................................................................. mercury

$Hg_{diss}$ ................................................................. total mercury in filtered (< 0.45 µm) fluid

$Hg^0$................................................................................................ elemental mercury

$Hg^{2+}$ ................................................................................................ ionic mercury

$Hg_{gas}$ ................................................................................. mercury in emitted gas

HgS ................................................................................................ mercury sulfide

ICP-MS.................................................... inductively coupled plasma mass spectrometry

K................................................................................................................ potassium

Li................................................................................................................. lithium

MDSHS........................................................... marine deep sea hydrothermal system

Mg ....................................................................................................... magnesium

MMHg................................................................................ monomethyl mercury

Mn ....................................................................................................... manganese

xiii

# Introduction

## 1.1   Motivation and objectives

Mercury (Hg) is a known biological toxin with significant health implications due to bioaccumulation. Allowable concentrations of mercury within drinking water, industrial waste, and products for agricultural use are set by national and international organizations such as the United States Environmental Protection Agency (EPA) and the World Health Organization (WHO). While Hg is not widely distributed geologically, high concentrations can be observed in veins. Hg occurs in the natural environment in two major inorganic species ($Hg^0$ and $Hg^{2+}$) and two organic species (dimethylmercury (DMHg) and monomethylmercury (MMHg)). The organic species can pass through the blood-brain barrier, therefore posing the greatest human health risk. However, inorganic species have been shown to affect human health when present in greater quantities.

Human activities have raised concentrations of mercury within marine waters and the atmosphere up to 230% and 450% respectively (Lamborg et al., 2002; Outridge et al., 2018). Natural sources to the environment, such as hydrothermal systems, are not as well constrained as their anthropogenic counterparts. For this reason, despite known close associations between Hg and hydrothermal systems, current ocean cycling models assume hydrothermal systems to have a minimal impact on the environment (Fitzgerald et al., 2007; Mason and Fitzgerald, 1996; Obrist et al., 2016; Outridge et al., 2018). However, these systems present unique opportunities to study the effects of prolonged mercury exposure on the environment. In the case of marine shallow water hydrothermal systems (MSWHS), emissions occur near human populations and local fishing areas.

Hydrothermal systems transfer heat and mass through circulating water in a permeable geological formation. The circulating water (hydrothermal fluid) undergoes multiple subsurface processes, gaining and losing constituents dependent upon physical, geological, and chemical factors. According to Beaulieu and Szafranski (2020), a total of 184 systems are confirmed active across the globe. Of these, 43 are considered MSWHS (above 200 m depth). Areas of emission are characterized by diffuse fluid or gas emission (diffuse), or distinct localized points of emission (point

sources). Both types of emission can be sedimented or unsedimented dependent upon local conditions.

The goal of the doctoral project was to provide a fundamental understanding of Hg prevalence in MSWHS from three systems (Milos, Greece; Vulcano, Italy; Panarea, Italy).

## 1.2 Study Sites

### 1.2.1 Paleochori Bay, Milos, Greece

Paleochori Bay is located in the southeast of Milos, which is part of the Southern Aegean Volcanic Arc (Fig. 3.1). The island consists primarily of rhyolitic to andesitic volcanic rock atop a greenschist metamorphic basement (Papachristou et al., 2014). The bay contains numerous hydrothermal fluid and gas discharge areas and is one of the world's largest marine shallow-water hydrothermal systems (MSWHS). Two geothermal reservoirs were identified beneath the island: a high enthalpy system of up to 350 °C in the metamorphic basement and an overlying low enthalpy system of up to 175 °C within rhyolitic lavas close to the surface (Naden et al., 2005; Papachristou et al., 2014).

### 1.2.2 Baia di Levante, Vulcano, Italy

The island of Vulcano belongs to the Aeolian volcanic arc and is comprised entirely of volcanic rock, with younger volcanic edifices in the north and northwest (Keller, 1980). Volcanic activity began during the Upper Pleistocene, and the last eruptive period was from 1888 to 1890; however variable fumarolic activity on land and offshore has continued to the present (De Astis et al., 1997). Baia di Levante is located between the La Fossa caldera and the Vulcanello peninsula. Following drilling campaigns in the 1950s, the Baia di Levante area has been known to be fed by a hydrothermal aquifer beneath the bay (Sommaruga, 1984). Since that time, several subsurface circulation models have been proposed (e.g., Aiuppa et al., 2020; Falcone et al., 2022; Federico et al., 2010; Fulignati et al., 1998; Inguaggiato et al., 2012; Madonia et al., 2015; Oliveri et al., 2019). All models agree that the system is driven by a shallow geothermal aquifer, which generates a boiling hydrothermal brine that feeds the MSWHS in Baia di Levante. However, the exact subsurface plumbing of the hydrothermal aquifer, the sources of various marine and sub-aerial point sources, and the relative significance of water sources (e.g., meteoric water and

seawater) are not conclusively established. Large variations in gas and liquid composition and temperature were reported for the La Fossa and Baia di Levante areas (e.g., Aiuppa et al., 2007; Aubert et al., 2008; Boatta et al., 2013; Rogers et al., 2007). In Baia di Levante, multiple shallow-water point sources emit metals, REEs, and other components to the seawater, which affect the water chemistry of the bay (e.g., Capaccioni et al., 2001; Oliveri et al., 2019; Sedwick and Stuben, 1996).

### 1.2.3 Panarea, Italy

The island of Panarea belongs to the Aeolian volcanic arc with several minor islets located to the east of the main island (Fig. 5.1). The hydrothermal system has been well studied (Chiodini et al., 2006; Italiano and Nuccio, 1991; Longo et al., 2021; Price et al., 2015; Sieland, 2009; Stanulla, 2021), however investigations into the composition of fluids and gases regarding Hg are limited (Bagnato et al., 2009a; Bagnato et al., 2017). This group of formations is the remnant of an eroded volcanic complex between the Vulcano-Lipari-Salina volcanic belt. The exposed land masses are composed of volcanic rocks, whose semi-circular formation surround a 1 km shallow depression (maximum depth 30 m) with multiple locations of hydrothermal activity (Lucchi et al., 2013). A deep hydrothermal body (< 220 °C) is overlayed by two hydrothermal reservoirs (170 to 210 °C) which feed the MSWHS (Italiano and Nuccio, 1991). One reservoir beneath the island of Panarea is recharged by circulated continental waters, and the other recharged by marine waters (Fig 5.1). The emitted hydrothermal gases are mainly comprised of $CO_2$, with variable concentrations of $H_2S$, Ar, $N_2$, $CH_4$, $H_2$, He, and CO (Chiodini et al., 2006; Gugliandolo et al., 2006; Italiano and Nuccio, 1991). Fluids are near seawater values or slightly depleted in Cl and $SO_4$, but some contain enrichments of Ca, K, and $SiO_2$ (Caracausi et al., 2005; Italiano and Nuccio, 1991; Price et al., 2015). Temperatures of hydrothermally active areas can exceed 130 °C. However, the chemical compositions of the MSWHS fluids and gases at Panarea are not static (Caracausi et al., 2005; Tassi et al., 2009). Following a 2002 gas burst, multiple studies were conducted on the stability of the system (Capaccioni et al., 2005; Caracausi et al., 2005; Chiodini et al., 2006; Tassi et al., 2009). Furthermore, recent studies have linked Panarea activity to Stromboli, where increases and subsidence of gaseous activity were observed prior to larger events on Stromboli (Heinicke et al., 2009; Longo et al., 2021). Panarea is an ideal system of study, combining point sources

with large emissions of gases and liquids at high temperature (< 100 °C), and large areas of diffuse emission with a thick sediment layer. Additionally, the system has been well studied, inclusive of Hg data in fluids and gases (e.g., Bagnato et al., 2017; Caracausi et al., 2005; Chiodini et al., 2006; Longo et al., 2021; Lucchi et al., 2013; Price et al., 2015; Sieland et al., 2009; Stanulla, 2021; Tassi et al., 2009).

## 1.4 Methodological approach

### 1.4.1 Fluid collection and field analysis

Fluids were collected using samplers constructed from PTFE tubing and 10 mL pipette tips at 10 cm depth using polypropylene 60 mL syringes. Porewater temperatures were monitored at the depth of the pipette tip. No large deviations in temperature were permitted as sampling was performed to ensure that samples were not contaminated with seawater.

The pH (Halo Wireless pH meter, Hanna Instruments), conductivity and ORP (Myron Ultrameter) were immediately determined in the field. The samples were filtered through a 0.45 µm membrane, and the sub-samples for trace elements and major cations were preserved with 2 % (m/v) concentrated nitric acid.

### 1.4.2 Hg analysis

#### 1.4.2.1 THg and Hg$_{diss}$

Total Hg samples were collected unfiltered and filtered (0.45 µm) and analyzed following the USEPA (2002) protocol with a Brooks Rand CV-AFS analyzer in duplicate. In preparation for the analysis, 40 mL of the sample were added to a 60 mL Volatile Organic Analysis (VOA) glass vial with a PTFE-lined cap. Then 400 µL acidified bromide/bromate, a 1:1 mixture of 0.01 M bromide/bromate solution (Tritrisol, Merck) and 32 % hydrochloric acid (Optima grade, Fisher Scientific) were added to the sample, and the light-yellow colored solution was left standing for at least 30 min at room temperature. The bromine chloride reactivity was then quenched by the addition of 100 µL 30 % (m/v) hydroxylamine hydrochloride solution (ReagentPlus, 99 %, Sigma-Aldrich) and shaken. Elemental Hg was produced in the solution by adding 200 µL of a 20 % (m/v) tin(II)chloride solution (Reagent grade, Alfa Aesar). The detection limit for this method was determined to be 0.04 ng/L (n = 10) for our laboratory. The certified reference material ORMS-5 (elevated Hg in river water, National Research Council Canada) was used for quality control. The

reference material was certified for a concentration of 26.2 ± 1.3 ng/L T-Hg and measured within 5% of certified values.

### 1.4.2.2 Sediment digestion

Sediment samples were digested in 10:1 aqua regia following Bloom et al. (2003) and THg was analyzed by CV-AFS. The certified reference material PACS-1, certified for a concentration of 4.57 ± 0.16 µg/g THg was used for quality control.

### 1.4.2.3 Volatile Hg species

Volatile Hg was collected by purging 1 L of hydrothermal fluid with Hg free nitrogen onto gold and carbo traps and analyzed by CV-AFS (Cossa et al., 2011; Lehnherr et al., 2011).

### 1.4.2.4 MMHg (MeHg)

Analysis of MeHg was carried out by species-specific isotope dilution gas chromatography. A 100 mL sample was spiked with a Me$^{201}$Hg solution (ISC Science, Spain) and left equilibrating for an hour. An optimal ratio of 4.25 for Me201Hg in the spike to Me$^{202}$Hg in the sample was the spiking aim. Based on the assumption of 5 % of T-Hg being present as Me$^{201}$Hg, the amount of the enriched isotopic solution was calculated for the initial spiking. An acetate buffer, prepared from trace metal grade acetic acid (Fisher Scientific) and 30 M NaOH (Suprapur, Merck), was added to the sample. The pH was adjusted to 3.9 with sodium hydroxide solution (30 M, Suprapur, Merck). Subsequently, 1 mL propylation reagent (1 g sodium tetra-propyl borate (Merseburger Spezialchemikalien, Germany) in 100 mL oxygen-free Milli-Q water) was added to the sample followed by 200 µL n-Hexane (Reagent Grade ACS, Riedel-de-Haen). The Hg species were extracted into the n-hexane phase by shaking for 10 min, and the n-hexane phase was taken out for analysis by gas chromatography coupled to ICP-MS (Element 2, Thermo Scientific) with an in-house-built heated transfer line (temperature of 160 °C). A cyclonic spray chamber was attached at the transfer line just before the ICP torch for wet plasma conditions giving the option of plasma tuning and monitoring with an internal Thallium standard.

### 1.4.2.5 Gas sample collection and analysis

Gas samples were collected into Tedlar© bags using a custom-built glass funnel connected to Teflon tubing in combination with a standard lift bag. The lift bag was attached to lead weights, which enabled the calculation of gas volume collected,

5

i.e., the volume of gas needed to displace enough seawater to lift the bag at a given depth and lead weight. To remove sulfur species from the gas, the samples were passed through an alkaline solution. The sample was then trapped in a 0.5 M permanganate solution in 2 N sulfuric acid and analyzed on the CV-AFS as THg (Brombach and Pichler, 2019).

### 1.4.3 Anions and cations collection and analysis

Anions were analyzed in a non-acidified, filtered sample (0.45 µm) using a Metrohm 883 Basic IC instrument with a 5 µL injection loop and a Metrosep A Supp5 (150 × 4.0 mm; 5 µm) column. Quality control samples were an internal standard and IAPSO, an artificial seawater. Major cations and some trace elements were measured by inductively coupled plasma-optical emission spectrometry (ICP-OES) using a Perkin Elmer Optima 7300 DV instrument. The detection limit for most elements was around 1 to 10 µg/L, which was not sensitive enough for trace elements but sufficient for the major elements present in the sample. All water samples were diluted by a factor of 100 due to the high salinity of the samples. Quality control was assured with different certified waters: EnviroMAT Groundwater Low (ES-L-2) and High (ES-H-2), both from SCP Science, Canada, are groundwater samples while CRM-SW (High Purity Standards, USA) was a certified seawater.

Trace elements were analyzed with inductively coupled plasma mass spectrometry (ICP-MS, Element 2 Thermo Scientific). The mass analyzer of the Element 2 instrument is based on a magnetic and electric sector field. Mass interference based on polyatomic and isobaric interference can be overcome by adjusting the mass resolution from low to high, which is essential for some trace elements, e.g., arsenic. The same principle for sample dilution for saline samples as was described for ICP-OES. Plasma fluctuations were monitored via the addition of internal standards to each sample.

### 1.4.4 Flux calculations

The flux (pmol/m2/hour) of $Hg^0$ to the atmosphere from each of the sampling sites was calculated using equations by Liss and Slater (1974) (1) and Wanninkhof (1992) (2), as implemented by Wängberg et al. (2001). Where kw (cm/hour) is the gas transfer velocity, u10 is the wind speed at 10 m height, ScHg is the Schmidt number for Hg in seawater and ScCO2 is the Schmidt number for CO2 in seawater (Kuss et al., 2009), and H' is Henry's law constant. An approximate value was used

for atmospheric Hg (7.5 pmol/m3), and the percent volatile Hg$^0$ was assumed to be 10 % of Hgdiss (Horvat et al., 2003). Schmidt numbers 689 for Hg and 660 for CO2 were used.

$$Flux\ to\ the\ Atmosphere = k_w\ (DGM - {}^{TGM}/_H) \tag{1}$$

$$k_w = 0.31\ u_{10}^2\ ({}^{Sc_{Hg}}/_{Sc_{CO2}})^{-0.5} \tag{2}$$

## 1.3 Thesis Structure

This thesis was written in a cumulative format. It is a collection of three manuscripts which have been published or prepared for submission as joint-author articles to international peer-reviewed journals. The thesis is divided into six main chapters. The introductory chapter provides an outline of the motivation, objectives, and goals of the doctoral project. It also establishes the importance of the subject matter.

The second chapter introduces the subject matter, beginning with a summary of the chemistry, biology, and cycling of Hg within the natural environment. It is then followed by an introduction to hydrothermal systems, their formation, and current understanding of their role in studies of marine chemistry and specifically Hg cycling.

The third chapter addresses the field location of Milos, Greece. It focuses on geochemical and biological cycling, and the impact of the MSWHS on the local environment. This chapter was published in *Marine Chemistry*.

The fourth chapter addresses the field location of Vulcano, Italy. It focuses on geochemical cycling and the impact of largely gaseous emissions on the shallow bay of Baia di Levante. This chapter was published in *Marine Chemistry*.

The fifth chapter addresses the field location of Panarea, Italy. It compares and contrasts the Panarea system with Milos and Vulcano, utilizing knowledge gained in each to illuminate larger conclusions on MSWHS as a whole. This chapter was prepared for publication in *Chemical Geology*.

The sixth and final chapter synthesizes the three manuscripts and identifies key areas of interest to further the study of MSWHS and Hg cycling.

**Declaration of co-author contributions**

This thesis includes two published research articles and one prepared manuscript. The chapters are prepared under consideration of the journal requirements to which they have been submitted or intended for submission. The style has been adapted to the thesis style and headings, figures, tables, and formulae are numbered consecutively throughout the thesis. A complete list of references is given at the end of the thesis. In the following, a detailed overview of the co-authors' contributions to each chapter is presented.

Chapter 3: *Mercury in the hydrothermal fluids and gases in Paleochori Bay, Milos, Greece*

Authors: Hannah Roberts, Roy Price, Christoph-Cornelius Brombach, Thomas Pichler

The sampling protocol and field work were organized by HR, CB, and TP. The acquisition and assessment of data were performed by HR. The initial text, graphics, and tables were prepared by HR. TP helped with data interpretation and reviewed the manuscript before submission. RP and CB contributed to the biological cycling section and method section respectively. The co-authors contributed content and reviewed the manuscript before submission.

Chapter 4: *Hg in the hydrothermal fluids and gases in Baia di Levante, Vulcano, Italy*

Authors: Hannah Roberts, Thomas Pichler

The sampling protocol and field work were organized by HR and TP. The acquisition and assessment of data were performed by HR. The initial text, graphics, and tables were prepared by HR. TP helped with data interpretation and reviewed the manuscript before submission. The co-authors contributed content and reviewed the manuscript before submission.

Chapter 5: *A marine shallow water hydrothermal system as an important Hg emitter to the local environment of Panarea, Italy*

Authors: Hannah Roberts, Thomas Pichler

The sampling protocol and field work were organized by HR and TP. The acquisition and assessment of data were performed by HR. The initial text, graphics, and tables

<u>1. Introduction</u>

were prepared by HR. TP helped with data interpretation and reviewed the manuscript.

Status. To be submitted to *Chemical Geology*

## 2. Mercury in the environment and hydrothermal systems

### 2.1 Mercury

#### 2.1.1 The mercury cycle

The greatest contributors to atmospheric Hg are anthropogenic sources (4.4 kt / yr), followed by soil and vegetation (1.0 kt / yr), biomass burning (0.6 kt / yr), and geogenic sources (0.5 kt / yr) (Outridge et al., 2018). However, of these sources all are considered re-emission or remobilization or natural apart from anthropogenic sources. Atmospheric Hg is transported and deposited to environmental reservoirs (e.g., soils and waters) through dry and wet deposition. The largest Hg reservoir, the surface ocean, has risen to 230% above pre-industrial levels (Lamborg et al., 2002; Outridge et al., 2018). The overall net evasion of Hg to the atmosphere from the surface ocean is estimated to be 3.4 kt / yr due to recycling of legacy Hg within the reservoir. However, constraints on natural sources to the ocean and atmosphere are largely uncertain. Hydrothermal sources to the environment are discounted as insignificant, however these estimations were made by limited or incomplete data (Lamborg et al., 2002; Mason and Sheu, 2002).

As the largest reservoir, cycling of Hg within the marine environment is an important component of the overall global system. Mercury is primarily deposited to surface waters from the atmosphere and fluvial sources. Sinks from this system include biological uptake, burial in sediments, and evasion to the atmosphere. An important secondary consideration of the marine cycle include recycling of evaded Hg back to surface waters, which elevates concentrations in the open ocean (Mason and Sheu, 2002).

#### 2.1.2 Hg Chemistry

Mercury is a soft Lewis acid, forming strong covalent bonds with soft Lewis bases. Mercury and mercury bearing minerals have long been shown to be of practical use as amalgams in dentistry to thermometers, and ceramics. In modern times, its use has been strongly discouraged due to human health and environmental concerns but remains prevalent throughout much of the globe. The toxicity of Hg is determined by its speciation, which consists primarily of two inorganic and two organic species.

Inorganic elemental mercury ($Hg^0$) is primarily found in the environment as a gas in the atmosphere (Lamborg et al., 2000). Relative toxicity of elemental mercury is low, however high concentrations lead to respiratory issues. Within the subsurface, $Hg^0$ likely plays a key role in ore transport processes (Varekamp and Buseck, 1984). The chalcophilic inorganic mercuric ion ($Hg^{2+}$) and the redox cycles between $Hg^{2+}$ and $Hg^0$ play a pivotal role in Hg bioavailability, biotoxicity, and transport. For example, uptake by microorganisms is higher in neutrally bound $Hg^{2+}$, thereby impacting mercury methylation rates (Mason, 2001).

Organic mercury, monomethyl mercury (MMHg, $[CH_3Hg]^+$) and dimethyl mercury (DMHg, $[(CH_3)_2Hg]$), are the most toxic common Hg species. Bioaccumulation in muscle and organ tissues of fish and marine mammals are responsible for population poisonings in humans and other higher trophic species (e.g. Fimreite, 1974; Harada, 1995). Historical poisonings within humans were directly resultant from industrial disposal practices of $Hg^{2+}$, where waste was dumped into marine waters and subsequently methylated and bioaccumulated in culturally traditional marine protein sources (Compeau and Bartha, 1984; Cossa et al., 2009; Mason, 2001). While MMHg is more prevalent within the environment, DMHg is remarkably more toxic (Siegler et al., 1999).

### 2.1.3 Hg geological considerations

Distribution of mercury within Earth's crust is not well distributed and relatively rare. Rather, high concentrations are observed in veins (Table 2.1). Large deposits of mercury, the largest being the Almaden mercury mining district in Spain, have been sourced to hydrothermal activity (e.g. Hall et al., 1997; Hernandez et al., 1999; Saupe, 1990). Hydrothermal fluid gains mercury (Hg) through three main sources: magmatic, mineral dissolution, and leaching from an unmineralized source or host rocks (Barnes, 1973; Giggenbach, 1997; Saupe, 1990; Varekamp and Buseck, 1984). Ore deposits of mercury are formed in the greatest abundance between 100° to 150° C, under saline (10 to 23 % eq. NaCl), near surface conditions (Barnes, 1979; Loredo et al., 1988). Additionally, organic-rich sediments and soils have higher mercury concentrations due to uptake by biological organisms (Fitzgerald and Lamborg, 2004).

Table 2.1: Distributions of Hg by rock type

| Rock Type | Hg (ug/g) | References |
|---|---|---|
| *Igneous* | | |
| Granites | 0.077 | (Marowsky and Wedepohl, 1971) |
| | 0.08 | (Turekian and Wedepohl, 1961) |
| Basalts | 0.07 | (Marowsky and Wedepohl, 1971) |
| | 0.09 | (Turekian and Wedepohl, 1961) |
| Ultramafics | 0.004 | (Marowsky and Wedepohl, 1971) |
| *Sedimentary* | | |
| Shales | 0.4 | (Marowsky and Wedepohl, 1971) |
| | 0.4 | (Turekian and Wedepohl, 1961) |
| Graywackes | 0.28 | (Marowsky and Wedepohl, 1971) |
| Sandstones | 0.03 | (Turekian and Wedepohl, 1961) |
| Limestones | 0.04 | (Marowsky and Wedepohl, 1971) |
| | 0.04 | (Turekian and Wedepohl, 1961) |
| *Representative metamorphic changes* | | |
| Initial shale | 0.35 | (Turekian and Wedepohl, 1961) |
| Greenschist facies | <.010 | (Turekian and Wedepohl, 1961) |
| Amphibolite facies | <.010 | (Turekian and Wedepohl, 1961) |
| *Crustal averages* | | |
| Upper crust | 0.056 | (Wedepohl, 1995) |
| Lower crust | 0.021 | (Wedepohl, 1995) |
| | | |
| *Hydrothermally Influenced* | | |
| Mid ocean ridge basalt | 29.3 | (Konovalov et al., 2018) |
| Inter-tidal hot spring | 74.3 | (Leal-Acosta et al., 2018) |
| Gorda Ridge pyrite vein | 0.0003 | (Lamborg et al., 2006) |
| Hot Spring Sediments | 25.2 | (Leal-Acosta et al., 2010) |
| Hot Spring Crust Wall | 60.3 | (Leal-Acosta et al., 2010) |
| Almada Mining District | 6-8 * | (Hernandez et al., 1999) |
| Sinter | 0.2 - 2 | (Sherman et al., 2009) |
| | | |
| *Marine Shallow Water Systems* | | |
| Vulcano, Italy | 0.6 to 3.4 | (Roberts and Pichler, 2022) |
| Milos, Greece | 83 to 243 | (Roberts et al., 2021) |

* Ore grade (%)

## 2.1.4 Hg biological considerations

As a toxic heavy metal, organisms have developed mechanisms to handle various mercury species. Elemental mercury is not readily absorbed through the skin or gastrointestinal tracts of humans. However, $Hg^0$ is highly volatile and readily releases Hg vapor which is then largely absorbed by the lungs. Ionic mercury,

particularly when bound in neutral chloride complexes, and methyl mercury can be passively taken up by microorganisms (e.g. Mason, 2001; Mason et al., 1996). Inorganic mercury is easily absorbed via ingestion and through the skin, primarily affecting the kidneys in humans. Organic mercury is also easily absorbed when ingested or through the skin. However, organic mercury species cross the blood-brain barrier, and concentrates in the kidneys and central nervous system. Bioaccumulation of methylmercury is of primary concern, as trophic transfer and bioaccumulation of organic species is higher (Mason, 2001). The methylation of mercury is primarily biologically mediated by microbes (King et al., 2000) through *mer* A and *mer* B genes. These pathways play a pivotal role mercury toxicity throughout the world (e.g. Boyd et al., 2009; Crepo-Medina et al., 2009). However, uptake of mercury is not limited to microbes, for example seagrasses and lichens have also been shown to accumulate Hg (e.g. Leal-Acosta et al., 2018; Loppi, 1996).

## 2.2 Hydrothermal systems

### 2.2.1 Hydrothermal system introduction

Hydrothermal systems are formed when a heat source fuels the circulation of water through a planet's crust. Therefore, hydrothermal systems are primarily associated with magma (volcanogenic) or tectonic activity. Water sources can be meteoric, juvenile, connate, or metamorphic water (Giggenbach, 1997). Convection or conduction drives fluid flow from water sources through the fractured crust towards the heat source in an area identified as the recharge zone (Alt, 1995). Through this process, the pressure and temperature of the water increases and initiates water-rock interactions. Proximal to the heat source, high temperature (> 350°C) reactions occur within the reaction zone, resulting in rapid changes in buoyancy. The hot positively buoyant fluid then passes through the upflow zone to the surface, losing pressure and heat while undergoing additional water-rock interactions.

Due to these changes, hydrothermal fluid undergoes a boiling process, where vapors separate from the fluid phase. This process strongly affects the water-rock interactions in the subsurface, and ultimately the chemistry of waters and vapors upon emission. Fluids at the surface are generally separated into three main groups according to their dominant constituents: neutral-chloride, acid-sulfate, and bicarbonate waters. Neutral-chloride waters are typical of high temperature systems with more direct flow from a deep fluid reservoir. These fluids are associated with

13

intense flow, such as those observed at geysers. Acid-sulfate waters are formed by condensed vapors mixing with near-surface oxygenated waters. Acid-sulfate waters are therefore resultant of boiling processes and found at areas such as the margins of major upflow areas and over boiling zones. Bicarbonate waters are produced when condensed vapors mix with poorly-oxygenated near-surface waters. Bicarbonate waters are more typical of non-volcanogenic high temperature systems. The complexity of hydrothermal systems often leads to a mixing of these fluids prior to emission.

Low temperature systems, with maximum temperatures of 30-60 °C, are also observed in many areas. These low-enthalpy systems contain meteoric water that returns to the surface after heating. Deep faulting and folding, regions of uplift, and cooling plutons, can result in this type of hydrothermal system.

Hydrothermal systems may be subaerial or submarine. Large differences in processes and emitted material exist between subaerial (SAHS), marine shallow water (MSWHS), and marine deep-sea (MDSHS) systems (e.g. Sherman et al., 2009). Dependent upon the type of hydrothermal system, gas, diffuse brine, focused hot fluid, or a mixture of the three, are possible. Due to the pressure of the overlying water column, gases do not separate from the hydrothermal fluid of MDSHS. Comparatively, SAHS and MSWHS do produce phase separated gases under various conditions (e.g. Bagnato et al., 2017; Dando et al., 1995). The primary differences between the three types of systems are observed beginning in the shallow subsurface, with surface conditions enhancing these differences.

The impact of a given hydrothermal system on its surrounding environment is highly variable. While low temperature, low flow springs can result in negligible changes, high temperature, high flow, or acidic point sources can result in drastic changes in geology, chemistry, and biological activity. While some relatively consistent hydrothermal systems range into the millions of years old, acute major disturbances to the surrounding environment also occur (e.g. explosions from plumbing instability).

**2.2.2 Subaerial systems (SAHS)**

Subaerial hydrothermal systems (also referred to as terrestrial hydrothermal systems) are areas of active hydrothermal activity above sea level. Emitted material

is under atmospheric pressure at the surface, however unlike MSWHS's, gases and liquids are not necessarily scrubbed of various constituents by overlying water before exposure to the atmosphere (e.g. Bagnato et al., 2017; Leal-Acosta et al., 2018).

### 2.2.3 Deep sea systems (DSHS)

Deep sea hydrothermal systems are largely associated with mid-ocean ridges (MOR). Due to the intense pressure at these depths, gases are not separated from fluids. Large fluxes of metals and other chemical constituents from these systems generate unique biological and chemical environments on the seafloor. The primary water source of these systems is seawater. Recharge zones for MDSHS's may be wide spread, with on-axis magmatically driven circulation or off-axis circulation associated with passive cooling of the crust (Alt, 1995). The plumes generated by deep sea systems are responsible for generating essential nutrients for not only localized deep sea ecosystems (Jannasch and Mottl, 1985; Ruelas-Inzunza et al., 2003), but for global biological activity as well (Wu et al., 2011).

### 2.2.4 Marine shallow water hydrothermal systems (MSWHS)

Similar to subaerial systems, MSWHS's emit gases and fluids due to lower pressures than those observed at MDSHS's. Primarily, MSWHS's are observed in association with island arc volcanoes (e.g. Milos, Greece), but are also observed at back-arc basins (e.g. White Island, New Zealand), mid-ocean ridges (e.g. Espalamaca, Azores), fault-related heat sources (e.g. Punta Mita Mexico), intra-plate activity (e.g. El Hierro Canary Islands), and serpentization processes (e.g. Prony Bay, New Caledonia). Due to the nature of MSWH's, most emit acidic fluids (Price and Giovannelli, 2017). However, neutral-chloride (Valsami-Jones et al., 2005) and bicarbonate fluids (Pichler et al., 1999b) have also been observed. In comparison to SAHS's, MSWHS's have the added complexity of an overlying water body. For example, microcirculation of oxygenated seawater within sediments surrounding gas point sources was shown to influence silica and manganese precipitation patterns observed on Milos, Greece (Wenzhofer et al., 2000). Gaseous emissions from shallow water systems may be large enough to reach the air-sea interface (Bagnato et al., 2017), or may dissolve in the water column (Dando et al., 1995). In the latter instance, the extent or presence of many shallow water systems may remain unknown (Esposito et al., 2018). The addition of photochemical reactions and terrigenous materials further separates shallow water systems from their pressurized

15

deep sea counter parts (e.g. Dando et al., 1999; Giovannelli et al., 2013; Gomez-Saez et al., 2015).

Features associated with shallow water systems are microbial mats (Price et al., 2013), chimneys (Esposito et al., 2018), brines (Valsami-Jones et al., 2005), and gaseous emissions (Bagnato et al., 2017). Additionally, the movement and settling of sediments and particles result in interactions between gases, fluids, and sediments (e.g. Dando et al., 1995; Pichler et al., 1999a). Limited research into the transport of buoyant fluids and particles from shallow water systems indicates the radius of impact of these systems may be far reaching (Dando et al., 2000; Lin et al., 2020).

The influence of shallow water systems is three-fold. Gases and liquids influence the environment of the surrounding seawater (e.g. Pichler et al., 1999b), volatile contaminants in fluids and vapors may reach the air-sea interface (Bagnato et al., 2017), and groundwaters utilized by local communities may be contaminated by upflowing hydrothermal fluids and gases (Bagnato et al., 2009a). The proximity of shallow water systems to local communities has potential health implications (e.g. Bagnato et al., 2009a; Davey and van Moort, 1986). Organisms dependent on hydrothermal activity, outside of microbes, is not present in shallow water systems as it is in the deep sea.

## 2.3 Environmental abundance of Hg

### 2.3.1 Mercury distribution in minerals, rocks, sediments, and soils

High mercury concentrations within sediments associated with hydrothermal discharge have been observed from SAHS, MSWHS, and DSHS (see Table 2.1). Mercury is most commonly observed in ore veins, with extreme concentrations in cinnabar (HgS) deposits. Concentrations of Hg observed in surface soils and minerals are influenced by anthropogenic and natural sources, with atmospheric deposition (dry and wet) as a significant source (Lamborg et al., 2002).

The pH, $H_2S$, temperature, and chloride concentrations associated with hydrothermal systems, particularly those of acid-sulfate fluids, facilitate HgS dissolution and transport. It is well known that Hg travels within the subsurface as a vapor. The formation of acid-sulfate waters, therefore, concentrates Hg species and preserves Hg within the fluid. Deposition of Hg from hydrothermal systems occurs under near surface conditions, where further mixing of hydrothermal fluid with other

waters and lower temperatures are achieved.  This process focuses mercury into concentrated veins (Barnes, 1973).

As was discussed by Schluter (2000), rates of evaporation of Hg from soils to the atmosphere are determined by a complex series of factors. The formation of volatile species by biological methylation to DMHg or (a)biological reduction from $Hg^{2+}$ to $Hg^0$ are impacted by $Hg^{2+}$ availability, microbial activity, the presence of organic matter, and redox potential. Diffusion and mass transport of volatile species can be interrupted by sorptive interactions and influenced by meteorological and hydrological conditions, along with chemical characteristics of the soil. Evaporation of volatile species are strongly influenced by meteorological factors. Rates of evaporation can reach up to 4.2 g $m^{-2}$ $hr^{-1}$ under laboratory conditions (Schluter, 2000), while fluxes in the natural environment have been found to be on the order of ng  $m^{-2}$ $hr^{-1}$ from enriched soils (e.g. Gustin et al., 1999)

Research on dissolution of Hg from hydrothermal deposits is primarily associated with mining, and geothermal energy production, (e.g. Covelli et al., 1999; Feng et al., 2010; Nicholson, 1992). Benthic flux to the overlying water column from the contaminated sediments of the Gulf of Trieste was highest in autumn and winter months with a total of 25% of deposited material recycled into the water column (Covelli et al., 1999). The presence of hydrogen sulfide immobilizes trace metals into sulfide complexes (Brumsack, 2006), however dissolution of HgS has been shown with changes in DOM (Slowey, 2010). As increasing DOM sorbes to cinnabar surfaces, dissolution rates decrease (Waples et al., 2005). The presence of organic rich material in combination with HgS-complexes was positively correlated with MMHg production within contaminated sediments (Drott et al., 2007). However, it should be noted that MMHg concentrations within hydrothermally influenced sites did not show increased MMHg concentrations (King et al., 2006). The balance between accumulation, dissolution, and deposition generates areas of extreme enrichment with the potential for further mobilization given proper environmental changes (Konovalov et al., 2018; Lacerda et al., 2004).

## 2.3.2 Mercury distribution in seawater

Mercury concentrations vary within seawater both spatially and temporally in the low pM range with elevated levels in surface waters strongly influenced by atmospheric deposition (Fitzgerald et al., 2007). The behavior of Hg within the water

17

column is non-conservative, and impacted by biological, chemical, and geological processes. Coastal waters may contain higher concentrations of Hg in both particulate and dissolved forms due to additional sources (e.g. fluvial waters, local pollution, etc).

Within porewaters, higher THg concentrations are associated with organic rich sediments (Baeyens et al., 1998; Choe et al., 2004; Lamborg et al., 2006). Benthic fluxes of THg in estuarine environments may be of similar magnitude as riverine flux during low flow (Choe et al., 2004), and elevated by transitional periods between seasons (Covelli et al., 1999). As much as 25% of deposited THg, with a large portion as MMHg, within the Gulf of Trieste was found to be recycled into the water column annually (Covelli et al., 1999). Major factors affecting benthic flux increases include anoxic environments coupled with increases in sulfate reduction and organic matter production (Baeyens et al., 1998; Covelli et al., 1999).

Within the water column, mercury concentrations are in the low pM range (Fitzgerald et al., 2007; Lamborg et al., 2006). Trace metals tend to fall within a 'scavenged-type' (net particulate removal) or 'nutrient-type' (biogenic particle removal followed by remineralization) distribution within the water column. However, THg does not follow either pattern, rather individual Hg species follow identifiable patterns (Bowman et al., 2015). More generally, mercury concentrations in the open ocean are controlled by the extent of both external sources and water column processes (Cossa et al., 1997; Laurier et al., 2004) such as evasion to the atmosphere in surface waters, and scavenging by particles and remineralization in deeper waters. Organic mercury species are generally at or below detection limits in non-contaminated waters (Bowman et al., 2015; Fitzgerald et al., 2007) and are therefore not well studied.

## 2.3.3 Mercury distribution in hydrothermal fluids and gases

Hydrothermal fluid gains mercury (Hg) through three main sources: magmatic, mineral dissolution, and leaching from an unmineralized source or host rocks (Barnes, 1973; Giggenbach, 1997; Saupe, 1990; Varekamp and Buseck, 1984). Hydrothermal systems were shown to be the source of large Hg deposits, as documented by the well-studied Almaden district which contains approximately one third of the world's mercury resources (e.g. Hall et al., 1997; Hernandez et al., 1999; Saupe, 1990). As hot hydrothermal fluid rises, temperature and pressure decreases

allowing Hg minerals to precipitate (Varekamp and Buseck, 1984). Mercury ores formed through hydrothermal processes are also associated with a variety of mineral deposits (Cabral et al., 2002; Tang et al., 2017).

### 2.3.4.1 Sub-aerial

Mercury within the hydrothermal fluids of sub-aerial systems have been found to range between pM and nM concentrations in the fluid phase (Table 2.2). Within the gas phase, concentrations fall within the nmol / $m^3$ range. Predictably, low concentrations of THg are frequently observed within acid-sulfate and bicarbonate waters.

Table 2.2: Distribution of THg from hydrothermal systems

| Source | Sample location | Hg Tot pM |
|---|---|---|
| *SAHS* | | |
| (Sherman et al., 2009) | Yellowstone | 0.1 - 0.7 |
| (Leal-Acosta et al., 2018) | Gulf of California | BDL - 6481 |
| | | |
| *DHSH* | | |
| (Lamborg et al., 2006) | Gorda Ridge | 4 - 10 |
| (Kádár et al., 2007) | Lucky Strike | 6000000 |
| (Crepo-Medina et al., 2009) | East Pacific Rise | 75 - 11000 |
| | | |
| *MSWHS* | | |
| Roberts (Roberts et al., 2021) | Milos, Greece | 34 - 2894 |
| Roberts (Roberts and Pichler, 2022) | Vulcano, Italy | 3 - 2888 |
| Roberts (In Prep.) | Panarea, Italy | 1 - 248766 |
| Kurzinger (Kürzinger, 2019) | Panarea, Italy | 12264 - 55835 |

### 2.3.4.2 Marine Shallow Water Systems

Shallow water systems contain pM to µM concentrations of THg (Table 2.2). Concentrations vary considerably within short distances with high variability between study sites (Leal-Acosta et al., 2018; Prol-Ledesma et al., 2004; Roberts and Pichler, 2022; Roberts et al., 2021). Despite the limited body of literature, multiple studies were conducted on the island of Panarea (Bagnato et al., 2017; Kürzinger, 2019; Roberts and Pichler, 2022). Unfortunately, these studies are not in agreement. Differences in sampling technique (such as the suggestion by Bagnato et al. (2017) of gases contaminating fluid samples), temporal variations (Aubert et al., 2008), or different point sources mistakenly measured (Roberts et al., 2021) could explain these differences. Despite large variations in concentrations between studies, no known study has reported measurable methylated mercury concentrations within MSWHS fluid (Roberts and Pichler, 2022; Roberts et al., 2021). Organisms primarily responsible for MMHg are present within these systems (Price and Giovannelli, 2017). However, their impact appears to be limited. Within the gaseous phase, concentrations are in the low nmol / $m^3$ to low µmol / $m^3$ $Hg_{gas}$.

### 2.3.4.3 Deep Sea

Concentrations of total mercury range from the low pM to the low µM upon emission (Table 2.2). The highest concentration found in the literature was from Lucky Strike, a deep-sea hydrothermal vent with high concentrations of dissolved gases indicating phase separation.

# 3. Mercury in the Hydrothermal Fluids and Gases in Paleochori Bay, Milos, Greece

Hannah Roberts[1*], Roy Price[2], Christoph-Cornelius Brombach[1], Thomas Pichler[1]

1    Universität Bremen, Fachbereich Geowissenschaften, Geochemistry and Hydrogeology, Klagenfurter Str. 2-4, 28359 Bremen, Germany

2    Stony Brook University, School of Marine and Atmospheric Sciences, Stony Brook, New York, USA

## Abstract

Seafloor hydrothermal activity may constitute a considerable mercury (Hg) source to the oceans, but the flux from marine shallow-water hydrothermal systems (MSWHS) remains poorly constrained to date. To study the presence of Hg in MSWHS in Paleochori Bay (Milos Island, Greece), sea surface, bottom, pore fluid and hydrothermal gas samples were collected in June of 2017, October of 2018 and July of 2020, and analyzed for Cl, Br, SO4, As, Ca, Fe, K, Mg, Mn, Na, Si, Sr, $H_2S$, unfiltered total Hg (THg), and filtered Hg (Hgdiss). Specific sites were selected for the analysis of volatile elemental Hg (Hgo), dimethylmercury (DMHg), monomethylmercury (MMHg), and Hg in the gas phase (Hggas). Concentrations of THg observed in samples collected from the sea surface were elevated compared to surface samples taken outside Paleochori Bay. The highest surface water concentrations (~10 to 15 pM) were measured in samples collected directly above shallow-water hydrothermal discharge areas. Pore fluids outside Paleochori Bay were significantly lower in THg (0.8 to 8.6 pM) than those taken inside (17.4 to 1511 pM). Porewaters collected from areas with visible gaseous or fluid emission were highly variable but generally elevated in THg concentrations (185 to 5066 pM). Concentrations within gases ranged from 0.7 to 2791 nmol/m3. The vast majority of samples with highly elevated THg (> 100 pM) had low Na/K ratios (< 15), indicative of rapidly rising fluid. Concentrations of $Hg^0$, DMHg, and MMHg were below detection limits in all samples.

Bottom substrate type (e.g., rocky vs. sediment covered) likely affected infiltration rates of oxygenated seawater below the sediment-water interface, thereby affecting

Hg speciation and removal by precipitation. Flux rates from porewaters compared to those with gaseous emission were high (12.56 to 1088 mol THg/year and 0.37 to 1.85 mol THg/year). Sites with slow gaseous emission rates are hypothesized to have extended subsurface reaction times, resulting in lower Hg concentrations emitted to bottom waters. However, increasing rates of gas emission did not necessarily indicate higher Hg concentrations. The scavenging of Hg in the sediments and advective flux out of Paleochori Bay likely prevent significant accumulations of THg in the water column of Paleochori Bay. The total atmospheric flux from Paleochori Bay using average flux calculations over the entire surface area would contribute 6 mmol Hg/year to the atmosphere.

We hypothesize that Hg concentrations within the pore fluids of Paleochori Bay reflect a balance between mixing and precipitation in the subsurface. A three-component mixing system of vapor, brine and seawater determines THg concentrations; however, precipitation due to sulfur cycling, changes in redox conditions and temperature, all play a crucial role in removing Hg from emitted fluids and gases.

## 3.1 Introduction

Mercury (Hg) is a post-transition metal with unique physicochemical properties and a rather distinct global biogeochemical cycle. Contrary to other trace metals, it is highly volatile and has a low chemical reactivity in its gaseous elemental form ($Hg^0$). Consequently, it has an atmospheric residence time of close to one year and is thus widely dispersed worldwide (Schroeder and Munthe, 1998). In the marine environment, Hg is a scavenged trace element and can be present in two oxidation states: elemental $Hg^0$ and ionic $Hg^{2+}$. Elemental Hg is generally present as a dissolved gas but can also be bound to particulates (Wang et al., 2015). Ionic Hg is mainly associated with sulfur minerals and methylated organic species monomethylmercury (MMHg) and dimethylmercury (DMHg). Biotic and abiotic processes control the speciation and complexation of Hg, which determine Hg availability for methylation and toxicity (Fitzgerald et al., 2007; Mason, 2001). Dissolved species (Hgdiss) include Hg bound to colloids (< 0.45 µm) and unbound $Hg^{2+}$ and $Hg^0$, and methylated species. Both $Hg^0$ and DMHg are volatile. Concentrations of bound $Hg^0$ can be significant and prevent the escape of $Hg^0$ to the atmosphere; however, their stability is unknown. Total Hg (THg) concentrations in

## 3. Mercury in the Hydrothermal Fluids and Gases in Paleochori Bay, Milos, Greece

unpolluted waters for the Mediterranean Sea were reported to be in the low pM range (Cossa et al., 1997; Horvat et al., 2003) with a varying temporal and spatial distribution in the water column (Fitzgerald et al., 2007; Gworek et al., 2016).

Methylmercury (MeHg) is of particular concern as it is a bioaccumulating toxin causing adverse health effects for organisms at higher trophic levels (Frederick and Jayasena, 2010) and their human consumers (Fitzgerald and Clarkson, 1991). Anthropogenic Hg emissions, mainly due to coal combustion and artisanal and small-scale gold mining, have exceeded natural emissions since the onset of the industrial revolution (Sun et al., 2014; UNEP, 2013). Those emissions increased the marine Hg inventory (Lamborg et al., 2014), amplified MeHg production and bioaccumulation, and increased human exposure. Therefore, the production of methylated species by biotic and abiotic mechanisms is of interest, along with inorganic Hg sources.

Fluid and gas emissions from subaerial, deep-sea and marine shallow-water hydrothermal systems (MSWHS) are enriched in Hg, but conclusions regarding the importance of MSWHS as part of the global Hg cycle remain uncertain. Studies regarding Hg concentrations in MSWHS are limited and data only exists for the sites in Bahia Concepcion and Panarea Island. (e.g., Bagnato et al., 2017; Leal-Acosta et al., 2010). Nevertheless, some view hydrothermal venting to be the single most important primary natural Hg source to the global Hg cycle (Sonke et al., 2013). Regardless, current global Hg cycling models have either excluded or discounted MSWHS due to limited data or by extrapolating reactions observed for deep-sea systems. These models report atmospheric flux as the primary transport mechanism to the ocean (Lamborg et al., 2002; Mason and Sheu, 2002).

MSWHS are defined as occurring at seawater depths less than ~200 m and are chiefly associated with island arc volcanoes, intraplate volcanoes, and mid-ocean ridges (Price and Giovannelli, 2017). Most sites of hydrothermal activity are characterized by the emissions of gases and fluids with elevated heavy metal concentrations, high temperatures, and low pH (e.g., McCarthy et al., 2005; Pichler et al., 2019; Pichler et al., 1999b; Price and Giovannelli, 2017; Valsami-Jones et al., 2005). Hydrothermal fluids often have elevated concentrations of THg as a result of water-rock interactions and magmatic degassing (e.g., Taran et al., 1995). While Hg is known to travel in the vapor phase, mixing with other fluids such as brines and seawater, combined with a decrease in pressure and temperature, leads to the

formation of $Hg^{2+}$ and thus Hg removal from the vapor phase (Christenson and Mroczek, 2003). Therefore, Hg is emitted as both a liquid and a gas in shallow water systems.

Here, we present the first estimate of Hg flux and Hg concentrations in gases and fluids for the marine shallow-water hydrothermal system in Paleochori Bay, Milos, Greece.

## 3.2.2 Materials and Methods

### 3.2.1 Geological Setting

Paleochori Bay is located in the southeast of Milos, which is part of the Southern Aegean Volcanic Arc (Fig. 3.1). The island consists primarily of rhyolitic to andesitic volcanic rock atop a greenschist metamorphic basement (Papachristou et al., 2014). The bay contains numerous hydrothermal fluid and gas discharge areas and is one of the world's largest marine shallow-water hydrothermal systems (MSWHS). Two geothermal reservoirs were identified beneath the island: a high enthalpy system of up to 350 °C in the metamorphic basement and an overlying low enthalpy system of up to 175 °C within rhyolitic lavas close to the surface (Naden et al., 2005; Papachristou et al., 2014).

## 3. Mercury in the Hydrothermal Fluids and Gases in Paleochori Bay, Milos, Greece
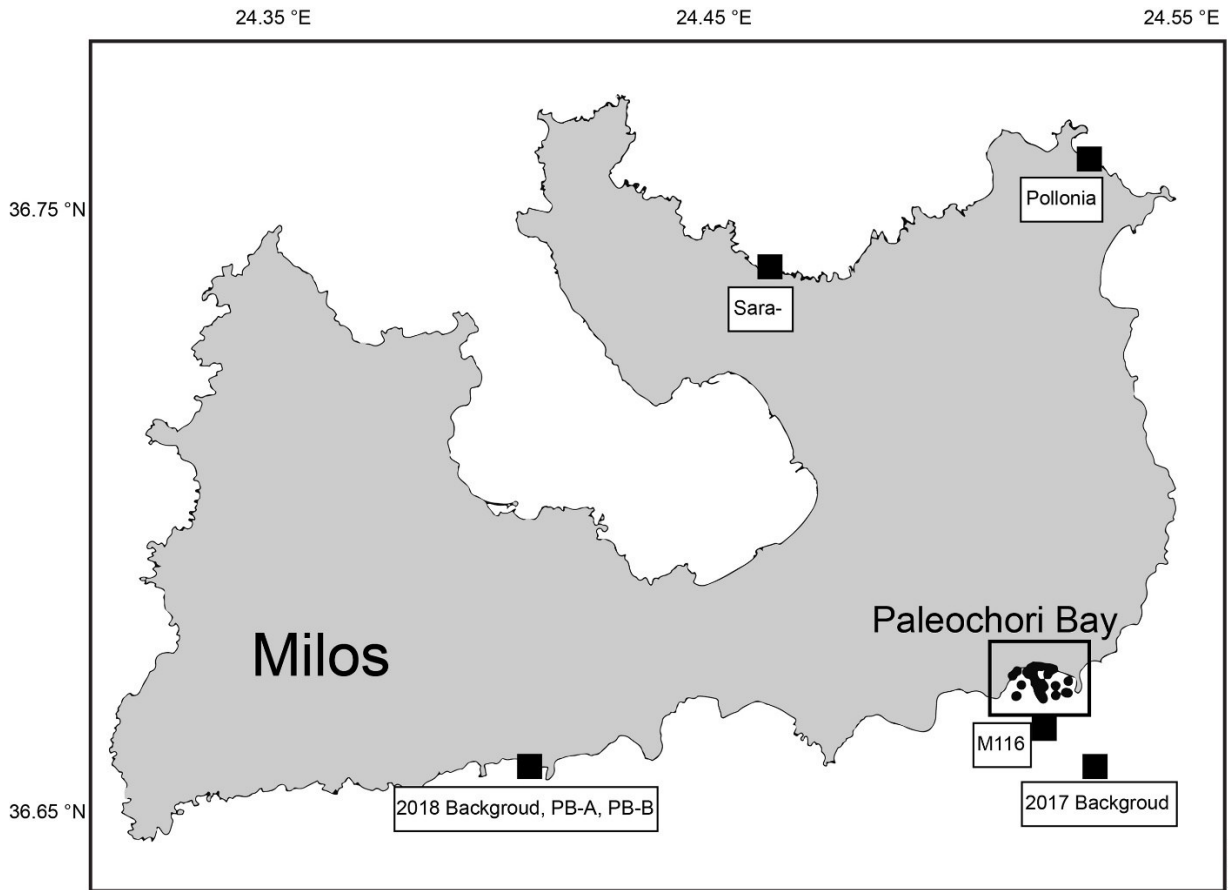


Figure 3.1: Map of Paleochori Bay and locations around Milos Island, where Hg samples were collected. The map was generated by Ocean Data View

Hydrothermal fluids in Paleochori Bay are enriched in various heavy metals and gases are primarily composed of $CO_2$, $CH_4$, $H_2S$, and $H_2$ (Botz et al., 1996; Dando et al., 1995; Fitzsimons et al., 1997; Price et al., 2013a; Stüben and Glasby, 1999; Valsami-Jones et al., 2005). Previously, hydrothermal fluids were grouped into low- and high-Cl types resulting from phase separation in the subsurface, additionally characterized by high temperatures in porewaters, low Mg, and $SO_4$ concentrations in comparison to seawater (Papachristou et al., 2014; Price et al., 2013a; Valsami-Jones et al., 2005). In both cases, the emitted fluid was considered a mixture of seawater, water-rock interaction modified seawater, and magmatic water (Dotsika et al., 2009; Pflumio et al., 1991; Price et al., 2013a; Valsami-Jones et al., 2005). Hydrothermal activity is present throughout the bay; however, its frequency is most significant in the west (Khimasia et al., 2021). The volume of emitted gas and fluid in the bay was variable both temporally and spatially (Aliani et al., 1998; Botz et al., 1996; Dando et al., 1995; Miquel et al., 1998; Naden et al., 2005). Previous studies

25

have linked low and high chloride fluids to phase separation and subsurface boiling (Price et al., 2013a; Valsami-Jones et al., 2005). However, recent findings suggested that subsurface transport could also be responsible for differing chemical compositions (Khimasia et al., 2021). Fluids were hypothesized to follow two different pathways, where greater permeability resulted in more substantial arc magmatic fluid influence and a secondary shallower pathway with meteoric water contributions.

In areas where hydrothermal discharge is present, the sediments are characterized by the occurrence of yellow-orange, white, or brown mats, hosting chemolithotrophic sulfur-oxidizing and sulfate-reducing bacteria (e.g., Yücel et al., 2013) (Fig. 3.2). The sediments may also appear red to yellow due to the precipitation of hydrous ferric oxides and arsenic sulfides from the hydrothermal fluids (e.g., Godelitsas et al., 2015) (Fig. 3.2). Voudouris et al. (2021) reported the presence of cinnabar (HgS) and arsenian pyrite (FeS2) in areas with increased gas venting. Mineral precipitation and microbial growth generally are controlled by steep redox gradients at the sediment-water interface and fueled by rising hydrothermal fluid (Price et al., 2013a; Price et al., 2013b; Sievert et al., 1999; Wenzhofer et al., 2000; Yucel et al., 2013).
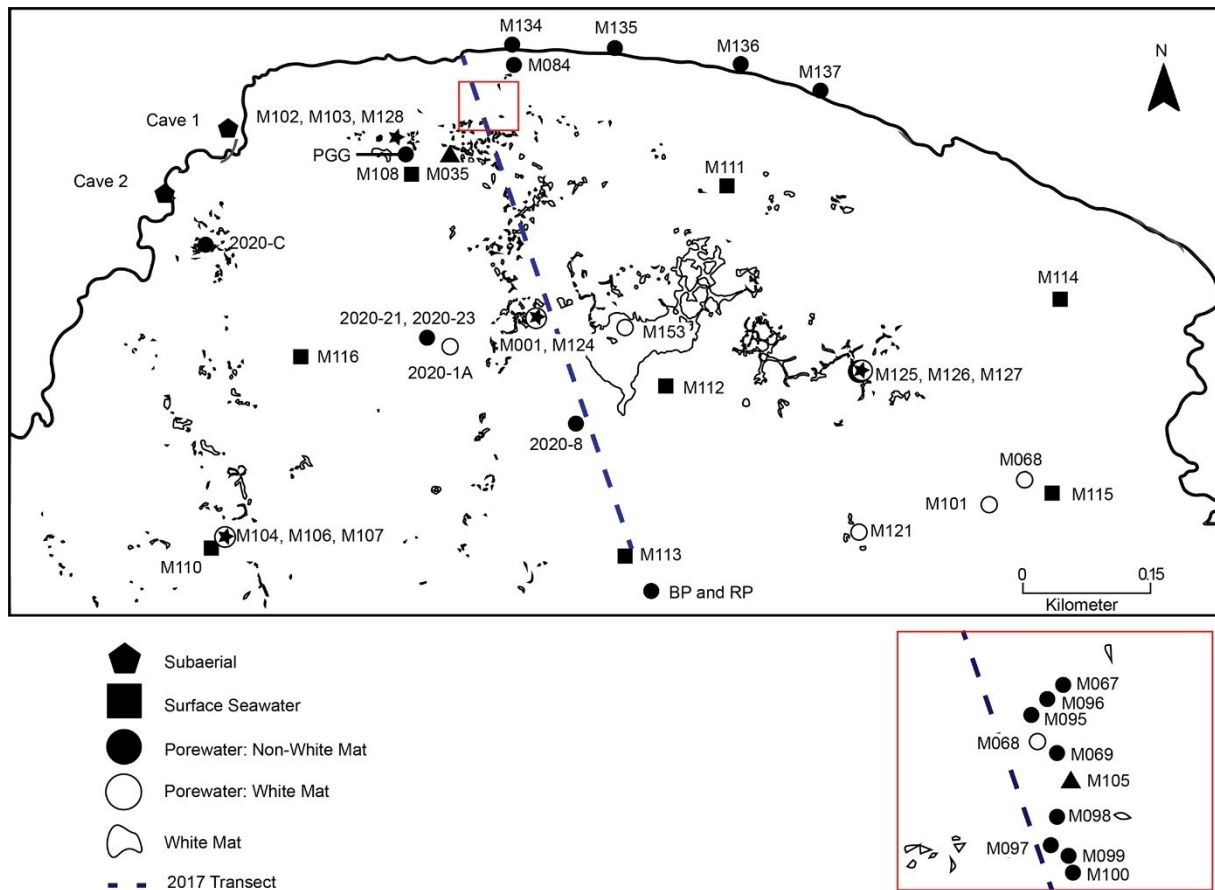
Figure 3.2: Map of sampling points in Paleochori Bay. The red box was an area of numerous porewater samples with numerous areas of white mats and precipitates. The map was adapted from Khimasia et al. (2021). The dashed line depicts the surface and bottom water transect sampled in 2017.

## 3.2.2 Methods

### 3.2.2.1 Field Sampling

Fieldwork was conducted in June 2017, October 2018 and June 2020. The absence of wind or prevailing northerly winds prevented circulation patterns and wave action within Paleochori Bay during fieldwork, as discussed by Khimasia et al. (2021). Scuba divers did not observe any current while sampling. A total of 95 samples were collected across the bay and around the island for Hg (filtered and unfiltered, i.e., $Hg_{diss}$ and THg), with select samples also analyzed for As, cations, and anions (Table 3.1, Appendix A). Most samples were a part of a larger dataset to estimate diffusive hydrothermal flux within Paleochori, including additional isotopic ($\delta 2H$, $\delta 18D$) measurements (Khimasia et al., 2021). Eight samples representative of different environmental conditions such as sedimented, un-sedimented, seagrasses, white

mats were selected for Hg speciation. Six of the eight samples included THg analysis of emitted gases. Point sources from Paleochori Bay were selected based on gaseous exhalations or fluid chemistry (Table 3.1, Fig. 3.3).  Background seawater samples were collected in areas with no visible hydrothermal activity from outside of Paleochori Bay. In 2017, surface and bottom waters were collected simultaneously to determine dissolved Hg along a transect perpendicular to the beach progressing from shallow (approx. 1 m) into deeper water (approx. 15 m). Samples were collected at the surface and the bottom of the water column simultaneously, with surface divers collecting GPS data. In 2020 sediment and porewater samples were collected simultaneously at three locations representing non-hydrothermal (background) and hydrothermal areas (2020-1A, 2020-C and 2020-8).
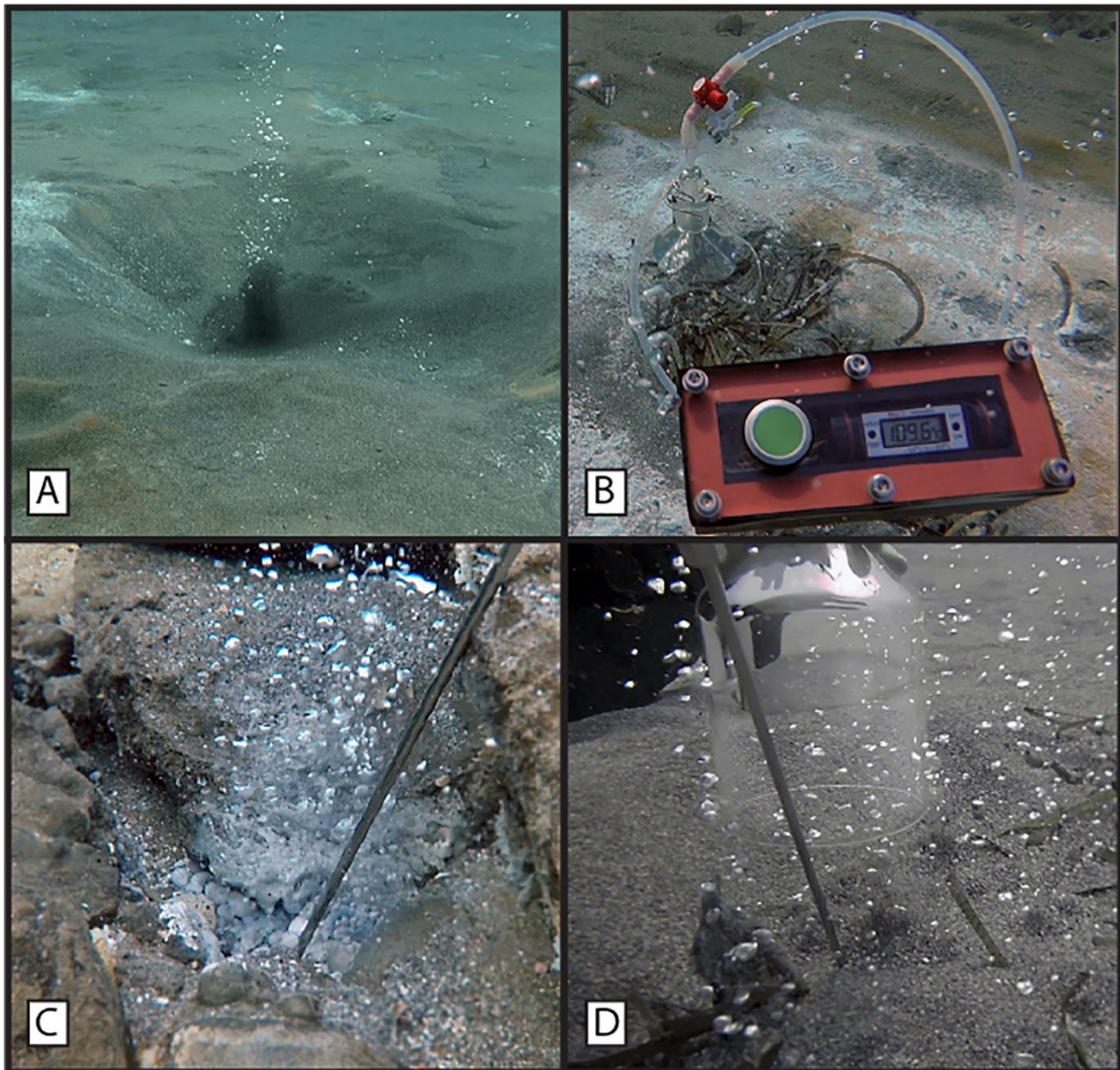
Figure 3.3: Examples of features of the submarine hydrothermal system within Paleochori Bay. A) Highly sedimented site (M102). Significant gas exhalations throw sediment into the water column and only coarser grains remained. B) Highly sedimented with white mat and precipitate accumulations on the sediment surface with porewater temperature probe and gas collection funnel. C) Site without sediment cover (M103) with significant gas exhalations. No sediment remained at the point of emission. D) Low to moderate sedimentation (M125) of only a few cm. Multiple smaller but continuous gas exhalations were collected by the gas funnel when the image was taken.

Fluids were collected using samplers constructed from PTFE tubing and 10 mL pipette tips at 10 cm depth using polypropylene 60 mL syringes. Porewater temperatures were monitored at the depth of the pipette tip. No large deviations in temperature were permitted as sampling was performed to ensure that samples were not contaminated with seawater.

### 3. Mercury in the Hydrothermal Fluids and Gases in Paleochori Bay, Milos, Greece

The pH (Halo Wireless pH meter, Hanna Instruments), conductivity and ORP (Myron Ultrameter) were immediately determined in the field. The samples were filtered through a 0.45 μm membrane, and the sub-samples for trace elements and major cations were preserved with 2 % (m/v) concentrated nitric acid.

# 3. Mercury in the Hydrothermal Fluids and Gases in Paleochori Bay, Milos, Greece

Table 3.1: Average values for chemical composition and temperature for seawater and porewater by sample grouping

| Sample | | T °C | pH | Cl mM | Br mM | SO$_4$ mM | As µM | Ca mM | Fe mM | K mM | Li mM | Mg mM | Mn mM | Na mM | Si mM | Sr mM | H2S µM | THg pM | Hg$_{diss}$ pM |
|---|---|---|---|---|---|---|---|---|---|---|---|---|---|---|---|---|---|---|---|
| Seawater | | | | | | | | | | | | | | | | | | | |
| | Outside P.B. | | | | | | | 29 | | 56 | 3 | 31 | | 553 | 2 | 0.2 | | 3 | |
| | Inside P.B. | 20 | 8.1 | 637 | 0.9 | 33 | 0.0 | 11 | 0.0 | 11 | 0.4 | 54 | 0.0 | 520 | 0.0 | 0.1 | | 5 | 6 |
| Porewater | | | | | | | | | | | | | | | | | | | |
| | Subaerial | 91 | 3.4 | 754 | 1.1 | 23 | | 16 | 0.8 | 24 | 2 | 20 | | 277 | 4 | 0.2 | | 2534 | 0.4 |
| | Sand and Precip. | 59 | 6.1 | 781 | 1.0 | 25 | 9 | 25 | 0.1 | 45 | 2 | 41 | 0.1 | 634 | 1.1 | 0.2 | 166 | 313 | 6 |
| | White Mats | 75 | 5.5 | 744 | 1.0 | 22 | 4 | 26 | 0.1 | 45 | 2 | 37 | 0.1 | 598 | 2 | 0.2 | 301 | 219 | 10 |
| | Point Sources | 114 | 6.5 | 605 | 0.9 | 31 | 0.2 | 11 | 0.0 | 11 | BDL | 52 | 0.0 | 506 | 0.2 | 0.1 | 4 | 1131 | 146 |
| | Large Volume | 97 | 5.7 | 889 | 1.1 | 20 | 35 | 30 | 0.1 | 61 | 2 | 35 | 0.1 | 688 | 2 | 0.3 | 1.0 | 37 | 2 |
| | Brines | 101 | 3.9 | 699 | 0.9 | 6 | | 54 | 0.3 | 110 | 7 | 16 | BDL | 739 | 3 | 0.4 | | 19 | 4 |

### 3.2.2.2 Mercury Analyses

Total Hg samples were collected unfiltered and filtered (0.45 µm) and analyzed following the USEPA (2002) protocol with a Brooks Rand CV-AFS analyzer in duplicate. In preparation for the analysis, 40 mL of the sample were added to a 60 mL Volatile Organic Analysis (VOA) glass vial with a PTFE-lined cap. Then 400 µL acidified bromide/bromate, a 1:1 mixture of 0.01 M bromide/bromate solution (Tritrisol, Merck) and 32 % hydrochloric acid (Optima grade, Fisher Scientific) were added to the sample, and the light-yellow colored solution was left standing for at least 30 min at room temperature. The bromine chloride reactivity was then quenched by the addition of 100 µL 30 % (m/v) hydroxylamine hydrochloride solution (ReagentPlus, 99 %, Sigma-Aldrich) and shaken. Elemental Hg was produced in the solution by adding 200 µL of a 20 % (m/v) tin(II)chloride solution (Reagent grade, Alfa Aesar). The detection limit for this method was determined to be 0.04 ng/L (n = 10) for our laboratory. The certified reference material ORMS-5 (elevated Hg in river water, National Research Council Canada) was used for quality control. The reference material was certified for a concentration of 26.2 ± 1.3 ng/L T-Hg and measured within 5% of certified values.

The sediment samples were digested in 10:1 aqua regia following Bloom et al. (2003) and THg was analyzed by CV-AFS. The certified reference material PACS-1, certified for a concentration of 4.57 ± 0.16 µg/g THg was used for quality control.

Volatile Hg was collected by purging 1 L of hydrothermal fluid with Hg free nitrogen onto gold and carbo traps and analyzed by CV-AFS (Cossa et al., 2011; Lehnherr et al., 2011).

Analysis of MeHg was carried out by species-specific isotope dilution gas chromatography. A 100 mL sample was spiked with a Me201Hg solution (ISC Science, Spain) and left equilibrating for an hour. An optimal ratio of 4.25 for Me201Hg in the spike to Me202Hg in the sample was the spiking aim. Based on the assumption of 5 % of T-Hg being present as Me201Hg, the amount of the enriched isotopic solution was calculated for the initial spiking. An acetate buffer, prepared from trace metal grade acetic acid (Fisher Scientific) and 30 M NaOH (Suprapur, Merck), was added to the sample. The pH was adjusted to 3.9 with sodium hydroxide solution (30 M, Suprapur, Merck). Subsequently, 1 mL propylation reagent (1 g sodium tetra-propyl borate (Merseburger Spezialchemikalien, Germany) in 100 mL

oxygen-free Milli-Q water) was added to the sample followed by 200 µL n-Hexane (Reagent Grade ACS, Riedel-de-Haen). The Hg species were extracted into the n-hexane phase by shaking for 10 min, and the n-hexane phase was taken out for analysis by gas chromatography coupled to ICP-MS (Element 2, Thermo Scientific) with an in-house-built heated transfer line (temperature of 160 °C).  A cyclonic spray chamber was attached at the transfer line just before the ICP torch for wet plasma conditions giving the option of plasma tuning and monitoring with an internal Thallium standard.

Gas samples were collected into Tedlar© bags using a custom-built glass funnel connected to Teflon tubing in combination with a standard lift bag. The lift bag was attached to lead weights, which enabled the calculation of gas volume collected, i.e., the volume of gas needed to displace enough seawater to lift the bag at a given depth and lead weight. To remove sulfur species from the gas, the samples were passed through an alkaline solution. The sample was then trapped in a 0.5 M permanganate solution in 2 N sulfuric acid and analyzed on the CV-AFS as THg (Brombach and Pichler, 2019). Exact rates of emission were not calculated; however, relative rates were established based on gas sample retrieval time. For simplicity, low emission samples required more than 30 minutes of dive time, and high emission samples needed less than 30 minutes. Each gas sample site was named (Fig. 3.3) and chosen based on visible physical characteristics (see Table 3.2, Fig. 3.3).

Table 3.2: Named gas emission sites with descriptors.

| Site | Emission Rate | Sediment Coverage | Descriptor |
|------|---------------|-------------------|------------|
| Red | Low | High | White mats and red metal precipitates surrounding |
| Seagrass | Low | High | White mats and seagrass growth surrounding |
| Crater | High | High | Sand covered by black precipitates |
| Eastern | Low | Medium | No white mats or metal precipitates, easternmost gas sample taken |
| Screamer | High | Low | No sediment coverage, cave-like structure above gas emission point |
| Boulder | High | Low | No sediment coverage, gas emitted from between two boulders |

## 3. Mercury in the Hydrothermal Fluids and Gases in Paleochori Bay, Milos, Greece

### 3.2.2.3 Other measurements

Anions were analyzed in a non-acidified, filtered sample (0.45 µm) using a Metrohm 883 Basic IC instrument with a 5 µL injection loop and a Metrosep A Supp5 (150 × 4.0 mm; 5 µm) column. Quality control samples were an internal standard and IAPSO, an artificial seawater. Major cations and some trace elements were measured by inductively coupled plasma-optical emission spectrometry (ICP-OES) using a Perkin Elmer Optima 7300 DV instrument. The detection limit for most elements was around 1 to 10 µg/L, which was not sensitive enough for trace elements but sufficient for the major elements present in the sample. All water samples were diluted by a factor of 100 due to the high salinity of the samples. Quality control was assured with different certified waters: EnviroMAT Groundwater Low (ES-L-2) and High (ES-H-2), both from SCP Science, Canada, are groundwater samples while CRM-SW (High Purity Standards, USA) was a certified seawater.

Trace elements were analyzed with inductively coupled plasma mass spectrometry (ICP-MS, Element 2 Thermo Scientific). The mass analyzer of the Element 2 instrument is based on a magnetic and electric sector field. Mass interference based on polyatomic and isobaric interference can be overcome by adjusting the mass resolution from low to high, which is essential for some trace elements, e.g., arsenic. The same principle for sample dilution for saline samples as was described for ICP-OES. Plasma fluctuations were monitored via the addition of internal standards to each sample.

### 3.2.2.4 Flux Calculations

The flux (pmol/m2/hour) of $Hg^0$ to the atmosphere from each of the sampling sites was calculated using equations by Liss and Slater (1974) (1) and Wanninkhof (1992) (2), as implemented by Wängberg et al. (2001). Where kw (cm/hour) is the gas transfer velocity, u10 is the wind speed at 10 m height, ScHg is the Schmidt number for Hg in seawater and ScCO2 is the Schmidt number for CO2 in seawater (Kuss et al., 2009), and H' is Henry's law constant. An approximate value was used for atmospheric Hg (7.5 pmol/m3), and the percent volatile $Hg^0$ was assumed to be 10 % of Hgdiss (Horvat et al., 2003). Schmidt numbers 689 for Hg and 660 for CO2 were used.

$$Flux\ to\ the\ Atmosphere = k_w\ (DGM - {}^{TGM}/_H) \qquad (1)$$

$$k_w = 0.31\ u_{10}^2\ ({}^{Sc_{Hg}}/_{Sc_{CO2}})^{-0.5} \qquad (2)$$

Samples were plotted against Na/K ratios, which have been used to indicate rapidly rising fluids (Henley, 1995) and, more recently, on Milos in conjunction with isotopic analysis (Khimasia et al., 2021).

## 3.3 Results

Conservative element data (Na, Cl, K, etc.) from porewaters and seawater samples were comparable to previously established mixing lines of hydrothermal fluid and seawater (Price et al., 2013a; Valsami-Jones et al., 2005). Samples taken at background sites in and outside Paleochori Bay were significantly lower in THg concentration than those influenced by hydrothermal activity (Table 3.1, Appendix A). All samples with a pH less than 4, temperatures above 65 °C, and Hg enrichment (THg and Hgdiss) were collected in Paleochori Bay.

Within Paleochori Bay porewaters, concentrations of Hg were highly variable between sampling sites. However, marked increases in the concentration were observed in hydrothermally influenced areas indicated by temperature, low Mg and high Cl concentrations. The high-Cl fluids of Paleochori Bay were found to contain low (< 15) Na/K ratios with a median value of 6.71 with isotopic values of δ2H and δ18O consistent with rapidly rising fluid (Khimasia et al., 2021).

### 3.3.1 Water Samples

### *3.3.1.2 Seawater*

Background seawater and samples taken outside of Paleochori Bay were comparable to previous studies concerning cations, anions, and Hg (Cossa et al., 1997; Horvat et al., 2003; Khimasia et al., 2021; Valsami-Jones et al., 2005). Within surface waters of Paleochori Bay, THg concentrations were higher than samples from outside of Paleochori Bay and background samples (Table 3.1, Appendix A). The concentration of all other elements (Cl, Br, SO4, Ca, Fe, K, Li, Mg, Mn, Na, Si, Sr) measured showed little variation (0.29 % to 6.5 % RSD) between samples. It reflected control group concentrations apart from As, which was highly variable (77 %).

Hg concentrations were highest near the shoreline for transect samples, where the known hydrothermal activity occurred directly beneath the sand surface (Fig. 3.4). Concentrations quickly returned to low pM values in surface and bottom waters but increased again when white mat accumulations were encountered (e.g., at approximately 0.3 km distance from shore, Fig. 3.4). Surface and bottom water samples were enriched by 314 to 18759 % over background Hgdiss.
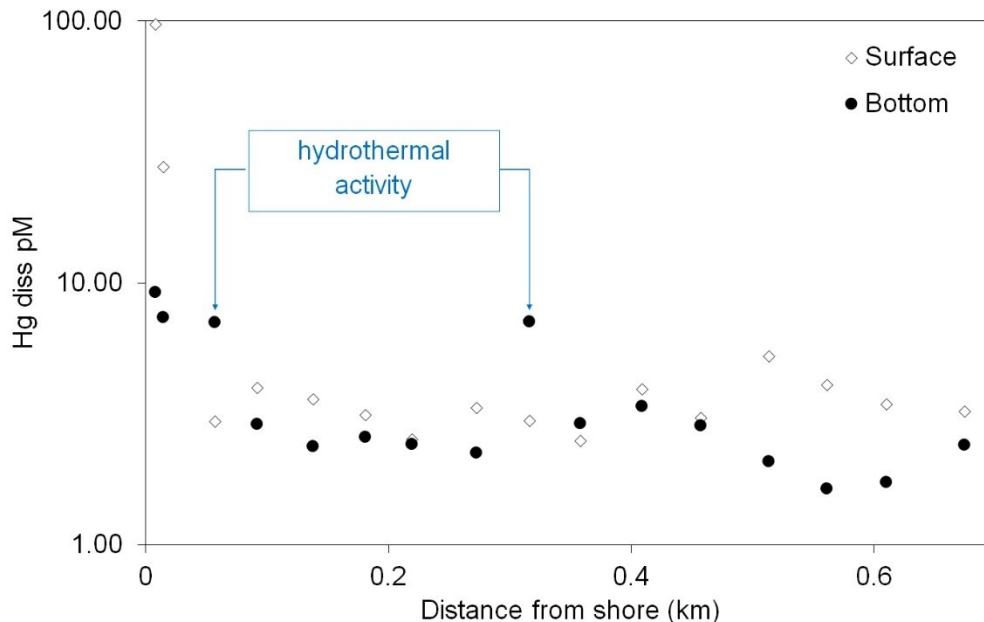


Figure 3.4: Transect of total Hg in filtered samples for the transect of surface and bottom samples in Paleochori Bay done in 2017. Surface samples were generally higher, except immediately adjacent to the shore and where hydrothermal activity was observed (i.e., white mats). The exact location of the transect is given in Fig. 3.2.

### 3.3.1.3 Paleochori Bay Vents, Porewater and Sediment

Porewaters included high- and low-Cl fluids with strong relationships between known hydrothermal indicators of active areas (Khimasia et al., 2021). Porewaters from within Paleochori Bay contained low (17 pM) to high (2894 pM) THg concentrations with a maximum of 69 % Hgdiss (Appendix A). Methylated and volatile species were all below detection limits. Hydrogen sulfide concentrations ranged from below the detection limit to 1.2 mM. Background porewater within Paleochori Bay contained 98 pM THg and 4 pM Hgdiss.

Water samples collected from the point sources (vents) shown in Figure 3.3 showed significant chemical composition variations except for THg, Hgdiss, and Hggas

## 3. Mercury in the Hydrothermal Fluids and Gases in Paleochori Bay, Milos, Greece

(Appendix A). The Boulder and Screamer sites were collected at the point of emission at the sediment-water interface due to the rocky hard bottom at those sites and thus, seawater contamination was unavoidable.

In 2017 an additional sample was taken from a point source, which discharged at sea level in a small cave. That sample (Cave-1) had higher than seawater Cl and Na but lower SO4 concentrations. The Cave-1 sample contained the highest measured concentration of THg for all samples (5066 pM), as well as the lowest pH (1.87).

The highest THg concentrations were associated with low Na/K ratios (Fig. 3.5). High Na/K ratios (> 15) were related to low-Cl fluid and low Si concentrations. The percentage of Hgdiss was more significant in high Na/K ratio samples.
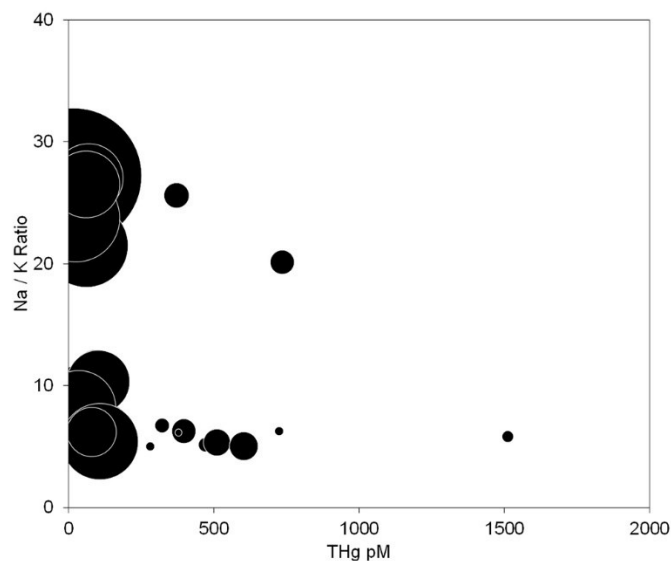


Figure 3.5: Total Hg (THg) concentration in porewaters vs Na/K ratios. The area of the circle corresponds to the percent dissolved Hg in the sample. Lower (< 15) Na/K ratios were associated with rapidly rising fluid along fault lines.

Data for THg of the three sediments samples and their corresponding porewater concentrations are presented in Table 3.3. Compared to the two hydrothermal samples, the "non-hydrothermal" sediment sample had higher THg in the porewater and lower concentration in the corresponding sediment, 97.9 pM and 414 pM/g. The background porewater sample's chemical composition was similar to seawater, and the area of sampling showed no physical indicators of hydrothermal activity.

37

Table 3.3: Sediment and porewater concentrations collected in 2020

| Sample | Temperature °C | pH | THg pM | Hg$_{diss}$ pM | Sediment THg pmol / g |
|--------|------|------|------|------|------|
| **2020-8** | 22 | 7.72 | 97.9 | 3.7 | 414 |
| **2020-C** | 86 | 1.87 | 23.7 | 5.0 | 1213 |
| **2020-1A** | 52.7 | 5.35 | 78.2 | 5.2 | 917 |

### *3.3.1.4 White Patch Flux Calculations*

White patch fluid flux calculations of Hg were completed using minimum and maximum concentrations of both total and dissolved Hg (347 to 777 µM/day THg, 51 to 210 µM/day Hgdiss) and flux estimates as described in Khimasia et al. (2021).

### 3.3.2 Gases

Gas concentrations of Hg were highly variable (0.7 to 2792 nmol/m3), and no statistical or otherwise significant relationship could be observed between Hg in gas and porewater. Elevated Hg in the gas phase did not necessarily indicate high or low Hg concentrations within the fluid phase and vice versa. However, the highest Hg concentrations in the liquid phase were observed at locations with intense gas emission, although intense gas emissions did not indicate high Hg concentrations within the gas phase (e.g., Crater site). However, it seemed that the absence of a sediment cover at the sampling site was responsible for higher Hggas concentrations (Fig. 3.6).
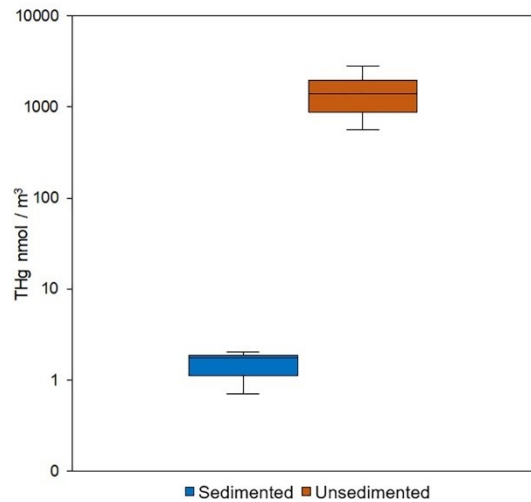
Figure 3.6: Concentration of total mercury (THg) in the gas phase. Sedimented sites are in blue and sites without a sediment cover are in orange.

Dando et al. (1995) estimated the release of 0.21 to 1.05 x 1011 moles per year of total gas. Based on this estimation, the contribution of Hg from the MSWHS to Paleochori Bay was calculated to be 3.3 x 10-4 to 6.6 mol Hg per year.

## 3.4 Discussion

### 3.4.1 Hg concentrations within the water column

Our data showed elevated total and dissolved Hg concentrations in Paleochori Bay compared to seawater unaffected by hydrothermal activity. Background concentrations of Hg for the Mediterranean are known to be in the low pM range. For example, Cossa et al. (1997) and Horvat et al. (2003) showed concentrations of THg ranging from 0.5 to 4 pM in the Western Mediterranean. The ratio of dissolved Hg to THg is elevated in open ocean Mediterranean waters (from 32 to 95 %) due to the low abundance of particulate matter (Horvat et al., 1999). Surface waters collected from Milos outside of Paleochori Bay were lower than average Mediterranean values.

In contrast, surface water THg samples from Paleochori were enriched by over 3000 % (15.4 pM) than this study's assumed background concentration (0.5 pM). The highest concentrations of THg in surface water were located above areas of known shallow-water hydrothermal activity in the western portion of Paleochori Bay (Fig. 3.2, Appendix A). The transect, where bottom and surface waters were sampled simultaneously (Fig. 3.4), showed that surface water was generally elevated above

bottom water, except at two locations where hydrothermal activity was present (Fig. 3.4). At a distance of approximately 60 and 300 m, elevated Hg concentrations were observed in bottom waters associated with a white mat. The high concentrations at the beginning of the transect are not considered representative because of substantial mixing within the surf zone and due to a shallow water depth of less than 1 m. Warm hydrothermal fluids are buoyant relative to seawater. Therefore, they are known to rise and transport trace metals to the sea surface, resulting in higher surface water concentrations than in the bottom water (Pichler et al., 2019; Pichler et al., 1999b). This overall strongly suggests hydrothermal emissions are a source of Hg to Paleochori Bay. The extent of this cycling may be restricted to local rather than regional areas. Therefore, the speciation of Hg from the pore fluids holds vital information on the fate of the Hg discharged.

**3.4.2 Hg Concentrations in Porewaters and Sediments**

The transformation of inorganic mercury to methylated species was negligible. Sub-optimal methylation conditions in the shallow subsurface (e.g.,> 75 °C, up to 1200 µM $H_2S$, < 18 pM Hgdiss) likely prevented appreciable MMHg and DMHg accumulation (Bayraktarov et al., 2013; King et al., 2000). Methylation rates under optimal conditions generate approximately 1 to 2 % MMHg of THg (King et al., 2000). Therefore, concentrations of up to 12 pM would be expected for Paleochori Bay porewater, well within the detection limit of the method. However, MMHg was not detected in any sample.

Relationships between Hg (THg and Hgdiss) and typical hydrothermal indicators (e.g., Cl, temperature, $SO_4$, etc.) were observed in areas without white mats. However, areas with white mats did not share these relationships. In particular, a significant positive trend (nonlinear) between THg and temperature was observed in areas without white mats (see Fig. 3.7A). Even by removing a single high THg sample (Crater site), the trend was maintained for the data, with an inflection point around 75 °C, where the slope increased significantly. Frequently used as an indicator of hydrothermal influences, a positive trend with THg concentrations is intuitive. However, this relationship was not present in the white mat areas, suggesting some removal mechanism or lack of an enriched Hg source, particularly at higher temperatures.
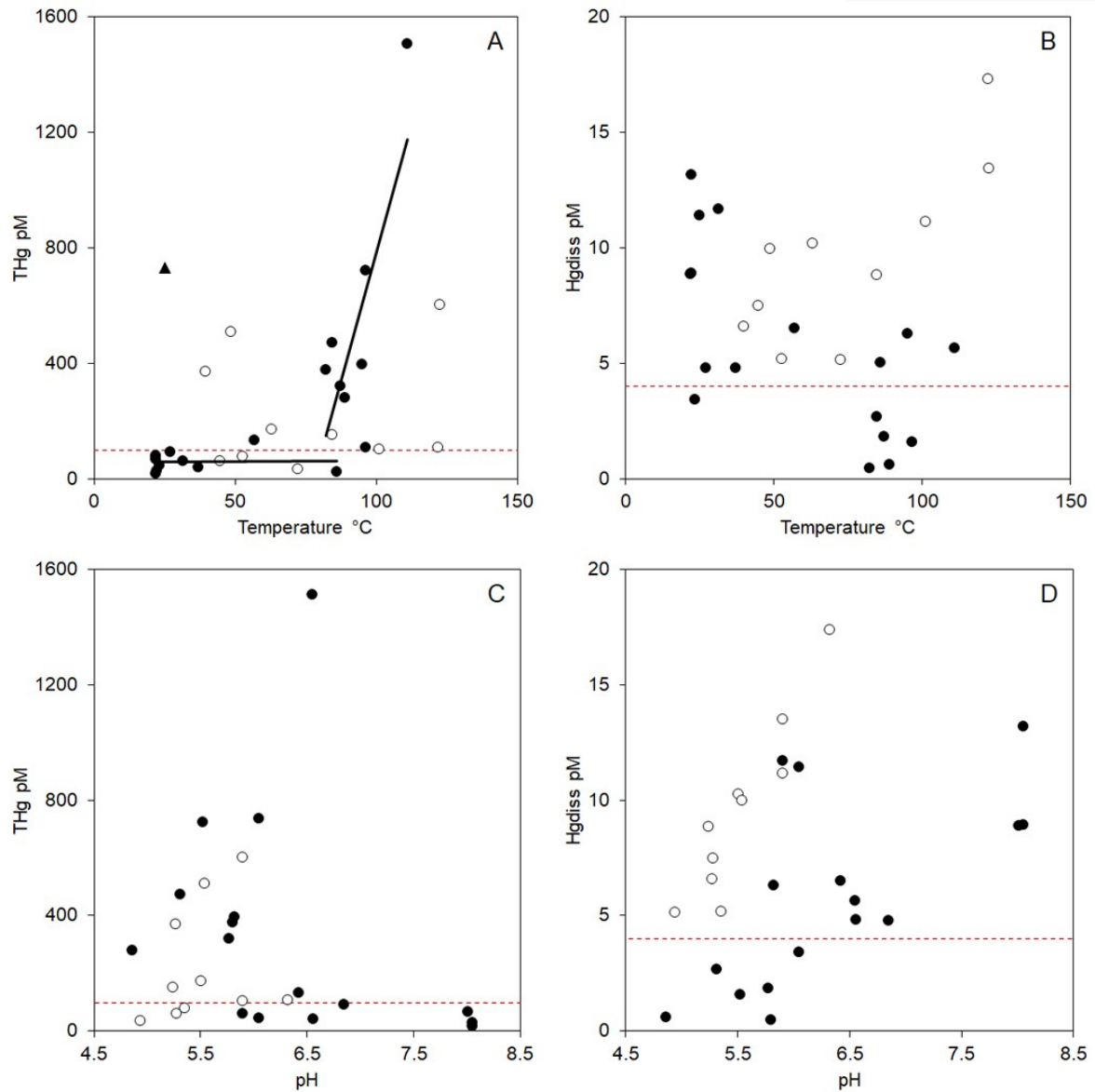
Figure 3.7: Scatterplots of THg and Hgdiss vs temperature (A and B) and pH (C and D). Samples from areas of white mat accumulations in white circles, non-white mat samples in black. Horizontal red lines represent background porewater concentration in THg and Hgdiss respectively. Black lines in (A) represent linear fit slopes of THg in non-white mat areas above and below 75 °C. The black triangle represents a sample with possible contamination or entrainment of a Hg rich precipitate.

Porewaters enriched with Hg were also enriched with arsenic, a metalloid extensively linked to hydrothermal activity (e.g., Pichler et al., 1999c; Price et al., 2013a). A significant positive correlation was observed between THg and As concentrations in areas without white mats. Mercury and As both belong to the so-called "epithermal suite" of elements (Au, Ag, Te, Se, Hg, As, Sb, and Tl) (Berger and Eimon, 1983; Saunders and Brueseke, 2012; Saunders et al., 2008). Two main chemical properties

of the "epithermal suite" of elements appear to control their similar behavior and common occurrence: (1) they are all "soft" Lewis acids, meaning they form covalent bonds with "soft" Lewis bases such as H2S, S2-, etc., and (2) they all have similar volatility, explaining why they are liberated together from the mantle. Enrichments of "epithermal elements" in vent fluids were identified in several MSWHS (Gamo and Glasby, 2003; Johnson and Cronan, 2001; McCarthy et al., 2005; Prol-Ledesma et al., 2004), making them excellent targets for Hg analysis. This was also confirmed for Paleochori Bay by Voudouris et al. (2021), who reported the presence of cinnabar within arsenian pyrite layers in areas with hydrothermal activity.

As a class b soft metal, Hg will more likely travel with sulfide ligands within shallow, low enthalpy systems, with vapor transport more likely within deeper, high enthalpy systems (Barnes and Seward, 1997; Barnes, 2015). Soft metal complexes are less sensitive to temperature changes, with deposition more likely with oxidation, dilution and pH. Chemical pathways of Hg within the subsurface of New Zealand hydrothermal environments were described in detail by Christenson and Mroczek (2003). As liquids and gases traveled through the upflow zone, precipitation of Hg as cinnabar, or coprecipitation with pyrite, occurred from liquids and directly from gases. As a result of changes in pH, Eh and temperature gas condensation happened and resulted in precipitation of said minerals causing the complete removal of THg from the gas phase. In gas-brine interactions, Hg behavior was strongly linked to heating and cooling regimes within the subsurface. Upon mixing with overlying oxygenated water, Hggas was oxidized by sulfur or oxygen to form Hg-S species or Hg-Cl species. This oxidation step removed volatile Hg species and flux to the atmosphere was limited.

The primary difference between white mat and non-white mat sample areas, in terms of sulfur concentration, is the balance of oxygen penetration into the shallow subsurface and hydrogen sulfide production, paired with large fluxes of an H2S-rich hydrothermal fluid. In previous studies, areas of high temperatures without white mats promoted increasing oxygenation of the subsurface and production of elemental sulfur from hydrogen sulfide, limiting S bioavailability  (Wenzhofer et al., 2000; Yucel et al., 2013). The sensitivity of Hg-S minerals to temperature changes follows known thermodynamic patterns established by Barnes et al. (1967). Areas with white mats provided enough flux of H2S to sustain microbial activity while minimizing

contamination with oxygenated seawater. Given those considerations, the effect of temperature on THg in non-white mat areas is more likely associated with hydrothermal fluid flow. This effect was seemingly masked in the shallow subsurface beneath white mat areas. There H2S did not oxidize to SO4 and thus could have resulted in HgS formation as discussed for aquatic environments by Hsu-Kim et al. (2013). This behavior has been similarly established for iron sulfide formations (Pichler et al., 1999a) and plays a substantial role in Paleochori Bay. The variations observed between samples of similar chemistry, geological location, or environmental conditions are indicative of a system precipitating Hg within the shallow subsurface and at the sediment-water interface.

Many porewater samples, although from hydrothermal areas, contained less THg than what is considered the background concentration of 98 pM (Fig. 3.7A), which would indicate that the source of the hydrothermal fluids could have been depleted in Hg (e.g., brine phase, meteoric water or seawater) and that any influence of potentially enriched sources (e.g., condensed vapor phase or gases) was limited. On the other hand, removing Hg in the shallow subsurface could have happened due to precipitation or scavenging. The majority of THg was bound to particles, as shown by the low Hgdiss concentrations in most porewater samples (Appendix A). Thus, hydrothermal solutions enriched in elements known to scavenge Hg, such as sulfur species, could therefore be depleted in THg compared to the background site. This has been observed in the water column in deep-sea plumes (e.g., Bowman et al., 2016), in the outflow from hot springs, where the oxidation of $Hg^0$ led to the precipitation of Hg-S minerals (Davey and van Moort, 1986) and in Paleochori Bay. Voudouris et al. (2021) reported grains of cinnabar up to 3 μm in size in arsenian pyrite layers. The pyrite precipitation was associated with high-Cl fluids. Indeed, the sediment sample from the hydrothermal site 2020-C had the highest THg, while its corresponding porewater had the lowest THg concentration relative to the other two sediments (Table 3.3).

The high THg concentrations observed in Paleochori Bay porewaters were related to low Na/K ratios, indicating a rapidly rising hydrothermal fluid along fault lines (Khimasia et al., 2021). Br/Cl ratios from all pore fluid samples from Paleochori Bay were comparable to those described by Valsami-Jones et al. (2005) and Price et al. (2013a) for this system. Based on Br/Cl ratios, subcritical phase separation was

suggested as an essential subsurface process. As discussed in (Khimasia et al., 2021; Wu et al., 2011), this ratio does not necessarily define samples as representative of vapor or brine phases. The THg and Hgdiss in samples collected from hydrothermally active areas were generally above background porewater concentrations regardless of high or low Cl values. However, samples with higher THg were generally high-Cl fluids. Additionally, those samples with low Na/K ratios contained the highest THg concentrations (see Fig. 3.5). Those samples corresponded to the ones described by Khimasia et al. (2021), which trended towards arc magmatic water. That was unsurprising given that various samples collected on land also indicated a magmatic fluid component in the Milos hydrothermal system (e.g., Dotsika et al., 2009).

One surprising aspect of porewater fluids sampled on Milos was the low ratio of Hgdiss to THg for most samples. If near-surface phase separation were happening, high concentrations of THg would be expected in low-Cl fluids. On the contrary, higher THg concentrations were observed in high-Cl samples, with high Hgdiss ratios in low-THg and low-Cl samples. A notable exception being the Eastern point source, where a relatively strong gas emission was also present, potentially influencing Hgdiss concentrations.

Papachristou et al. (2014) described the Milos system as containing two geothermal reservoirs, a deep high enthalpy system and a shallow (< 150 m below surface) lower enthalpy system with temperatures between 50 and 100 °C. The geothermal gradient is high in the island's central and eastern areas, with the low enthalpy system primarily associated with the central Vounalia area. Condensation of $Hg^0$ from hydrothermal vapors would fall within the temperature range of the low enthalpy system, where concentrations may be high (e.g., Davey and van Moort, 1986; Migdisov and Bychkov, 1998). The lack of $Hg^0$ within samples, coupled with high ratios of particle-bound Hg species, indicates that assuming low-Cl fluids result from a condensed vapor phase, Hg would be removed from solution before emission, potentially due to oxidation in the shallow subsurface. The high ratios of particulate bound Hg in high-Cl fluids with low Na/Cl, coupled with the isotopic data described in Khimasia et al. (2021), point towards a rapidly rising deep-seated hydrothermal fluid to be the primary source of Hg to Paleochori Bay.

### 3.4.3 Diffuse Flux Modeling

Diffusive flux modeling assumed THg and Hgdiss from 10 cm depth to be transported to the water column. However, as discussed above and as observed by Lamborg et al. (2006), removing Hg before emission is possible. Discharge through sediments can effectively remove Hg and other metals from hydrothermal fluids (e.g., Leal-Acosta et al., 2010; Pichler et al., 1999a; Pichler and Veizer, 2004; Price and Pichler, 2005). Besides, scavenging in hydrothermal plumes can be an important process for Hg speciation and sedimentation (Bowman et al., 2015). Nevertheless, the transect showed increases in Hgdiss in bottom water where white mats were noted (Fig. 3.4). This supports diffusive flux as a contributor to water column Hgdiss concentrations despite the potential for precipitation.

The minimum estimated daily flux from the white mat areas of 347 µM THg and 51 µM Hgdiss was far higher than the estimated daily flux of $Hg^0$ to the atmosphere of 0.76 µM. An average elemental Hg flux of 1.3 pmol/m2/hour to the atmosphere, with a maximum flux of 2.7 pmol/m2/hour, was calculated (Table 3.4). This flux is similar to estimates observed for some Panarea sites, e.g., 3.48 pmol/m2/hour at Bottaro North (Bagnato et al., 2017) and the open waters of the Mediterranean and polluted coastal areas (e.g., 3.99 to 25.9 pmol/m2/hour, respectively) (Andersson et al., 2007). It should be noted that estimates on flux values would vary significantly based upon deviations from the assumed 10 % $Hg^0$ speciation of Hgdiss. However, even if all Hgdiss would be present as a volatile species, this would result in only a 10-fold increase in flux. Without substantial increases in wind speed coupled with high volatile Hg concentrations, the flux of Hg to the atmosphere cannot balance the diffusive flux of Hg to the system. Some portion of Hg must, therefore, be removed before venting.

Table 3.4: Surface water concentrations and flux to the atmosphere

| Sample | Temperature °C | pH | GPS Lat | GPS Lon | THg Filtered pM | Flux pmol / m$^2$ / hr |
|--------|----------------|------|----------|----------|-----------------|------------------------|
| M108 | 20.1 | 7.87 | 36.67371 | 24.51567 | 4.2 | 2.7 |
| M109 | 20.1 | 8.11 | 36.67180 | 24.51420 | 1.4 | 0.9 |
| M110 | 20.1 | 8.19 | 36.66983 | 24.51301 | 0.7 | 0.4 |
| M111 | 20.1 | 8.03 | 36.67359 | 24.51989 | 2.1 | 1.3 |
| M112 | 20.1 | 8.05 | 36.67150 | 24.51904 | 1.3 | 0.8 |
| M113 | 20.1 | 8.14 | 36.66973 | 24.51851 | 1.7 | 1.0 |
| M114 | 20.1 | 8.01 | 36.67241 | 24.52428 | 3.3 | 2.1 |
| M115 | 20.1 | 7.99 | 36.67040 | 24.52418 | 2.1 | 1.3 |
| M116 | 20.1 | 8.01 | 36.66472 | 24.51906 | 1.5 | 0.9 |

### 3.4.4 Point Sources

The complexity of the hydrothermal system in Paleochori Bay concerning Hg was highlighted by the heterogeneity of the point source samples. Valsami-Jones et al. (2005) concluded that subaerial low Cl and Mg fluids were likely representative of an end-member equilibrated at depth. Additionally, Price et al. (2013a) concluded low Cl fluids were resultant from condensed vapor phases with some mixing of seawater and the brine phase.

The Cave-1 fluid contained elevated cations, anions, and metals, including the highest THg measured in the study (5066 pM). This sample was collected closer to high-temperature areas observed in Paleochori Bay (Khimasia et al., 2021). Enrichment of Cl, depletion of Mg, and low pH indicated a strong influence of hydrothermal fluid. The Cave-1 sample is indicative of a high THg arc magmatic water. Simmons and Brown (2007) described Hg concentrations from deep hydrothermal solutions in New Zealand, an area of known high hydrothermally sourced Hg. Concentrations ranged from 3400 pM to over 400 nM in hydrothermal fluids ranging in temperature from 195 to 322 °C.

Despite sampling difficulties, the extreme enrichment of THg from the Eastern, Boulder, and Screamer sites warranted further investigation. These fluid samples are

likely better representations of the localized impact of hydrothermal fluid on seawater based upon fluid chemistry and sampling environment.

The Eastern Site was moderately sedimented and contained the lowest THg and Hgdiss concentrations of the three. Despite a high porewater temperature (122 °C), pH remained close to neutral (6.04). The depleted cation and anion concentrations of the Eastern sample indicate a contribution of a low-Cl fluid. With MMHg, DMHg, and $Hg^0$ concentrations below detection limits, the high concentration of Hgdiss was comprised entirely of $Hg^{2+}$. The depletion of cations and anions within the Eastern site fluid was slight, with SO4 close to background values, indicating a strong influence of oxygenated seawater. The Na/K ratio of the Eastern site was high, and the site was located along proposed fault lines (Khimasia et al., 2021). However, the porewater concentration of THg was only moderately elevated compared to background porewater. If low Cl concentrations were caused by a condensed vapor phase, higher THg concentrations would be expected. Therefore, either the low Cl concentration was due to meteoric water, or THg was removed from the fluid before emission. Given that the sample's location lies on a fault line with a strong gas emission, the porewater's low THg is surprising. Further investigations into the area would be needed to understand the site further.

Like the Eastern site, the Screamer site contained high Hgdiss (217 pM) relative to THg (312 pM) and close to seawater concentrations of anions and cations. The Boulder site contained over twice the Hggas of the Screamer site and close to ten times the THg in the liquid sample. However, the Hgdiss concentration was comparable to that of the Screamer site (115 pM). However, these sites had hard rocky bottoms where clean fluid samples could not be obtained. Instead, the Hg concentrations at these sites reflected a mixture of emitted pore fluid, seawater, and equilibrated gas. As was observed at the Eastern site, MMHg, DMHg, and $Hg^0$ were below detection limits; therefore, all Hgdiss was in the form of $Hg^{2+}$.

Above the Boulder and Screamer sites, THg values within surface waters were high (9.6 pM). The large quantity of point sources (Khimasia et al., 2021) along with the high concentrations of THg from fluid samples and overlying surface waters, indicates transport from the point source to the surface, as was observed for other metals from hydrothermal systems (Pichler et al., 2019; Pichler et al., 1999b). Measurement of

surface waters directly above the Eastern site was not completed; however, the surrounding surface water sites were elevated compared to background samples.

With no visible fluid emission at the Boulder and Screamer site and major elements similar to local seawater values, the liquid samples taken from the point sources are hypothesized to be seawater primarily affected by hydrothermal gases. High THg and Hgdiss suggest rapid oxidation of $Hg^0$, the assumed primary Hg species within the gas, as was discussed in Christenson and Mroczek (2003).

### 3.4.5 Mercury in Hydrothermal Gases

Lower gas emission rates were observed at the Seagrass and Red sites, where Hggas concentrations were low. The low gas emission rates provide for increased subsurface reaction times and, therefore, the greater potential for removal (Bower et al., 2008; Christenson and Mroczek, 2003; Pichler et al., 1999a). However, given the gas sites' locations in relation to the proposed fault lines (Khimasia et al., 2021), high Hggas would have been expected.

The two highest Hg concentrations measured had limited sediment coverage (Boulder and Screamer sites). Both sites had high gas emission rates; however, the third high gas emission site (Crater) did not contain high Hg concentrations in the gas phase. This result was astounding given the low Na/K ratio and proximity to the Boulder and Screamer site. A large amount of overlying sulfur-rich sediment at the point of emission is hypothesized to be a primary removal mechanism for Hggas. The sediment cover acts as a filter for Hg species while at the same time facilitating the percolation of oxygenated seawater further into the subsurface due to the formation of circulation cells caused by the constant gas stream (e.g., O'Hara et al., 1994). The introduction of oxygen and subsequent oxidation of $Hg^0$ facilitates Hg removal, as described previously by Davey and van Moort (1986) for the Hg deposition at Ngawha Springs in New Zealand. The large concentration of Hg bound to particulates in the fluid phase compared to Hgdiss supports extensive scavenging at this site. The differences between concentrations in the fluid and gas phases are likely the result of rapid oxidation described by Christenson and Mroczek (2003).

### 3.5 Conclusions and Summary

Elevated concentrations of THg within surface waters within Paleochori Bay were due to the contributions of hydrothermal fluids and gases in the form of diffusive flux and

high THg point sources. We argue that these contributions must be substantial, given the potential for dilution and removal mechanisms (e.g., transport, sedimentation, atmospheric flux). The highest fluxes to the atmosphere were those closest to shore and associated with shallow water hydrothermal activity. At the same time, Hgdiss tended to be higher in samples with higher THg, while the Hgdiss fraction of THg did not. Direct measurement of volatile $Hg^0$ from the surface would be needed to measure this flux more accurately.

Environmental conditions commonly associated with Hg speciation and behavior, such as epithermal elements (As), scavenging species (S), and indications of hydrothermal activity (high temperatures, pH, salinity, emission site proximity) proved to be irrelevant outside of the specified sample groupings. Areas of white mat accumulation showed Hgdiss correlated with pH, while areas without visible white mat accumulation showed correlations with pH and other factors. Concentrations of THg within the non-white mat areas showed some correlation with multiple factors; however, not all of these were shared with the white mat areas, despite similarities in the ranges of concentrations of cations and anions. Smaller groupings showed potential similarities; however, these groupings were too small (n < 4) for meaningful statistical analysis. The highest THg concentrations from porewaters were found in samples associated with arc magmatic fluid, with sedimentation having a pivotal role in removing Hg (e.g., Crater site). Sediment samples showed elevated THg concentrations in the background and hydrothermally active areas, with active areas containing over double the background concentration. Duran-Toro et al. (2019) showed that suspended nanoparticles in the water column in Paleochori Bay were enriched in arsenic. Considering the Hg concentration difference between filtered and unfiltered samples, nanoparticles rich in Hg may exist in Paleochori Bay, which should be included in future research.

In summary, despite its substantial enrichment, we found Hg to be an elusive element in Paleochori Bay. Further investigations into the role of chemical reactions and fluid circulation in the shallow subsurface (before venting into seawater) will be necessary to better understand the source, transport and fate of Hg.

Appendix A
All collected data from Milos

| Sample | Gas | Depth | Lat. | Long. | Temp. | pH | Cl | Br | SO4 | As | Ca | Fe | K | Li | Mg | Mn | Na | Si | Sr | H2S | THg | Filtered THg | Gas THg | Methyl. Hg | Volatile Hg | Sed. THg |
|---|---|---|---|---|---|---|---|---|---|---|---|---|---|---|---|---|---|---|---|---|---|---|---|---|---|---|
| | | m | | | °C | | mM | mM | mM | µM | mM | mM | mM | mM | mM | mM | mM | mM | mM | µM | pM | pM | nmol/m³ | pM | pM | pmol/g |
| **Background Seawater** | | | | | | | | | | | | | | | | | | | | | | | | | | |
| *Seawater* | | | | | | | | | | | | | | | | | | | | | | | | | | |
| 2018 | | 0 | 36.657718 | 24.408037 | 20 | 8.25 | 639 | 0.92 | 32.8 | 0.02 | 11.1 | 0.00 | 11.2 | 0.00 | 52.3 | 0.00 | 528 | | 0.00 | | 0.11 | 0.5 | BDL | | | |
| 2017 | | | 36.657321 | 24.529800 | | | | | | | 11.3 | 0.0 | 11.0 | 0.82 | 54.3 | 0.00 | 461 | | 0.0 | | 0.1 | 1.8 | 0.52 | | | |
| *Porewater* | | | | | | | | | | | | | | | | | | | | | | | | | | |
| 2020-8 | | | 36.669960 | 24.519120 | 22 | 7.72 | 628 | 0.96 | 31.5 | 0.05 | 13.6 | BDL | 13.0 | 0.15 | 67.6 | BDL | 635 | | BDL | BDL | 0.11 | 98 | 4.00 | | | 414 |
| **Outside of Paleochori Bay Seawater** | | | | | | | | | | | | | | | | | | | | | | | | | | |
| *Seawater* | | | | | | | | | | | | | | | | | | | | | | | | | | |
| PB-A | | | 36.657942 | 24.408080 | | | | | | | 31.0 | BDL | 73.1 | 4.24 | 25.4 | BDL | 607 | | 3.5 | 0.3 | | 2.8 | | | | |
| PB-B | | | 36.656892 | 24.407711 | | | | | | | | | | | | | | | | BDL | | 0.5 | | | | |
| Pollonia | | | 36.762378 | 24.527809 | | | | | | | 26.4 | BDL | 39.5 | 2.44 | 37.5 | BDL | 498 | | 1.0 | 0.2 | | 3.1 | | | | |
| Sara-A | | | 36.743880 | 24.458935 | | | | | | | | | | | | | | | | | | 4.59 | | | | |
| Sara-B | | | 36.744748 | 24.459493 | | | | | | | | | | | | | | | | | | 3.71 | | | | |
| **Inside Paleochori Bay** | | | | | | | | | | | | | | | | | | | | | | | | | | |
| *Seawater Samples* | | | | | | | | | | | | | | | | | | | | | | | | | | |
| *Transect Samples* | | | | | | | | | | | | | | | | | | | | | | | | | | |
| 2017S-P1 | 0 | | 36.674770 | 24.516207 | | | | | | | | | | | | | | | 0.01 | | | 98 | | | | |
| 2017S-P2 | 0 | | 36.674698 | 24.516214 | | | | | | | | | | | | | | | 0.01 | | | 28 | | | | |
| 2017S-P3 | 0 | | 36.674419 | 24.516550 | | | | | | | | | | | | | | | 0.01 | | | 3.0 | | | | |
| 2017S-P4 | 0 | | 36.674122 | 24.516699 | | | | | | | | | | | | | | | 0.01 | | | 4.0 | | | | |
| 2017S-P5 | 0 | | 36.673706 | 24.516731 | | | | | | | | | | | | | | | 0.01 | | | 3.6 | | | | |
| 2017S-P6 | 0 | | 36.673321 | 24.516790 | | | | | | | | | | | | | | | 0.01 | | | 3.1 | | | | |
| 2017S-P7 | 0 | | 36.673000 | 24.516951 | | | | | | | | | | | | | | | 0.01 | | | 2.5 | | | | |
| 2017S-P8 | 0 | | 36.672562 | 24.517178 | | | | | | | | | | | | | | | 0.01 | | | 3.3 | | | | |
| 2017S-P9 | 0 | | 36.672226 | 24.517450 | | | | | | | | | | | | | | | 0.01 | | | 3.0 | | | | |
| 2017S-P10 | 0 | | 36.671875 | 24.517632 | | | | | | | | | | | | | | | 0.01 | | | 2.5 | | | | |
| 2017S-P11 | 0 | | 36.671413 | 24.517658 | | | | | | | | | | | | | | | 0.01 | | | 3.9 | | | | |
| 2017S-P12 | 0 | | 36.670986 | 24.517767 | | | | | | | | | | | | | | | 0.01 | | | 3.1 | | | | |
| 2017S-P13 | 0 | | 36.670502 | 24.517944 | | | | | | | | | | | | | | | 0.01 | | | 5.2 | | | | |
| 2017S-P14 | 0 | | 36.670261 | 24.518364 | | | | | | | | | | | | | | | 0.01 | | | 4.1 | | | | |
| 2017S-P15 | 0 | | 36.669865 | 24.518560 | | | | | | | | | | | | | | | 0.00 | | | 3.4 | | | | |
| 2017S-P16 | 0 | | 36.669392 | 24.518833 | | | | | | | | | | | | | | | 0.00 | | | 3.2 | | | | |

## 3. Mercury in the Hydrothermal Fluids and Gases in Paleochori Bay, Milos, Greece

Appendix A
All collected data from Milos

| Sample | Gas | Depth | Lat. | Long. | Temp. | pH | Cl | Br | SO4 | As | Ca | Fe | K | Li | Mg | Mn | Na | Si | Sr | H2S | THg | Filtered THg | Gas THg | Methyl. Hg | Volatile Hg | Sed. THg |
|---|---|---|---|---|---|---|---|---|---|---|---|---|---|---|---|---|---|---|---|---|---|---|---|---|---|---|
|  |  | m |  |  | °C |  | mM | mM | mM | µM | mM | mM | mM | mM | mM | mM | mM | mM | mM | µM | pM | pM | nmol/m³ | pM | pM | pmol/g |
| 2017B-P1 |  | 1.5 | 36.674770 | 24.516207 |  |  |  |  |  |  |  |  |  |  |  |  |  |  |  | 0.02 |  |  | 9.2 |  |  |  |
| 2017B-P2 |  | 2.4 | 36.674698 | 24.516214 |  |  |  |  |  |  |  |  |  |  |  |  |  |  |  | 0.01 |  |  | 7.4 |  |  |  |
| 2017B-P3 |  | 3.9 | 36.674419 | 24.516550 |  |  |  |  |  |  |  |  |  |  |  |  |  |  |  | 0.01 |  |  | 7.0 |  |  |  |
| 2017B-P4 |  | 5.3 | 36.674122 | 24.516699 |  |  |  |  |  |  |  |  |  |  |  |  |  |  |  | 0.00 |  |  | 2.9 |  |  |  |
| 2017B-P5 |  | 6 | 36.673706 | 24.516731 |  |  |  |  |  |  |  |  |  |  |  |  |  |  |  | 0.00 |  |  | 2.4 |  |  |  |
| 2017B-P6 |  | 7.2 | 36.673321 | 24.516790 |  |  |  |  |  |  |  |  |  |  |  |  |  |  |  | 0.01 |  |  | 2.6 |  |  |  |
| 2017B-P7 |  | 8 | 36.673000 | 24.516951 |  |  |  |  |  |  |  |  |  |  |  |  |  |  |  | 0.00 |  |  | 2.4 |  |  |  |
| 2017B-P8 |  | 9 | 36.672562 | 24.517178 |  |  |  |  |  |  |  |  |  |  |  |  |  |  |  | 0.00 |  |  | 2.2 |  |  |  |
| 2017B-P9 |  | 9.8 | 36.672226 | 24.517450 |  |  |  |  |  |  |  |  |  |  |  |  |  |  |  | 0.00 |  |  | 7.1 |  |  |  |
| 2017B-P10 |  | 11.3 | 36.671875 | 24.517632 |  |  |  |  |  |  |  |  |  |  |  |  |  |  |  | 0.00 |  |  | 2.9 |  |  |  |
| 2017B-P11 |  | 12.4 | 36.671413 | 24.517658 |  |  |  |  |  |  |  |  |  |  |  |  |  |  |  | 0.00 |  |  | 3.4 |  |  |  |
| 2017B-P12 |  | 13.8 | 36.670986 | 24.517767 |  |  |  |  |  |  |  |  |  |  |  |  |  |  |  | 0.00 |  |  | 2.9 |  |  |  |
| 2017B-P13 |  | 14.7 | 36.670502 | 24.517944 |  |  |  |  |  |  |  |  |  |  |  |  |  |  |  | 0.00 |  |  | 2.1 |  |  |  |
| 2017B-P14 |  | 16.1 | 36.670261 | 24.518364 |  |  |  |  |  |  |  |  |  |  |  |  |  |  |  | 0.00 |  |  | 1.6 |  |  |  |
| 2017B-P15 |  | 18 | 36.669865 | 24.518560 |  |  |  |  |  |  |  |  |  |  |  |  |  |  |  | 0.00 |  |  | 1.7 |  |  |  |
| 2017B-P16 |  | 20.7 | 36.669392 | 24.518833 |  |  |  |  |  |  |  |  |  |  |  |  |  |  |  | 0.00 |  |  | 2.4 |  |  |  |
| *Surface* |  |  |  |  |  |  |  |  |  |  |  |  |  |  |  |  |  |  |  |  |  |  |  |  |  |  |
| M108 | 0 |  | 36.673707 | 24.515665 | 20.1 | 7.87 | 636 | 1.04 | 32.5 | 0.05 | 11.1 | BDL | 11.2 | BDL | 53.8 | BDL | 518 |  | BDL | 0.11 |  | 9.6 | 4.2 |  |  |  |
| M109 | 0 |  | 36.671798 | 24.514197 | 20.1 | 8.11 | 638 | 0.88 | 32.7 | 0.06 | 11.8 | BDL | 11.7 | BDL | 55.4 | BDL | 544 |  | 0.01 | 0.10 |  | 1.8 | 1.4 |  |  |  |
| M110 | 0 |  | 36.669833 | 24.513008 | 20.1 | 8.19 | 634 | 0.89 | 32.5 | 0.02 | 11.0 | BDL | 11.0 | BDL | 54.0 | BDL | 505 |  | BDL | 0.10 |  | 3.1 | 0.7 |  |  |  |
| M111 | 0 |  | 36.673587 | 24.519885 | 20.1 | 8.03 | 638 | 0.86 | 33.0 | 0.04 | 11.5 | BDL | 11.6 | BDL | 55.7 | BDL | 534 |  | BDL | 0.11 |  | 5.1 | 2.1 |  |  |  |
| M112 | 0 |  | 36.671504 | 24.519043 | 20.1 | 8.05 | 637 | 0.88 | 32.7 | 0.04 | 11.0 | BDL | 11.0 | BDL | 53.5 | BDL | 517 |  | BDL | 0.10 |  | 3.0 | 1.3 |  |  |  |
| M113 | 0 |  | 36.669733 | 24.518515 | 20.1 | 8.14 | 639 | 0.87 | 32.8 | 0.15 | 11.5 | BDL | 11.6 | BDL | 53.6 | BDL | 528 |  | BDL | 0.10 |  | 4.1 | 1.7 |  |  |  |
| M114 | 0 |  | 36.672409 | 24.524276 | 20.1 | 8.01 | 639 | 0.91 | 32.7 | 0.03 | 11.6 | BDL | 11.6 | BDL | 56.3 | BDL | 529 |  | BDL | 0.11 |  | 15 | 3.3 |  |  |  |
| M115 | 0 |  | 36.670400 | 24.524177 | 20.1 | 7.99 | 640 | 0.90 | 32.9 | 0.04 | 11.3 | BDL | 11.5 | BDL | 53.5 | BDL | 526 |  | BDL | 0.10 |  | 9.0 | 2.1 |  |  |  |
| M116 | 0 |  | 36.664723 | 24.519062 | 20.1 | 8.01 | 635 | 0.82 | 32.7 | 0.04 | 11.4 | BDL | 11.4 | BDL | 52.5 | BDL | 527 |  | BDL | 0.10 |  | 1.7 | 1.5 |  |  |  |
| *Subaerial* |  |  |  |  |  |  |  |  |  |  |  |  |  |  |  |  |  |  |  |  |  |  |  |  |  |  |
| Cave-1 |  |  | 36.674167 | 24.513236 | 91 | 3.37 | 754 | 1.07 | 22.9 |  | 27.9 | 0.1 | 47.8 | 2.81 | 38.1 | BDL | 550 | 2.2 | 0.2 |  |  | 5066 |  |  |  |  |
| Cave-2 |  |  | 36.673370 | 24.512271 |  |  |  |  |  |  | 4.4 | 1.5 | 0.6 | 0.80 | 1.8 | BDL | 5 | 5.2 | BDL |  |  | 2.5 | 0.4 |  |  |  |
| ***Porewaters*** |  |  |  |  |  |  |  |  |  |  |  |  |  |  |  |  |  |  |  |  |  |  |  |  |  |  |

51

Appendix A
All collected data from Milos

| Sample | Gas | Depth | Lat. | Long. | Temp. | pH | Cl | Br | SO4 | As | Ca | Fe | K | Li | Mg | Mn | Na | Si | Sr | H2S | THg | Filtered THg | Gas THg | Methyl. Hg | Volatile Hg | Sed. THg |
|---|---|---|---|---|---|---|---|---|---|---|---|---|---|---|---|---|---|---|---|---|---|---|---|---|---|---|
| | | m | | | °C | | mM | mM | mM | µM | mM | mM | mM | mM | mM | mM | mM | mM | mM | µM | pM | pM | nmol/m³ | pM | pM | pmol/g |
| *Sand, Red and Yellow Precipitates* | | | | | | | | | | | | | | | | | | | | | | | | | | |
| M067 | | 2.4 | 36.674574 | 24.516776 | 89 | 4.86 | 1115 | 1.33 | 15.0 | 4.68 | 46.0 | 0.10 | 99.0 | 3.73 | 25.0 | 0.16 | 847 | 2.57 | 0.38 | | 130 | | 281 | 0.6 | | |
| M069 | | 2.5 | 36.674514 | 24.516772 | 82.2 | 5.8 | 996 | 1.27 | 19.0 | 21.42 | 45.9 | 0.32 | 94.4 | 3.33 | 45.0 | 0.14 | 989 | 2.52 | 0.39 | | 174 | | 377 | 0.5 | | |
| M084 | | 2.4 | 36.674865 | 24.517017 | 84.5 | 5.31 | 1090 | 1.32 | 15.6 | 4.94 | 43.8 | 0.11 | 94.5 | 3.61 | 26.1 | 0.15 | 832 | 2.47 | 0.37 | | 86 | | 472 | 2.7 | | |
| M095 | | 2.4 | 36.674551 | 24.516751 | 37 | 6.56 | 798 | 1.04 | 25.9 | 10.35 | 24.4 | 0.22 | 41.0 | 1.33 | 42.6 | 0.08 | 628 | 0.64 | 0.21 | | 19 | | 41 | 4.8 | | |
| M096 | | 2.4 | 36.674565 | 24.516760 | 27 | 6.85 | 743 | 0.96 | 28.2 | 2.30 | 20.3 | 0.04 | 31.1 | 0.90 | 47.6 | 0.04 | 598 | 0.37 | 0.16 | | 959 | | 93 | 4.8 | | |
| M097 | | 2.3 | 36.674411 | 24.516768 | 95 | 5.82 | 934 | 1.19 | 21.2 | 18.78 | 32.8 | 0.06 | 66.5 | 2.26 | 35.7 | 0.09 | 709 | 1.59 | 0.25 | | 4 | | 395 | 6.3 | | |
| M098 | | 2.2 | 36.674431 | 24.516777 | 96.4 | 5.52 | 944 | 1.25 | 21.1 | 18.01 | 33.5 | 0.06 | 68.3 | 2.33 | 35.4 | 0.09 | 728 | 1.75 | 0.26 | | 34 | | 724 | 1.6 | | |
| M099 | | 2.3 | 36.674402 | 24.516782 | 87.2 | 5.77 | 909 | 1.17 | 22.4 | 16.99 | 30.5 | 0.09 | 60.2 | 2.10 | 37.0 | 0.09 | 689 | 1.51 | 0.26 | | 56 | | 321 | 1.8 | | |
| M100 | | 2.5 | 36.674394 | 24.516791 | 57 | 6.42 | 901 | 1.12 | 22.1 | 15.62 | 31.5 | 0.29 | 61.0 | 2.05 | 38.5 | 0.10 | 701 | 0.58 | 0.23 | | 34 | | 133 | 6.5 | | |
| M102 (Crater) | High | 4.0 | 36.673985 | 24.515777 | 111 | 6.55 | 936 | 1.15 | 20.2 | 30.47 | 35.6 | 0.09 | 70.7 | 2.58 | 30.0 | 0.10 | 701 | 1.74 | 0.30 | | 1511 | | 5.7 | 1.7 | BDL | BDL |
| M127 | | 11.6 | 36.671625 | 24.521533 | 23.2 | 6.05 | 633 | 0.87 | 32.9 | 0.54 | 11.2 | 0.06 | 11.4 | | 53.4 | BDL | 527 | 0.05 | 0.10 | | 45 | | 3.4 | | | |
| M134 | | 0.1 | 36.675058 | 24.517004 | 22 | 7.89 | 640 | 0.87 | 32.7 | 0.08 | 12.0 | BDL | 12.2 | 0.05 | 54.2 | BDL | 540 | 0.03 | 0.10 | | 80 | | 33 | | | |
| M135 | | 0.1 | 36.674994 | 24.518398 | 22.1 | 8.05 | 644 | 0.91 | 32.8 | 0.04 | 11.9 | BDL | 11.9 | BDL | 55.5 | BDL | 553 | 0.01 | 0.10 | | 28 | | 13 | 0.5 | | |
| M136 | | 0.1 | 36.674756 | 24.520011 | 22 | 8.05 | 638 | 0.83 | 33.0 | 0.04 | 11.7 | BDL | 11.6 | BDL | 57.2 | BDL | 538 | 0.01 | 0.10 | | 17 | | 8.9 | | | |
| M137 | | 0.1 | 36.674517 | 24.521070 | 21.9 | 8.05 | 637 | 0.92 | 32.5 | 0.03 | 11.7 | BDL | 11.6 | BDL | 54.4 | BDL | 534 | 0.01 | 0.10 | | 67 | | 8.9 | | | |
| M160 | | | 36.671970 | 24.516420 | 25 | 6.05 | 646 | 0.96 | 30.9 | BDL | 17.1 | 0.01 | 16.9 | 0.24 | 59.4 | 0.03 | 593 | 0.34 | 0.11 | | 735 | | 11 | | | |
| PGG | | | 36.673501 | 24.516503 | 96.4 | 5.9 | 572 | 0.90 | 27.4 | | 11.0 | BDL | 11.9 | 0.92 | 47.7 | BDL | 427 | 0.3 | 0.1 | | 110 | | 2.7 | | | |
| 2020-C | | | 36.672638 | 24.512690 | 86 | 1.87 | 74 | 0.10 | 24.7 | 4.85 | 6.1 | 0.14 | 6.5 | 0.22 | 3.3 | 0.05 | 66 | 2.81 | 0.02 | | 24 | | 5 | | | 1213 |
| *White Mats* | | | | | | | | | | | | | | | | | | | | | | | | | | |
| M068 | | 2.4 | 36.674531 | 24.516756 | 84.5 | 5.24 | 1026 | 1.28 | 17.8 | 6.17 | 42.6 | 0.09 | 90.6 | 3.43 | 27.0 | 0.14 | 812 | 2.31 | 0.37 | | 108 | | 152 | 8.9 | | |
| M101 | | 12.0 | 36.670450 | 24.523800 | 48.6 | 5.54 | 774 | 0.93 | 15.2 | 0.07 | 37.9 | BDL | 64.4 | 2.45 | 20.5 | 0.11 | 584 | 1.49 | 0.25 | | 12 | | 510 | 10 | | |
| M104 | | 11.1 | 36.669917 | 24.513164 | 122.4 | 5.9 | 814 | 0.96 | 10.7 | 3.59 | 36.6 | BDL | 72.8 | 2.91 | 16.9 | 0.11 | 625 | 2.47 | 0.29 | | 19 | | 603 | 13 | | |
| M106 | | 11.0 | 36.669918 | 24.513176 | 63 | 5.51 | | | | | | | | | | | | | | | 172 | | 10 | | | |
| M107 (Seagrass) | Low | 11.1 | 36.669921 | 24.513156 | 122 | 6.32 | 803 | 0.93 | 12.7 | 3.39 | 33.6 | BDL | 65.8 | 2.60 | 20.1 | 0.10 | 607 | 2.24 | 0.27 | | 108 | 107 | 17 | 2.0 | BDL | BDL |
| M121 | | 17.1 | 36.669998 | 24.521608 | 44.6 | 5.28 | 693 | 0.90 | 27.2 | 0.19 | 11.4 | BDL | 11.6 | BDL | 54.8 | BDL | 522 | 0.11 | 0.11 | | 12 | | 60 | 7.5 | | |
| M124 | | 9.5 | 36.672110 | 24.517157 | 72.4 | 4.94 | 580 | 0.74 | 20.7 | 15.61 | 18.2 | BDL | 33.0 | 1.03 | 29.0 | 0.06 | 460 | 3.80 | 0.15 | | 655 | | 34 | 5.2 | | |
| M126 | | 11.6 | 36.671621 | 24.521566 | 39.7 | 5.27 | 633 | 0.83 | 32.7 | 0.04 | 11.7 | 0.01 | 12.2 | BDL | 53.7 | BDL | 533 | 0.06 | 0.11 | | 371 | | 6.6 | | | |
| M153 | | 10.1 | 36.672109 | 24.518504 | 101.2 | 5.9 | 727 | 1.02 | 26.7 | 4.38 | 24.4 | BDL | 32.8 | 0.94 | 43.1 | 0.03 | 577 | 1.61 | 0.16 | | 1196 | | 103 | 11 | | |

## 3. Mercury in the Hydrothermal Fluids and Gases in Paleochori Bay, Milos, Greece

Appendix A
All collected data from Milos

| Sample | Gas | Depth | Lat. | Long. | Temp. | pH | Cl | Br | SO4 | As | Ca | Fe | K | Li | Mg | Mn | Na | Si | Sr | H2S | THg | Filtered THg | Gas THg | Methyl. Hg | Volatile Hg | Sed. THg |
|---|---|---|---|---|---|---|---|---|---|---|---|---|---|---|---|---|---|---|---|---|---|---|---|---|---|---|
| | | m | | | °C | | mM | mM | mM | µM | mM | mM | mM | mM | mM | mM | mM | mM | mM | µM | pM | pM | nmol/m³ | pM | pM | pmol/g |
| 2020-1A | | | 36.671930 | 24.516670 | 52.7 | 5.35 | 646 | 0.97 | 29.8 | 5.17 | 18.7 | BDL | 20.1 | 0.29 | 65.0 | 0.03 | 661 | 0.93 | 0.13 | | | 78 | 5 | | | 917 |
| *Point Sources* | | | | | | | | | | | | | | | | | | | | | | | | | | |
| M01 (Red) | Low | 9.9 | 36.672140 | 24.517190 | 113 | 7.16 | 630 | 0.94 | 32.2 | 0.20 | 11.2 | 0.01 | 11.4 | BDL | 52.0 | BDL | 522 | 0.06 | 0.10 | | | | | 0.7 | BDL | BDL |
| M103 (Boulder) | High | 4.0 | 36.674030 | 24.515350 | 110 | 6.78 | 612 | 0.88 | 31.7 | 0.23 | 10.8 | BDL | 10.9 | BDL | 53.7 | BDL | 508 | 0.09 | 0.09 | | | 2894 | 115 | 2792 | BDL | BDL |
| M125 (Eastern) | Low | 11.1 | 36.671630 | 24.521580 | 122 | 6.04 | 558 | 0.77 | 28.5 | 0.21 | 9.9 | BDL | 10.4 | BDL | 47.8 | 0.01 | 470 | 0.47 | 0.10 | | 7.74 | 186 | 107 | 561 | BDL | BDL |
| M128 (Screamer) | High | 4.0 | 36.673961 | 24.515771 | 111 | 6.03 | 621 | 0.85 | 32.1 | 0.23 | 11.5 | BDL | 11.6 | BDL | 52.8 | BDL | 524 | 0.01 | 0.09 | | 0.12 | 312 | 217 | 1383 | BDL | BDL |
| *Large Volume Samples* | | | | | | | | | | | | | | | | | | | | | | | | | | |
| M035 | | 4.5 | 36.673880 | 24.516167 | 98.9 | 5.96 | 773 | 0.95 | 21.9 | 25.11 | 21.7 | 0.03 | 44.3 | 1.42 | 39.4 | 0.04 | 602 | 1.91 | 0.19 | | 0.12 | 28 | 1.4 | | | |
| M105 | | 2.3 | 36.674489 | 24.516778 | 95 | 5.35 | 1006 | 1.26 | 18.9 | 45.32 | 37.8 | 0.11 | 78.2 | 2.91 | 31.2 | 0.11 | 773 | 2.10 | 0.33 | | 1.97 | 45 | 2.3 | | | |
| *Brines* | | | | | | | | | | | | | | | | | | | | | | | | | | |
| BP | | | | | 105 | 3.18 | 520 | 0.63 | 3.2 | | 77.0 | 0.3 | 147.0 | 9.13 | 6.2 | BDL | 870 | 2.9 | 0.6 | | | 44 | 3.7 | | | |
| Rocky Point | | | 36.673672 | 24.516004 | 96.4 | 4.54 | 877 | 1.18 | 8.3 | | 31.3 | BDL | 72.9 | 4.36 | 25.0 | BDL | 607 | 3.6 | 0.3 | | | 22 | | | | |

## 4. Hg in the hydrothermal fluids and gases in Baia di Levante, Vulcano, Italy

Hannah Roberts, Thomas Pichler

Universität Bremen, Fachbereich Geowissenschaften, Geochemistry and Hydrogeology, Klagenfurter Str. 2-4, 28359 Bremen, Germany

This chapter corresponds to a manuscript published to the journal *Marine Chemistry*

**Abstract**

The importance of fluid and gaseous mercury (Hg) emissions from hydrothermal systems in the shallow, coastal ocean is poorly constrained. However, there are indicators that they could be a significant natural Hg source. We evaluated the hydrothermal Hg emissions around Vulcano Island, Aeolian Arc, Italy, which is host to a marine shallow-water hydrothermal system (MSWHS) in Baia di Levante. Fluids were collected with porewater probes, and gases were collected into Tedlar© bags. Total Hg (THg) concentrations in the hydrothermal fluids ranged from 2.9 to 2888 pM. The concentrations of volatile Hg were below 8 pM and trended positively with increasing temperature. Monomethyl Hg (MMHg) was not detected. Total Hg in the gases ranged from 0.03 to 1.82 µmol / $m^3$.

High concentrations of THg were associated with low Cl-concentrations, low pH-values, and high K / Cl and Mg / Cl ratios. Concentrations of THg in the hydrothermal fluids resulted from mixing between meteoric water, seawater, condensed fumarolic vapor, and a deep hydrothermal fluid. However, not all low-Cl fluids were high THg samples. Samples taken along the coast of the La Fossa crater contained substantially less THg (2.9 to 29.4 pM), despite similar hydrothermal indicators as those in the Baia di Levante samples. These data support subsurface circulation models, which discuss the downslope flow of condensed La Fossa crater gases to the coast. In the hydrothermally active area of Baia di Levante, concentrations of THg were elevated relative to background surface seawater, ranging from 40 to 5110 pM. In comparison, the remainder of the bay ranged from 0.8 to 2.4 pM.

## 4. Hg in the hydrothermal fluids and gases in Baia di Levante, Vulcano, Italy

The flux of Hg to the atmosphere from surface waters was calculated through dissolved Hg concentrations. The flux at each sampled site ranged from 0 to 19.6 pmol / m2 / hr. The highest flux rates were determined for those areas with visible hydrothermal activity, particularly those with high gaseous emission rates. Surface water concentrations declined rapidly away from point sources, indicating atmospheric emission, dilution through mixing, or scavenging and sedimentation. In hydrothermally active areas, Baia di Levante sediments contained THg concentrations of 2.42 nmol / g and 49.52 nmol / g, which were significantly above background (0.03 nmol / g).

The largest gaseous point source, Bambino, released more than 2 L of gas per second. Although, Hg concentrations in the gas were low (113 to 122 nmol / m3) relative to other measured point sources near the beach (1768 to 1817 nmol / m3), due to the volume of discharge, surface water concentrations were elevated (131 pM).

The Hg present in the hydrothermal system of Vulcano contributes Hg to the atmosphere and local seawater as a natural source.

### 4.1.1 Introduction

Mercury (Hg) is a well-known biological toxin affecting environmental and human health. Anthropogenic Hg emissions are the primary source to the environment, while natural sources of Hg play a lesser role and are poorly constrained in global models (Lamborg et al., 2002; Outridge et al., 2018). In the marine cycle, Hg is primarily deposited from the atmosphere to surface waters as elemental Hg ($Hg^0$) or ionic Hg ($Hg^{2+}$) (Mason and Fitzgerald, 1996; Mason and Sheu, 2002). Abiotic and biotic reactions oxidize $Hg^0$ to ionic Hg ($Hg^{2+}$), after which primarily biological processes generate methylated species monomethylmercury and dimethylmercury (MMHg and DMHg) (Fitzgerald et al., 2007). These organic Hg compounds are highly toxic, given their ability to pass through the blood-brain barrier. Additionally, organic species bioaccumulate to levels that can affect human health. Dissolved species (Hgdiss) include colloidally bound Hg (< 0.45 μm) and unbound $Hg^{2+}$, $Hg^0$, and methylated species. Volatile species include $Hg^0$ and DMHg. Total Hg (THg), which includes dissolved and particle-bound Hg, in the Mediterranean Sea, is generally in the low pM (< 5 pM) concentration range with variable concentrations in

the water column spatially and temporally (e.g., Cossa et al., 2018; Cossa et al., 1997b; Fitzgerald et al., 2007; Horvat et al., 2003).

Marine shallow-water hydrothermal systems (MSWHS) are sparingly described natural sources of Hg to the atmosphere and marine environment (e.g., Bagnato et al., 2017; Leal-Acosta et al., 2010; Roberts et al., 2021; Stoffers et al., 1999). Emission types can be concentrated at a single point (point sources) or occur diffusely across a wide area (diffusive flux) and are generally associated with elevated temperatures of up to 120 °C (Pichler et al., 1999b; Price and Giovannelli, 2017; Roberts et al., 2021). Features associated with MSWHS include microbial mats (e.g., Price and Giovannelli, 2017; Price et al., 2013b); chimneys and hydrothermal precipitates (e.g., Esposito et al., 2018; Pichler and Veizer, 2004); and fluid, brine, and gas emission (e.g., Bagnato et al., 2009; Pichler et al., 1999a; Valsami-Jones et al., 2005). As a volatile element, Hg can be present in hydrothermal systems in the gas or fluid phase (Roberts et al., 2021; Varekamp and Buseck, 1984). Depending upon depth and gas flow, emissions from MSWHS can contribute Hg directly to the atmosphere or dissolve constituents into the water column (e.g., Bagnato et al., 2017; Pichler et al., 1999a; Pichler et al., 1999c; Roberts et al., 2021). At the point of emission, no methylated species have been observed in fluids from MSWHS (Roberts et al., 2021). However, contributions of inorganic Hg species to local waters, seagrasses, and sediments have been reported (Bagnato et al., 2017; Leal-Acosta et al., 2013; Leal-Acosta et al., 2010; Roberts et al., 2021). Additionally, the methylation of inorganic species within the water column is a significant factor within the marine Hg cycle (Lehnherr et al., 2011; Monperrus et al., 2007; Munson et al., 2018).

Here, we present Hg and water chemistry data for the hydrothermal fluids and gases of the Vulcano MSWHS, along with data for surface waters in Baia di Levante (Fig. 4.1). We hypothesize the source of Hg to be a rising hydrothermal vapor phase. The final concentration of Hg is controlled by mixing seawater and meteoric water. These findings support previous studies of subsurface circulation models (Oliveri et al., 2019; Zambardi et al., 2009) and groundwater studies (Aiuppa et al., 2000; Bagnato et al., 2009).

## 4.1.2 Geological Setting

The island of Vulcano belongs to the Aeolian volcanic arc and is comprised entirely of volcanic rock, with younger volcanic edifices in the north and northwest (Keller, 1980). Volcanic activity began during the Upper Pleistocene, and the last eruptive period was from 1888 to 1890; however variable fumarolic activity on land and offshore has continued to the present (De Astis et al., 1997). Baia di Levante is located between the La Fossa caldera and the Vulcanello peninsula. Following drilling campaigns in the 1950s, the Baia di Levante area has been known to be fed by a hydrothermal aquifer beneath the bay (Sommaruga, 1984). Since that time, several subsurface circulation models have been proposed (e.g., Aiuppa et al., 2020; Falcone et al., 2022; Federico et al., 2010; Fulignati et al., 1998; Inguaggiato et al., 2012; Madonia et al., 2015; Oliveri et al., 2019). All models agree that the system is driven by a shallow geothermal aquifer, which generates a boiling hydrothermal brine that feeds the MSWHS in Baia di Levante. However, the exact subsurface plumbing of the hydrothermal aquifer, the sources of various marine and sub-aerial point sources, and the relative significance of water sources (e.g., meteoric water and seawater) are not conclusively established. Large variations in gas and liquid composition and temperature were reported for the La Fossa and Baia di Levante areas (e.g., Aiuppa et al., 2007; Aubert et al., 2008; Boatta et al., 2013; Rogers et al., 2007). In Baia di Levante, multiple shallow-water point sources emit metals, REEs, and other components to the seawater, which affect the water chemistry of the bay (e.g., Capaccioni et al., 2001; Oliveri et al., 2019; Sedwick and Stuben, 1996).

Figure 4.1: Map of all hydrothermal sample locations on Vulcano island with A) regional map, B) map of Baia di Levante and the La Fossa samples with locations of hydrothermal samples. LF samples were distinctive from Baia di Levante samples with greater influence from the La Fossa crater. The maps were generated in QGIS. C) Map of Baia de Levante hydrothermally active area showing named point sources including subaerial low-Cl, shore, rock boulder, tidal cave, Bambino, white mat, and the mud bath area (MB). Created from drone images that were stitched with Microsoft ICE.

Hydrothermal activity is present north of the Vulcano port along the beach and in the shallow bay (Fig. 4.1 and 4.2). Activity in the bay was observed primarily in the form of gaseous exhalations. An area of diffuse hydrothermal fluid flux is indicated by the formation of white biomats north of the port (Fig. 4.1). A large, acidic mud bath frequented by tourists sits to the west of the bay, immediately onshore and north of the port. The rocky outcropping that divides the beach and port areas contains at least three acidic hydrothermal sources below or above sea level. The area in Baia di Levante north of the outcropping area and directly east of the mud bath is considered the mud bath area (MB) for purposes of data discussion. North of MB is the largest gaseous exhalation in the bay, named Bambino. Eastward from Bambino are many small gaseous exhalations in addition to a point source northeast of Bambino (Mini-Bambino). Between the rocky outcropping and Bambino, the bottom substrate is rocky with little sedimentation close to shore. Waters are often murky, with large flocculants visible in the water column. The area to the north of Bambino contains only a few small gaseous point sources (Aiuppa et al., 2020; Boatta et al., 2013). Small, low-Cl point sources emit gas and fluid onshore to the north of MB. Fluids are transparent with some coloration on the surrounding fine sediment. To the south of the port is the La Fossa area (LF). A cooler hydrothermal fluid point source was discovered near a mermaid statue in that area.
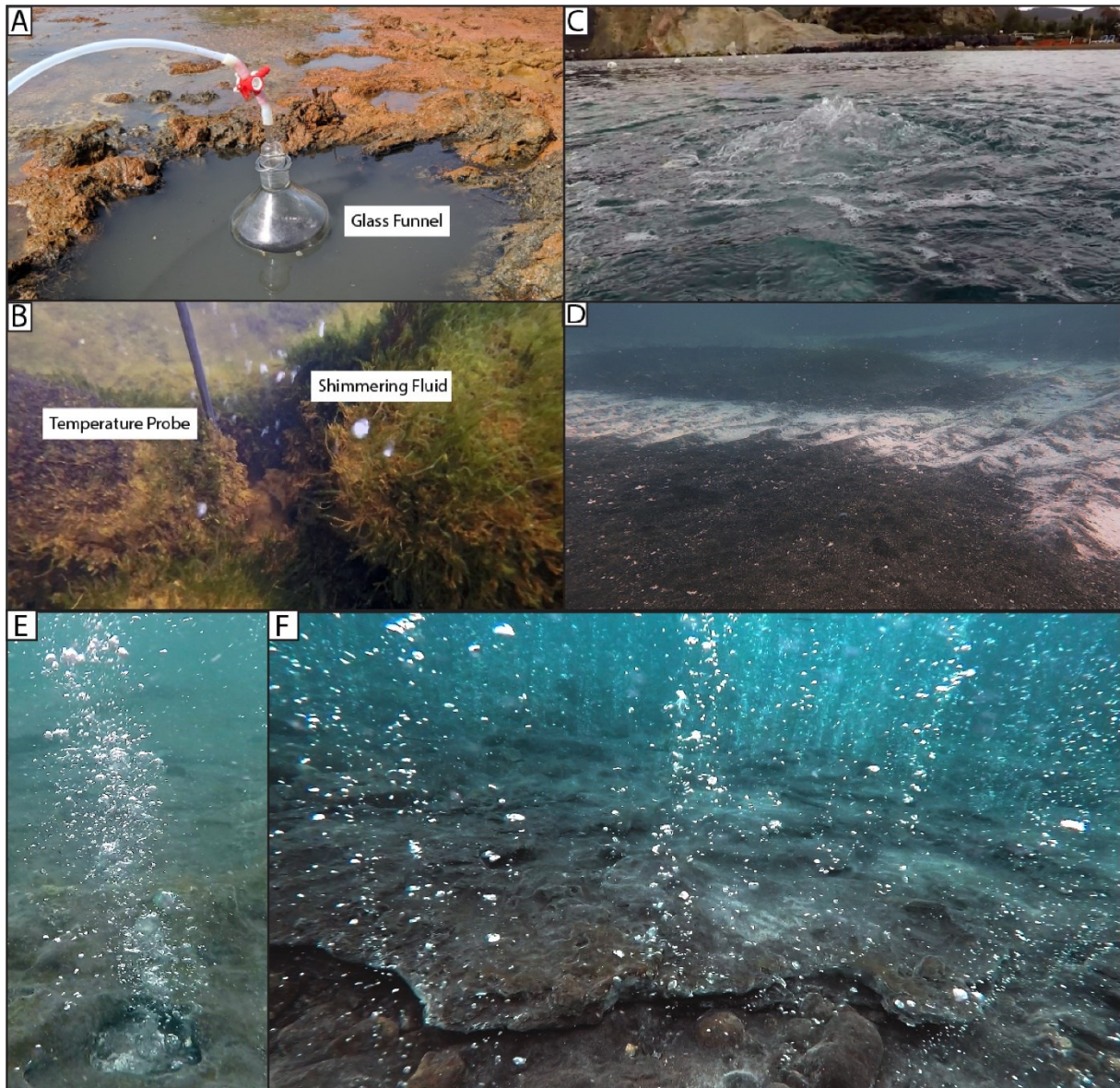
Figure 4.2: Point source examples on Vulcano island. A) gas sampling of subaerial low-Cl, B) submarine low-Cl with shimmering hydrothermal fluid, C) Bambino surface emission, D) white mat area. Point sources in the area of Bambino E) gaseous point source (Mini-Bambino), F) extensive gaseous exhalations to the east of Bambino.

Concentrations of Hg were reported for La Fossa cone fumaroles (e.g., Bagnato, 2007; Ferrara et al., 2000; Zambardi et al., 2009) and groundwaters (Aiuppa et al., 2000; Bagnato et al., 2009). However, there were no data reported for Hg in the hydrothermal gases and fluids collected at the point of emission in Baia di Levante.

## 4.2. Methods

In June 2019 and September 2021, a total of 85 samples were collected across the bay and around the island for Hgdiss (filtered) and THg (unfiltered) in surface waters, the water column, and from hydrothermal point sources (PS), along with As, cations, and anions (Appendix 1 and 2). In a subset of samples, Hg was speciated (V25, V26, V29, V30, and V36), which included the determination of THg, Hgdiss, $Hg^0$, DMHg, and MMHg and required a sample volume of 1 L. Surface waters (n = 32) were collected by boat using 60 mL polypropylene syringes and filtered immediately onboard through a 0.45 μm membrane. Hydrothermal fluids were collected using pore fluid samplers constructed from PTFE tubing and 10 mL pipette tips at 10 cm sediment depth using polypropylene 60 mL syringes. Porewater temperatures were monitored at the pipette tip, and deviations in temperature were not observed during sampling. This ensured that samples were not contaminated with seawater. Measurements of pH (Halo Wireless pH meter, Hanna Instruments), conductivity and ORP (Myron Ultrameter) were immediately taken in the field. The subsample for anion analysis was filtered with a 0.45 μm syringe filter, and the subsamples for elemental analysis (ICP-OES and ICP-MS) were additionally preserved with 2 % (m / v) concentrated nitric acid.

The syringes that were collected for Hg speciation were carefully expelled into a 1 L glass jar in the field lab for $Hg^0$ collection. To avoid the potential loss of $Hg^0$, utmost care was taken to prevent turbulent flow while transferring the sample.

A total of six gas samples were collected for analysis of Hggas (Table 4.1). Background surface seawater samples were collected in areas with no visible hydrothermal activity outside Baia di Levante to the east (V36) and on the other side of the island to the west (V47-V50).

# 4. Hg in the hydrothermal fluids and gases in Baia di Levante, Vulcano, Italy

Table 4.1: Concentrations of Hg in the gas phase on Vulcano

| Sample Number | Sample Description | Gas nmol / m^3 |
|---|---|---|
| | **Bambino** | |
| V51 | Low Tide | 122 |
| V52 | High Tide | 113 |
| B-B-06 | 2021 Low Tide | 120 |
| B-MB | Mini-Bambino | 282 |
| | **White Patch** | |
| V29 | White Patch 10 cm | 7 |
| V39 | White Patch T Map: White | 5 |
| | **Baia di Levante** | |
| V30 | Subaerial low-Cl | 3 |
| V42 | Shore Sample | 1768 |
| V43 | Rock Boulder at Mud Bath | 1817 |

Liquid Hg samples were collected as unfiltered and filtered (0.45 µm), stored and analyzed following the USEPA (2002) protocol with a Brooks Rand CV-AFS analyzer. The acidified samples arrived from the field in the laboratory and were held at 4 °C until analysis. On the day of analysis, 40 mL sample were transferred into a 60 mL Volatile Organic Analysis (VOA) glass vial with a PTFE lined cap. 400 µL acidified bromide / bromate (1:1 mixture of 0.01 M bromide / bromate solution (Tritrisol, Merck) and 32 % hydrochloric acid (Optima grade, Fisher Scientific)) were added to the sample and left standing for at least 30 min at room temperature. The reactivity of the bromine chloride was then quenched by adding 100 µL 30 % (m / v) hydroxylamine hydrochloride solution (ReagentPlus, 99 %, Sigma-Aldrich). Elemental Hg was generated in the solution upon the addition of 200 µL 20 % (m / v) tin(II)chloride solution (Reagent grade, Alfa Aesar). Each sample was analyzed in duplicate whenever the sample volume allowed. The limit of detection for this method in our laboratory was determined to be 0.04 ng / L (n = 10). The certified reference material ORMS-5 (elevated Hg in river water, National Research Council Canada)

was used for quality control. The reference material is certified for a concentration of 26.2 ± 1.3 ng / L THg.

The sediment samples were digested in 10:3 aqua regia following Bloom et al. (2003) and THg was analyzed by CV-AFS. The certified reference material PACS-1, certified for a concentration of 4.57 ± 0.16 µg / g THg was used for quality control.

$Hg^0$ in the liquid phase was collected from selected samples (Table 4.2) by purging 1 L of hydrothermal fluid with Hg free nitrogen onto gold and carbo traps and analyzed by CV-AFS (Cossa et al., 2011; Lehnherr et al., 2011).

Table 4.2: Concentrations of dissolved $Hg^0$ in collected fluid samples from Vulcano

| Sample Number | Sample Description | $Hg^0$ |
|---------------|--------------------|--------|
| | | pM |
| V36 | Background (Vulcano) | 0.98 |
| B-B-06 | Bambino | 7.27 |
| V29 | White Patch 10 cm | 5.33 |
| V30 | Subaerial low-Cl | 1.52 |
| V25 | Tidal Cave | 3.3 |
| V26 | Submarine Cave | 2.58 |

MeHg was analyzed by species-specific isotope dilution-gas chromatography-inductively coupled plasma-mass spectrometry (SSID-GC-ICP-MS) (Brombach et al., 2015). A 100 mL sample was spiked with a solution of Me201Hg (ISC Science, Spain) and left standing for an hour for equilibration. An optimal ratio of 4.25 for Me201Hg in the spike to Me202Hg in the sample was the aim of the spiking. Based on the assumption that 5 % of THg was present as Me201Hg, the amount of the enriched isotopic solution was calculated for the initial spiking. An addition of 5 mL of a 1 M acetic acid – acetate buffer at pH 3.9, prepared from trace metal grade acetic acid (Fisher Scientific) and 30 M NaOH (Suprapur, Merck), was added to the sample, and the pH was adjusted to 3.9 with sodium hydroxide (30 M, Suprapur, Merck). Subsequently, 1 mL propylation reagent (1 g sodium tetrapropylborate ;Merseburger Spezialchemikalien, Germany) in 100 mL oxygen-free Milli-Q water was added to the

sample followed by 200 μL n-hexane (Reagent Grade ACS, Riedel-de-Haen). The Hg species were extracted into the n-hexane phase by shaking for 10 min, and the n-hexane phase was analyzed using a Thermo Scientific Trace 1300 GC coupled to a Thermo Scientific Element 2 ICP-MS. A cyclonic spray chamber was attached to the transfer line just before the ICP torch for wet plasma conditions giving the option of plasma tuning and monitoring with an internal Thallium standard. General settings of the GC and the ICP-MS can be found elsewhere (Brombach et al., 2015).

Gas samples were collected into Tedlar© bags using a custom-built glass funnel connected to Teflon tubing in combination with a standard underwater lift bag. The lift bag was attached to lead weights which enabled the calculation of the gas volume collected, i.e., the volume of gas needed to displace enough seawater to lift the bag at a given depth and lead weight. In some instances, gas point sources were located at depths too shallow to use the lead weights. In these instances, gas sample bags were filled as much as possible without damaging the sample bag. H2S was removed from the gas in an alkaline trap, to prevent the formation of HgS within sample vials. The sample was then trapped in 0.5 M permanganate solution in 2 N sulfuric acid and analyzed by CV-AFS as THg (Brombach and Pichler, 2019).

Anions were analyzed using a Metrohm 883 Basic IC plus instrument fitted with a 5 μL injection loop and a Metrosep A Supp5 (150 × 4.0 mm; 5 μm) column for anion separation in combination with a mobile phase consisting of 3.2 mmol / L Na2CO3 (Analytical reagent grade, Fisher Scientific) and 1.0 mmol / L NaHCO3 (puriss. p.a., ≥ 99.7 %, Sigma-Aldrich). Quality control was assured with an internal laboratory standard and the artificial seawater standard IAPSO. Major cations were measured by inductively coupled plasma-optical emission spectrometry (ICP-OES) using a Perkin Elmer Optima 7300 DV instrument. Quality control was assured by using the EnviroMAT Groundwater Low (ES-L-2) and High (ES-H-2) standards and a certified seawater (CRM-SW, High Purity Standard). Trace elements were analyzed by inductively coupled plasma-mass spectrometry (ICP-MS, Element 2 Thermo Scientific). Quality control was identical to that of the ICP-OES measurements.

The flux (pmol / m2 / h) of $Hg^0$ to the atmosphere from each of the sampling sites was calculated using the equations by Liss and Slater (1974) (1) and Wanninkhof (1992) (2), as implemented by Wängberg et al. (2001), where DGM is the dissolved gaseous Hg concentration, TGM is an approximate gaseous Hg

concentration for the area of Sicily as field blank values were below detection limits (10.86 pmol / m3 (Kotnik et al., 2014)), kw (cm / h) is the gas transfer velocity, u10 is the wind speed at 10 m height, ScHg is the Schmidt number for Hg in seawater and ScCO2 is the Schmidt number for CO2 in seawater (Kuss et al., 2009), and H' is the dimensionless Henry's law constant as calculated by Clever et al. (1985) (3). An approximate value was used for atmospheric Hg (7.5 pmol / m3), and the percent volatile $Hg^0$ was assumed to be 10 % of Hgdiss in seawater samples (Horvat et al., 2003). Schmidt numbers 689 for Hg and 660 for CO2 were used.

$$Flux\ to\ the\ Atmosphere = k_w\ (DGM - {}^{TGM}/_{H'}) \tag{1}$$

$$k_w = 0.31\ u_{10}^2\ ({}^{Sc_{Hg}}/_{Sc_{CO2}})^{-0.5} \tag{2}$$

$$H' = \exp\left(\frac{-4633.3}{T_w} + 14.53\right) \tag{3}$$

## 4.3. Results

### 4.3.1 Seawater

In general, the surface water samples of Baia di Levante, outside of the mud bath area (MB), had similar concentrations of cations, anions, and metals as background seawater (Appendix 1). Significant deviations were observed in samples from areas with visible hydrothermal influences. These variations included a lower pH and elevated concentrations of SO4, Si, H2S, Sr, Mn, THg, and Hgdiss (Fig. 4.3 and 4.4). Among the surface water samples outside MB, a positive linear trend was observed between THg and Hgdiss (Fig. 4.5). The samples within the Vulcano Port area (V04 to V06, V10 to V12, and V16 to V17) were not included within the surface maps to improve data visualization.
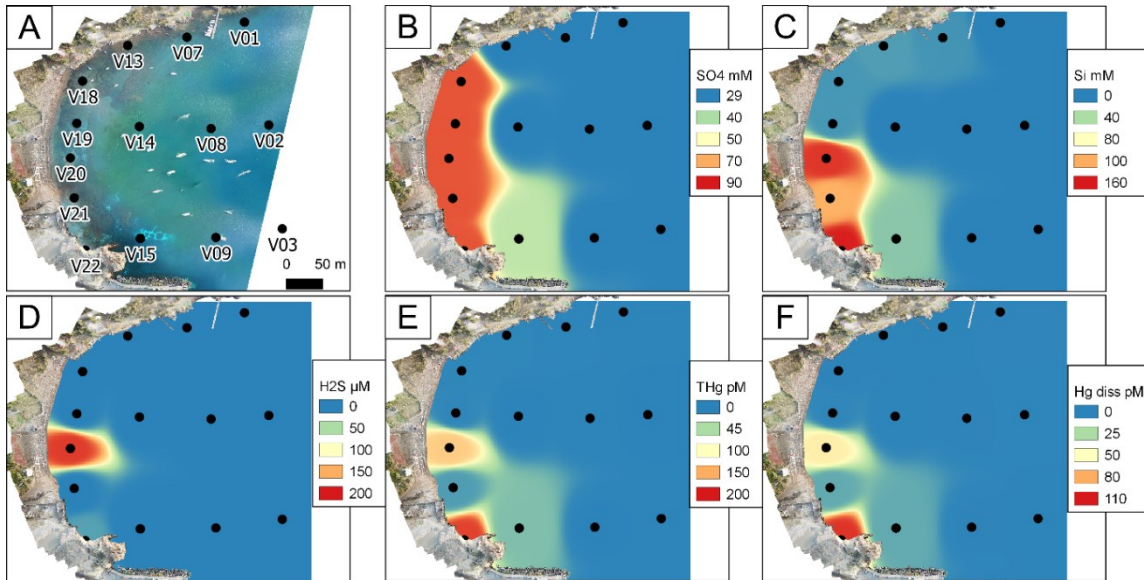
Figure 4.3: Surface water maps of 2019 data of A) sample locations, B) SO4 (mM), C) Si (mM), D) H2S (µM), E)THg (pM), and F) Hgdiss (pM). Maps were generated in QGIS. For mapping purposes, values below detection limits were replaced with 0. Distance coefficient (P) was 6.5. Output raster size was 1026 by 2019.
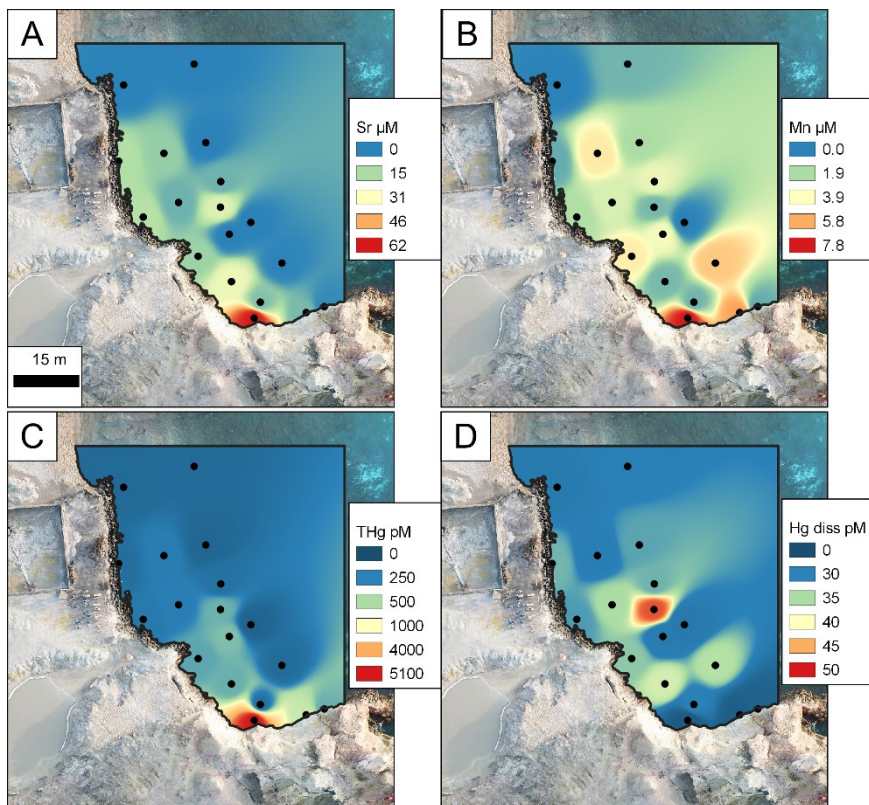


Figure 4.4: Surface seawater water concentrations for September 2021 within the MB area of A) Sr (µM), B) Mn (µM), C) THg (pM) with extreme concentration gradient (3 m) highlighted by white points, and D) Hgdiss (pM). Maps were generated in QGIS. For mapping purposes, values below detection limits were replaced with 0. Distance coefficient (P) was 5. Output raster size was 1000 by 986.

## 4. Hg in the hydrothermal fluids and gases in Baia di Levante, Vulcano, Italy

In MB, high THg concentrations were observed in seawater and gas samples (Fig. 4.4). Samples taken at the orifices of two-point sources (Rock Boulder (V43) and Shore Sample (V42)) near the beach contained up to 2800 pM THg and 270 pM Hgdiss in 2019 (Appendix 3) with over 1800 nmol / $m^3$ $Hg^0$ in the emitted gas phase. Surface water samples above the point sources (V17 and V18, respectively) were higher than the surrounding surface water samples (Appendix 1). Hgdiss concentrations were lower closer to shore near the rocky outcropping and higher in areas of gaseous point source activity.

To the east of MB, white mats were observed. There, concentrations of THg in the gases were low (5 to 7 nmol / m3) (Table 4.1), while pore fluids were low to high in THg (7 to 276 pM) and Hgdiss (0 to 7 pM) (Appendix 1). A significantly lower pH (pH 6.7) than that of seawater (pH 8.1) was observed above the white mats at location V15. Three vertical water column samples were collected at that station. The concentration of THg decreased substantially from 71 pM at the surface (V34) to 5 pM at a depth of 3 m (V33) and 3 pM at a depth of 5 m (V32).
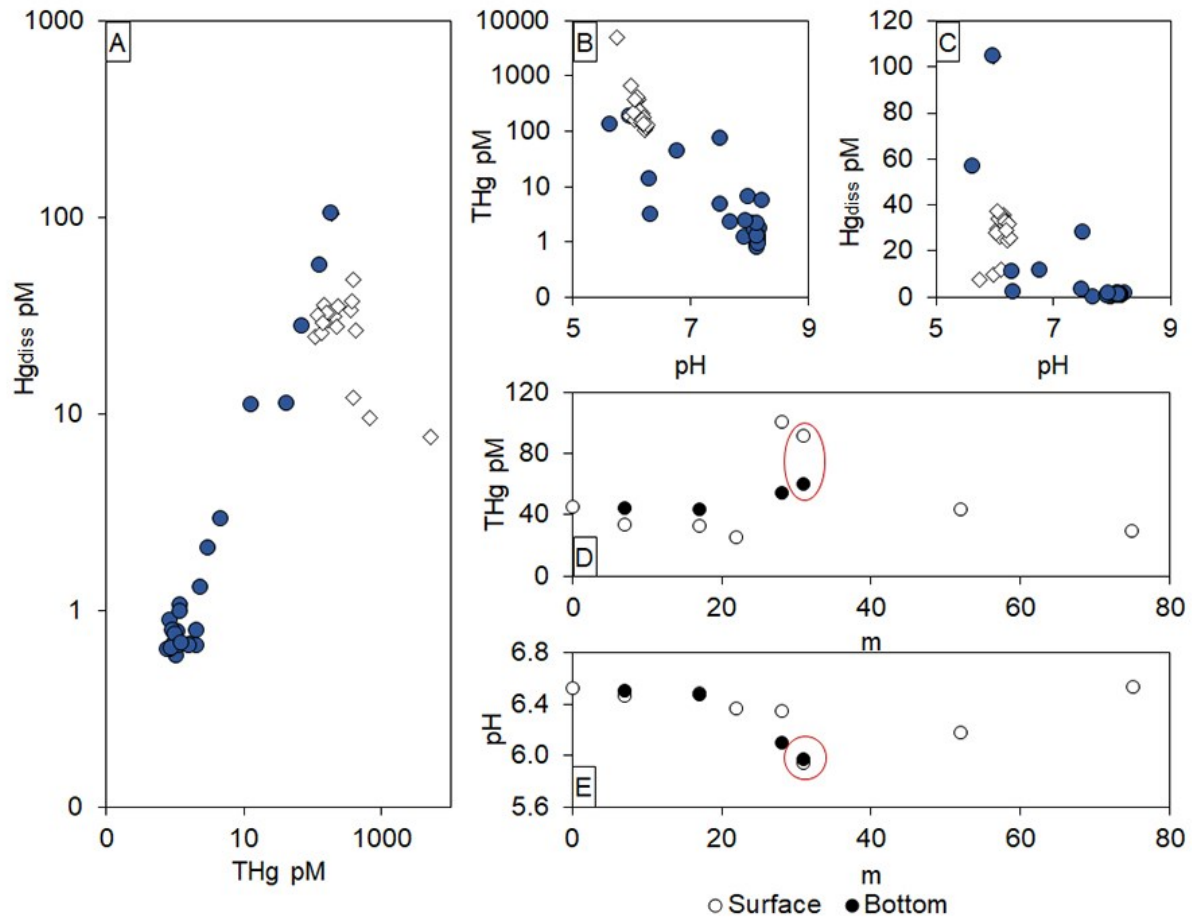
Figure 4.5: Seawater (blue circles) and MB (white diamonds) concentrations of A) THg (pM) vs Hgdiss (pM), B) THg (pM) vs pH, C) Hgdiss (pM) vs pH. Bambino transect with distance (m) from shore. D)THg (pM) and E) pH. The location of Bambino is circled in red.

Flux to the atmosphere was estimated at each surface site and ranged from 0.1 to 19.6 pmol / m2 / h1 in 2019 (Appendix 2). Estimations for the MB area ranged between 1.4 and 9.0 pmol / m2 / h1. Emission rates were highly dependent on Hgdiss concentrations. This is not necessarily surprising, as other factors affecting emission rates (wind speed, atmospheric Hg concentration, etc.) were considered the same for all sites.

The Bambino gaseous point source contained 113 nmol / m3 Hg at high tide and 122 nmol / m3 at low tide in 2019 and 120 nmol / m3 in 2021 (Table 4.1). It should be noted that the Bambino site was too shallow to use lead weights to determine the gas collection volume. Due to the potential for sampling error, those two values were considered the same for both low and high tide and 2019 and 2021.

## 4. Hg in the hydrothermal fluids and gases in Baia di Levante, Vulcano, Italy

An emission rate was measured at the Bambino site. A 2 L graduated cylinder was filled with seawater and placed over the point source. The rising gas displaced the seawater from the cylinder, with the timing of full displacement indicative of an emission rate. However, gas emissions exceeded 2 L / s when approximations were attempted. The cylinder overflowed with gas immediately. Therefore, a minimum of 2 L / s was established for calculation purposes. Under these assumptions, Bambino contributed 235 pmol / s of Hg to the area on average. In surface waters directly above Bambino (V20), 131 pM THg was observed in 2019, with 56 pM as Hgdiss (Appendix 1). A sample of $Hg^0$ from surface waters was taken above Bambino in 2021 with a concentration of 7.3 pM (Table 4.2), with THg 92 pM (Appendix 1). The resulting flux to the atmosphere using the $Hg^0$ concentration was estimated at 13.6 pmol / m2 / h1.

A surface and bottom water transect, including Bambino (B-S-06 and B-B-06), were completed at ebb tide (Appendix 1, Fig. 4.5). Additional samples were taken on separate days (B-01 and B-02). Surface water samples only were collected at stations where the depth was too shallow (B-S-01 and B-S-04) or too deep to sample without diving equipment (B-01 and B-02). Concentrations of THg ranged from 33 and 101 pM at the surface and 43 to 61 pM at depth. The concentrations of THg were highest directly above or adjacent to Bambino in the surface waters. Bottom water concentrations were similar to surface water concentrations at stations B-S-02 and B-S-03 but were significantly less than surface waters at B-S-05 and B-S-06. Temperatures were the same for all samples except for B-01 and B-02. Values of pH decreased with proximity to Bambino.

### 4.3.2 Pore fluids

In general, pore fluid samples had a lower pH, higher temperature, elevated concentrations of Ca, K, Li, Mn, Si, H2S, THg, and Hgdiss, and lower concentrations of Cl, Br, Na, and Sr than the background sample (Appendix 3). No linear relationship was observed between THg and Hgdiss. The tidal cave (V25 and F-01) was depleted in Cl, Br, Mg, Na, and Sr but contained elevated concentrations of THg, Si, Fe, and SO4. The two additional point sources on the rocky outcropping on the port side (F-02 and F-03) were similar in anion and cation concentration to the tidal cave, but with higher As (0.5 and 1.3 μM), lower THg (27 and 26 pM) and Hgdiss (6.5 and 5.5 pM) concentrations. The shore sample contained depleted but near background

69

concentrations of major constituents. However, concentrations of THg, Hgdiss, Si, and Li were elevated. An onshore subaerial site (V30) was sampled during an ebb tide. The chemical composition of V30 was depleted in major constituents, acidic, and elevated in Si and THg. Gas concentrations of Hg were low (3 nmol / m3).

The LF samples contained hot, acidic fluid with close to background concentrations of major constituents. THg and Hgdiss were elevated in all samples but highest in the sample with no Fe or H2S. The fluid of V27 was similar to the La Fossa Submarine Cave sample (V26), except for higher As concentrations (3.3 µM). Si concentrations were high in all samples. A similar chemical composition was observed for a nearby submarine point source (V26).

A five-point transect was completed in 2019 of porewaters within the white mat area. Each sample represented different environmental conditions: seagrass (V37), sand (V38), a dense white mat (V39), bubbling sand (V40), and a sparse white mat (V41). Each sampled location showed differences in chemical composition (Appendix 3). Metals and metalloids (Fe, Mn, Si, Hg, As) and H2S were elevated relative to seawater in bubbling and white mat samples. However, Mg was not depleted. The sample named 'seagrass' was near white mat activity; however, the chemical composition was similar to seawater except for elevated THg and Si.

### 4.3.3 Sediments

Sediments were collected as general representations of background (Black Beach, 0.03 nmol / g), the MB area (MB-15, 2.4 nmol / g), and an active point source (B-Bowl, 49.5).

### 4.3.4 Gases

Gases were collected from point sources onshore, nearshore, and the white mat area (Table 4.1). Concentrations ranged from 3 nmol / m3 onshore, 113 to 1817 nmol / m3 in nearshore samples, and 5 to 7 nmol / m3 in white mat samples.

### 4.3.5 Speciation

Neither MMHg nor DMHg was detected in the fluids from point sources of the Vulcano MSWHS. Measurements of volatile Hg ranged in concentration from 0.98 to 7.27 pM. $Hg^0$ pM

### 4.3.4 Chloride ratios

Ratios of conservative elements (e.g., Cl, Na, Mg, Ca, K) follow linear trends in seawater, with changes in concentration due primarily to mixing with fresh water. Hydrothermal and seawater samples were distinctly different with respect to conservative elements (Fig. 4.6). The seawater and MB samples generally followed a linear trend between Na and K when normalized to Cl, while hydrothermal pore fluid samples did not (Fig. 4.6B). High THg concentrations in hydrothermally influenced samples were associated with lower Mg / Cl and K / Cl (g) ratios (Fig. 4.6B and 4.6C).
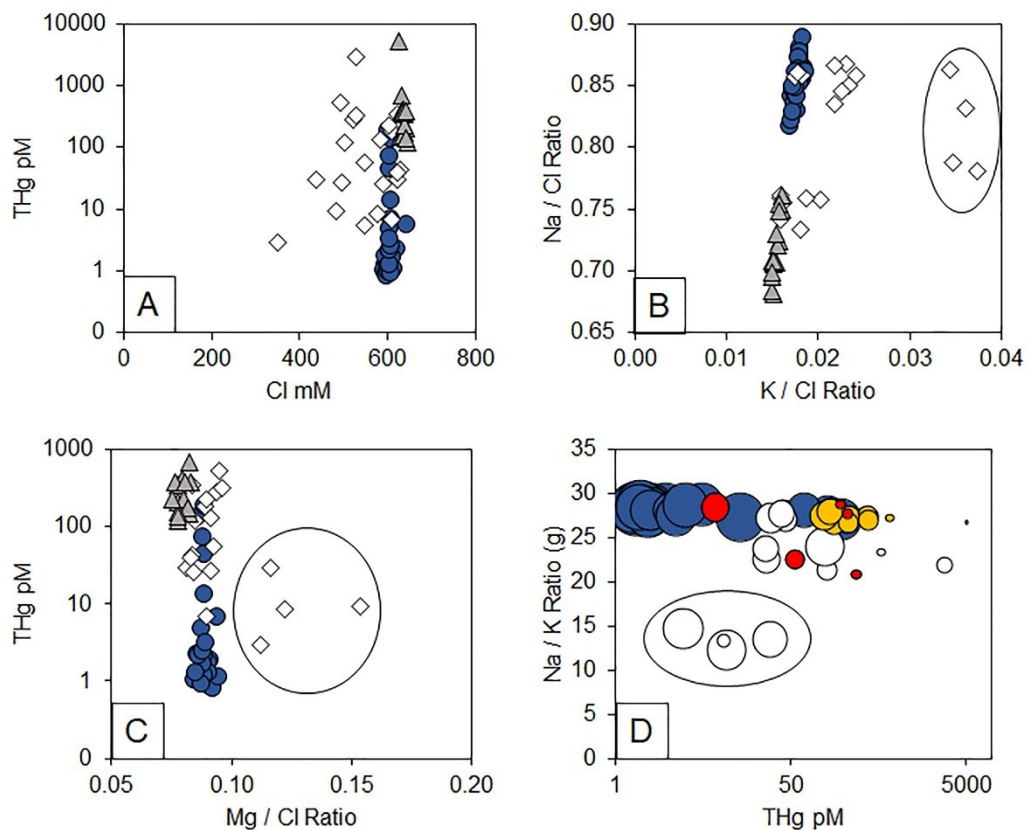


Figure 4.6: Plots of hydrothermal (white diamonds), MB seawater (grey triangles), and seawater (blue circles) samples. LF samples are circled. A) THg (pM) vs Cl (mM), B) Na / Cl vs K / Cl ratio, C) THg (pM) vs Mg / Cl ratio, D) Na / K ratio (mg) vs THg (pM) in seawater (blue), hydrothermal (white), white mat area (red), and MB (yellow), with bubble size indicating percent THg as Hgdiss.  MB samples contained greater THg concentrations compared to seawater throughout Baia di Levante but maintained Na and K linear mixing trends. Hydrothermal samples did not show linear mixing trends.

## 4.4. Discussion

### 4.4.1 Overview

The enrichment of Hg in surface water samples in Baia di Levante was due to intense and shallow hydrothermal activity (Fig. 4.7). Fluxes of fluids and gases containing high concentrations of Hg relative to background concentrations mix with overlying seawater upon emission. However, due to the buoyancy of the warm fluid, significant concentrations of Hg accumulated in the surface waters. Removal of Hg from Baia di Levante included flux to the atmosphere from fluids, sedimentation due to changing redox conditions and temperature (see 4.2), and dilution and transport in the water column.
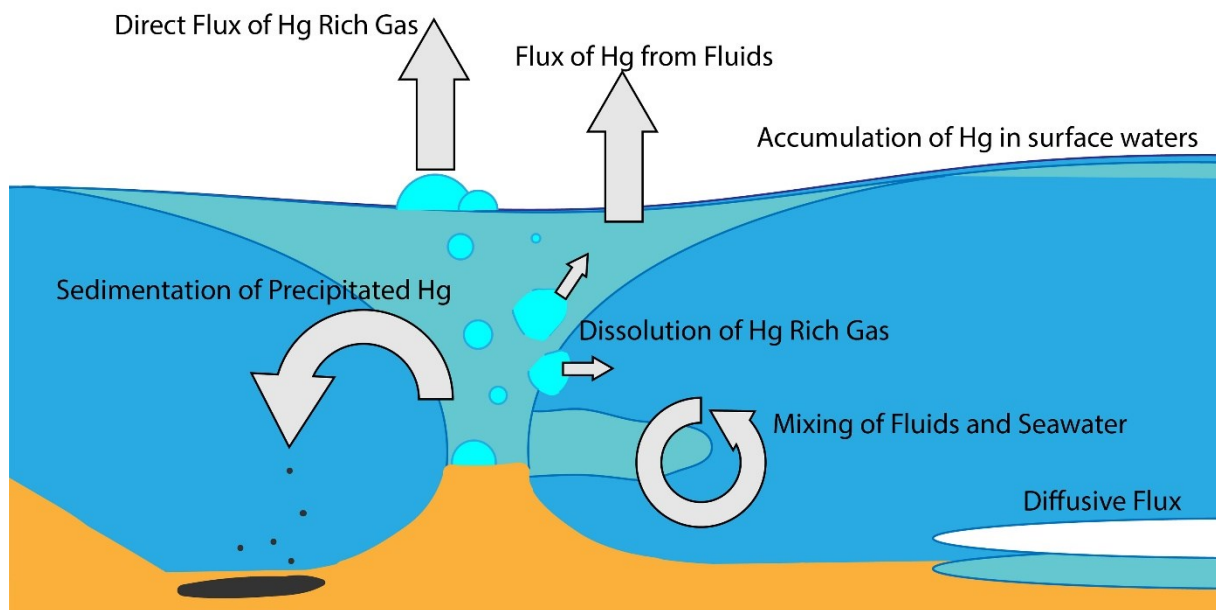


Figure 4.7: Schematic of Hg cycling from Vulcano point sources. Fluxes of fluids mix with the surrounding seawater, however due to the buoyancy of the warm fluid, significant concentrations of Hg accumulate in the surface waters. Due to changes in temperature and redox conditions, Hg may also precipitate from the water column. Gaseous Hg species may partially or fully dissolve in the water column during their ascent to the surface. In cases of shallow depth and high rates of gas emission, gaseous Hg may primarily be emitted to the atmosphere. For the Vulcano system, diffusive fluxes did not appear to play a large role in Hg accumulation within surface waters.

### 4.4.2 Hg in Bahia di Levante Seawater

The dominant source of THg to the surface water in Baia di Levante was the accumulation of buoyant hydrothermal fluid. This was demonstrated by water column

## 4. Hg in the hydrothermal fluids and gases in Baia di Levante, Vulcano, Italy

samples collected at V15, the Bambino transect (Fig. 4.5), and was previously established for other systems and metals (Pichler et al., 2019; Pichler et al., 1999b; Roberts et al., 2021). Alternative sources of Hg to Baia di Levante (anthropogenic influences and atmospheric deposition) were not significant compared to the MSWHS discharge. Increases in THg concentrations in proximity to the coast, and therefore human activity, were observed (Fig. 4.3). However, these enrichments were associated with hydrothermal activity. In areas with increased boating activity and fewer hydrothermal influences, THg values were equivalent to or below background values. Atmospheric deposition is known to generate supersaturated concentrations of Hg in the ocean surface and mixed layer waters due to $Hg^0$ oxidation (Fitzgerald et al., 2007). However, the magnitude of supersaturation due to atmospheric deposition was found to be comparatively low in the Mediterranean (e.g., Cossa et al., 1997a; Horvat et al., 2003). In addition to physical proximity to hydrothermal sources, elevated Hg concentrations were observed together with elevated concentrations of As, deviation from linear mixing patterns of cations and anions (Fig. 4.6), and a lower pH than background seawater. These factors are commonly associated with hydrothermal activity (e.g., Khimasia et al., 2021; Pichler et al., 1999b; Pichler et al., 1999c; Price et al., 2013a; Roberts et al., 2021). The mobilization of As by hydrothermal systems due to changing redox conditions is well established (Pichler et al., 1999b; Price and Pichler, 2005) and both As and Hg belong to the "epithermal suite" of elements (Au, Ag, Te, Se, Hg, As, Sb, and Tl) (Berger and Eimon, 1983; Saunders and Brueseke, 2012; Saunders et al., 2008). The grouping is generally controlled in their similar behavior by two main properties: (1) they are all soft Lewis acids and therefore form covalent bonds with soft Lewis bases, and (2) they have similar volatility resulting in their liberation from the mantle. Several studies identified enrichments of epithermal suite elements in MSWHS (Gamo and Glasby, 2003; Johnson and Cronan, 2001; McCarthy et al., 2005; Prol-Ledesma et al., 2004; Roberts et al., 2021) and following mixing with seawater, hydrothermally derived As and Hg have been shown to accumulate in surface waters (Pichler et al., 2019; Pichler et al., 1999b; Roberts et al., 2021). Therefore, elevated concentrations of THg and Hgdiss were considered to be caused by the hydrothermal activity in Baia di Levante.

The fate of Hg from the MSWHS of Baia di Levante is strongly tied to surface water conditions because, due to hydrothermal fluid buoyancy, Hg accumulates at

73

the surface and is potentially transported over large distances. For example, Leal-Acosta et al. (2013) reported dissolved Hg at a significant distance (km) away from hydrothermal sources in the Gulf of California. Elevated Hg$_{diss}$ concentrations in Baia di Levante, which trended positively with THg in surface waters outside of MB (Fig. 4.5), indicated the potential for transport and biological uptake. However, the surface water concentrations of Hg in Baia di Levante did not mirror the extent of other hydrothermal indicators (e.g., SO4 and Si, see Fig. 4.4). Despite high concentrations of THg and Hg$_{diss}$ in surface waters directly above or adjacent to point sources (e.g., MB-01), surface waters decreased in THg from 5110 pM to 164 pM over a distance of less than 5 m (Fig. 4.4). In contrast, Hg$_{diss}$ increased from 7.6 pM to 29.8 pM. Additionally, a negative trend was observed between pH and THg and Hg$_{diss}$ (Fig. 4.5). With an increasing seawater pH, the adsorption of Hg onto particles is enhanced, specifically for clay minerals and iron oxyhydroxides (Anderson, 1979). The sedimentation of particles, as previously discussed for other submarine and subaerial systems (e.g., King et al., 2006; Leal-Acosta et al., 2010; Roberts et al., 2021), would result in a reduction of THg in addition to Hg$_{diss}$ due to sedimentation. Sediment collected in the MB (2.42 nmol / g) and Bambino (49.52 nmol / g) areas reflected this process when compared to sediment collected within Black Beach (0.03 nmol / g). A previous study of a subaerial system showed a similar pattern, where THg concentrations rapidly declined away from hydrothermal sources, with amorphous S precipitates dominating removal (King et al., 2006). In accordance with those findings, surface waters above the MSWHS in Bahia di Levante could be considered a reservoir of THg and, therefore, may play a crucial role in the ultimate fate of Hg discharged from any MSWHS.

The MSWHS in Baia di Levante discharged large volumes of hydrothermal gases, which rapidly percolated through the water column and into the atmosphere. Therefore, gas emissions from this system directly affected the overlying water through bubble dissolution and the atmosphere through evasional and ebullitive flux (Fig. 4.7). Previous studies indicated efficient dissolution of gases in deep and shallow waters (e.g., McGinnis et al., 2011; Zhao et al., 2016), and Pichler et al. (1999a) highlighted the impact of gases on water chemistry and sedimentation. The highest calculated atmospheric flux of Hg to the atmosphere from surface waters (19.6 pmol / m2 / hr) was significantly higher than that observed by Roberts et al. (2021) for the Milos MSWHS (2.7 pmol / m2 / hr) but not as high as the flux

## 4. Hg in the hydrothermal fluids and gases in Baia di Levante, Vulcano, Italy

calculated by Bagnato et al. (2017) for the Panarea MSWHS (45 pmol / m2 / hr). While not intended to provide precise evasional flux measurements, the calculation illustrated the magnitude of hydrothermal impacts on surface waters with distance from point sources. Significant differences were observed in the surface waters of Baia di Levante. The highest were near, or directly above, shallow point sources. The Hg in hydrothermal gases is presumed to be $Hg^0$ (Brombach and Pichler, 2019). Bambino represents an ideal point source to study, with a high volume of gas output at a shallow depth where evasional and ebullitive flux are potentially significant. However, only 43 % of the THg was Hgdiss above Bambino, and less than 10 % of Hgdiss was $Hg^0$. After a distance of 9 m to the west and 21 m to the east of Bambino, the THg concentrations in surface water were reduced to 28 % and 48 % of the Bambino surface water concentration. This result was surprising, given the numerous point sources at a lower depth east of Bambino (Fig. 4.2F). The formation of bound Hg species was likely due to oxidative reactions, which rapidly reduced Hgdiss away from point sources. The rapid (first-order rate constant k = 0.1 $hr^{-1}$) oxidation of $Hg^0$ before reaching surface waters is expected to be driven by photochemical reactions and enhanced with the presence of Cl (Amyot et al., 1997; Lalonde et al., 2001). The oxidation of $Hg^0$ to $Hg^{2+}$ prevented the evasion of dissolved $Hg^0$ to the atmosphere and, thus, preserved Hg in seawater.

It should be noted that sample B-S-05, located 3 m west of Bambino, was higher in THg concentration than B-S-06 taken directly above Bambino in the bubbling area. Two scenarios could account for this phenomenon. First, transport away from Bambino during ebb tide would result in overall eastward movement of surface waters, although the distance between the stations was minimal. Displacement and mixing due to Bambino itself or anthropogenic activities (e.g., boating activities) could account for an increase in concentrations adjacent to the point source. This scenario is less likely, as the pH is lowest at the Bambino site, with a significant difference between the surface and bottom waters pH at B-S-05. This is despite the higher THg concentrations in the surface water samples than in the bottom water samples. Second, the slight decrease in concentration at B-S-06 could be due to intense bubbling directly above the point source. The decrease was approximately equal to the concentration of $Hg^0$ at B-S-06, which was taken less than 1 m away from the bubbling area. While oxidation of $Hg^0$ is expected to be efficient at

75

this location, $Hg^0$ present in surface seawater would be expected to be transferred to the atmosphere due to wind and bubbling.

### 4.4.3 Source of Hg

The MSWHS on Vulcano is thought to be fed by a combination of meteoric water, seawater, magmatic water, and a boiling aquifer beneath the bay (Aiuppa et al., 2020; Federico et al., 2010; Fulignati et al., 1998; Inguaggiato et al., 2012; Madonia et al., 2015; Oliveri et al., 2019). The boiling aquifer resulted in a Hg-rich vapor phase that was the primary contributor of Hg to the system. Hg concentrations in groundwaters and subaerial fumarole gases on Vulcano are linked to magmatic and hydrothermal origins (Aiuppa et al., 2007; Bagnato et al., 2009; Nuccio et al., 1999; Paonita et al., 2002; Zambardi et al., 2009). Bagnato et al. (2009) concluded that the THg found in Vulcano groundwaters was of hydrothermal origin and transported as $Hg^0$ in a vapor phase and oxidized to $Hg^{2+}$ in shallow groundwaters. A similar scenario, i.e., a Hg-rich vapor as the source for Hg in the Bahia di Levante MSWHS should also be likely. Low-Cl, high THg hydrothermal fluids are discharging in Baia di Levante (Fig. 4.6A), which would indicate the condensation of a hydrothermal vapor low in Cl, but enriched in Hg. The white patch area, where diffuse fluid flow and limited gas emission are present, also revealed higher THg concentrations in pore fluids at or below background Cl concentrations.

In a previous study, Roberts et al. (2021) described the MSWHS on the island of Milos with regard to Hg concentrations. There, elevated THg was associated with high Cl and low Na / K ratios, which indicated a greater arc-magmatic input coupled with fast ascension rates. This result was surprising, given the volatility of Hg and its association with the hydrothermal vapor phase in the subsurface (Barnes and Seward, 1997; Varekamp and Buseck, 1984). In contrast to the Milos system, the Hg concentrations of the MSWHS of Baia di Levante were associated with low-Cl fluids, a more intuitive result given the above. The presence of Hg, and its association with major elements, is descriptive of significant subsurface properties and processes. The proposed subsurface reactions can be supported by the relative concentrations and behavior of Hg in comparison to major elements. This study supports previous work associating localized elevated environmental Hg concentrations in the areas surrounding hydrothermal systems (Leal-Acosta et al., 2018; Leal-Acosta et al., 2010; Prol-Ledesma et al., 2004; Roberts et al., 2021). In particular, this study and Roberts

et al. (2021) emphasize the importance of sampling both fluids and gases from MSWHS. In two distinct sampling areas with notably different subsurface processes, the concentrations of THg, Hgdiss, and Hggas demonstrate reactions in the shallow subsurface. These reactions played a crucial role in Hg emissions from MSWHS and potential further transport.

Volatile species constituted a considerable portion of Hgdiss in some samples (Table 4.2). This finding further supports hydrothermal vapor as the primary Hg source in this system. The $Hg^0$ concentrations increased linearly with increasing temperature (Fig. 4.8). Similarly, pH decreased with increasing temperature. While not definitive, temperature and increasing acidity indicate hydrothermal activity (e.g., Khimasia et al., 2021; Roberts et al., 2021). Longer, slower transport increases the potential for redox reactions and therefore changes in speciation, particularly for the white mat and sedimented areas (Hsu-Kim et al., 2013; Roberts et al., 2021). The hotter, more acidic fluid may indicate a more direct, less seawater diluted hydrothermal gas and fluid flow. Higher $Hg^0$ concentrations would reflect greater proportions, or faster ascension of, the hydrothermal vapor phase. In one instance (V26), the volatile measurement exceeded Hgdiss concentrations. This result may be from measurement error or the result of volatile species bound to particulates (Wang et al., 2015).
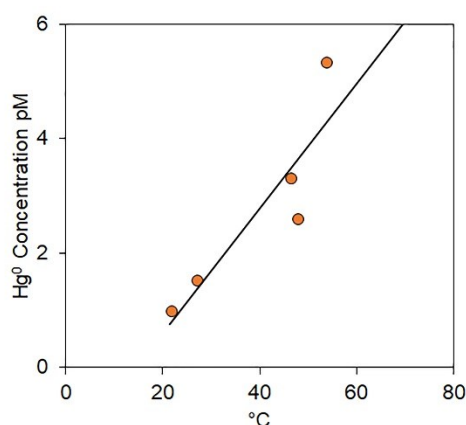


Figure 4.8: Plot of $Hg^0$ (pM) and temperature (°C)

## 4.4.4 White Mat Area

The hydrothermal white mat areas did not contribute significantly to THg concentrations in Baia di Levante. While the pore fluids concentrations of THg were

generally high (Appendix 3), the evidence did not support significant diffusive transport to the overlying water column. White mat areas have previously been found to affect Hg concentrations in the gas streams of MSWHS through subsurface removal of Hg species (Roberts et al., 2021). The white mat area of Baia di Levante was the only sedimented area where gases were measured (V29, V39). Gas flow was low, and Hg concentrations were between 5 and 7 nmol m-3 (8). Nearby (V15) water column measurements at depths of 2.7 m and 5.4 m did not indicate vertical transport as a significant contributor to surface concentrations. Additionally, the Na / K ratios of the white mat area fluid samples indicated slower ascension rates through the subsurface (Fig. 5.6D) (Khimasia et al., 2021; Nicholson, 1993; Roberts et al., 2021). Slower ascension rates were previously hypothesized to reduce THg concentrations in gases and fluids through HgS formation in the subsurface (Roberts et al., 2021). Contributions of the white mat area were therefore not significant to surface concentrations due to limited surface area in Baia di Levante and lack of vertical transport.

**4.4.5 Bambino**

The point sources responsible for elevated Hg concentrations in Baia di Levante surface seawater were not necessarily those with the highest Hg concentrations. The intensity and volume of flow were also important factors. The Bambino point source had less Hg in the gas phase (113 to 121 nmol / m3) than the MB point sources (1800 pM) but at the same time had a higher emission rate. A nearby smaller point source (Mini-Bambino) emitted gases with a higher Hg concentration (281 nmol / m3), however, it emitted significantly less gas volume than Bambino. Further east of Bambino, several small point sources emitted gases at 2 m depth (Fig. 4.2F). Despite the larger overall number of point sources east of Bambino, the surface water concentrations of THg were highest near Bambino. The THg concentrations observed in the 2021 transect decreased from 92 pM to 26 pM over a distance of 9 m towards the shoreline and to 44 pM over a distance of 21 m to the east. Despite many point sources with elevated THg concentrations (342 pM THg, VB-7B, surface water concentrations were not higher than concentrations observed closer to shore. Additional water depth led to two significant differences. First, water depth increases the dilution of hydrothermal fluids and gases by increasing the water volume between sources and the surface. Second, there is additional potential for the

removal by precipitation and sedimentation, since fluid and gas are exposed to oxygenated seawater and photochemical reactions for a longer period before reaching the surface (Davey and van Moort, 1986; Lalonde et al., 2001 ). Therefore, despite lower concentrations of Hggas than MB point sources, the Bambino area significantly impacted surface water concentrations of THg and Hgdiss (56 pM), as well as pH (Fig. 4.5).

Bambino was estimated to output 235 pmol / sec Hg, with a surface water atmospheric flux of 25 pmol / m2 / h. As a primarily gaseous point source (e.g., Fig. 4.2E), a surprisingly significant portion of THg was bound to particulates in the fluid sample in 2019 (75 pM). Despite high Hgdiss concentrations in 2019 (56 pM), $Hg^0$ was only 7.3 pM when measured in 2021. Amyot et al. (1997) estimated $Hg^0$ loss due to oxidation as roughly half of the flux to the atmosphere at a depth of 1 m. This rate of oxidation would account for the high Hg concentration bound to particulates despite a source enriched in $Hg^0$. The emission of THg from Bambino is 10-times the rate of flux from the seawater surface to the atmosphere. This leaves a significant portion of THg not accounted for. If all THg from Bambino remained within the water column, concentrations of THg in B-S-06 would exceed 1 nM in five minutes despite the flux of Hgdiss from the surface to the atmosphere. Considering THg concentrations throughout Baia di Levante and the Bambino area (Fig. 4.3 and 4.4), transport away from the site was limited.

Additionally, THg from Bambino affected surface seawater but had little impact on the bottom water concentrations (Fig. 4.5). Therefore, THg emitted by Bambino not accounted for in the surface was likely emitted directly to the atmosphere. The study of oxidation rates at the concentrations and environmental conditions at hydrothermal systems is necessary to support this hypothesis further.

### 4.4.6 La Fossa (LF) Samples

The LF samples (V26, V44-V46) likely originated as condensed vapors from the La Fossa crater, which were transported downslope. This contrasts the Baia di Levante samples, which were likely generated by a boiling hydrothermal aquifer. La Fossa crater gases are a mixture of magmatic water and seawater (Chiodini et al., 1995), and soil temperatures exceed 100 °C with concentrations averaging 12 nmol / m3 Hggas (Aiuppa et al., 2007; Barde-Cabusson et al., 2009; Zambardi et al., 2009). Magmatic vapors condense to form a salt-rich, acidic fluid, which is then transported

and diluted by seawater or groundwater (Madonia et al., 2015; Williams-Jones and Heinrich, 2005). Oxidation of Hg caused by low pH drives speciation to $Hg^{2+}$ and changes in temperature and oxidation remove Hg from solution, particularly at near-surface pressures and temperatures (Varekamp and Buseck, 1984; Williams-Jones and Heinrich, 2005). We propose that the LF samples resulted from mixing between condensed La Fossa crater vapor, meteoric water, and seawater. Notably, the LF samples were below 65 °C. This temperature was previously associated with a turning point of lower THg concentrations on the island of Milos (Roberts et al., 2021). Bagnato et al. (2009) discussed the groundwaters of Vulcano, where increases in THg were associated with SO4 and therefore hydrothermal or magmatic activity. However, the LF samples contain higher cation / anion concentrations and significantly lower THg concentrations than can be explained by mixing between seawater and groundwater. Similarly, the influence of a hydrothermal brine is unlikely. The LF samples do contain high Mn concentrations in comparison to background samples. High Mn is associated with rising hydrothermal brines (Valsami-Jones et al., 2005). Models of the Vulcano system also indicate the existence of a rising hydrothermal brine (Bolognesi and D'Amore, 1993) with the potential to affect groundwaters (Bagnato et al., 2009) and subaerial fumaroles (Chiodini et al., 1995; Di Liberto et al., 2002). However, low Cl coupled with high Li concentrations in these samples does not support this theory.

## 4.5 Conclusions

The Vulcano system highlights the complexity of Hg cycling in MSWHS. The Vulcano system demonstrated the direct influence of gaseous point sources on the Hg concentration in surface waters followed by rapid oxidation. Hg concentrations (THg and Hgdiss) were elevated in Baia di Levante, particularly in the MB area, due to hydrothermal activity as highlighted by water column concentrations, hydrothermal fluid and gas THg concentrations and surface water maps of THg. The area north of Vulcano port and close to shore contained the highest Hg concentrations in fluids and gases. Condensed vapor from La Fossa crater and diffuse venting from white mat areas are unlikely to contribute significantly to surface coastal Hg concentrations for this system. Therefore, the elevated THg in Baia di Levante was due to hydrothermal point sources located in the shallow waters of the bay.

## 4. Hg in the hydrothermal fluids and gases in Baia di Levante, Vulcano, Italy

The Hg present in the hydrothermal system of Vulcano impacts local groundwaters and the coastal waters of Baia di Levante and constitutes a natural source of Hg to the atmosphere. High volumes of gas emissions rich in Hg, coupled with highly elevated localized concentrations of THg and Hgdiss, warrant further investigation, particularly into the sediments and organisms of Baia di Levante.

Appendix 1. Surface water samples from in and outside of Baia di Levante, Vulcano. Updated with missing Bambino bottom water data

| Sample Number | Sample Description | Lat. | Long. | °C | pH | Cl | Br | SO4 | As | Ca | Fe | K | Li | Mg | Mn | Na | Si | Sr | H2S | THg | Hg_diss | Volatile | Sed. |
|---|---|---|---|---|---|---|---|---|---|---|---|---|---|---|---|---|---|---|---|---|---|---|---|
| | | | | | | mM | mM | mM | uM | mM | uM | mM | uM | mM | uM | mM | uM | uM | uM | pM | pM | pM | nmol/g |
| | **2019** | | | | | | | | | | | | | | | | | | | | | | |
| | **Outside Baia di Levante** | | | | | | | | | | | | | | | | | | | | | | |
| V36 | Background (Vulcano) | 38.418 | 14.983 | 22 | 8.11 | 610 | 0.94 | 29 | BDL | 11 | BDL | 10 | BDL | 56 | BDL | 513 | BDL | 99 | BDL | 2 | 1.1 | 0.98 | |
| V23 | WP 100 | 38.407 | 14.976 | 22.7 | 7.69 | 622 | 0.95 | 83 | 4.19 | 11 | BDL | 11 | BDL | 53 | BDL | 516 | 15 | 99 | BDL | 2 | 0 | | |
| V24 | WP 101 | 38.409 | 14.974 | 23 | 7.99 | 611 | 0.94 | 82 | BDL | 12 | 25 | 11 | BDL | 57 | BDL | 527 | 34 | 101 | BDL | 7 | 0 | | |
| V47 | WP102 | 38.424 | 14.952 | 22 | 8.1 | | | | | | | | | | | | | | | 2 | 1.4 | | |
| V48 | WP103 | 38.425 | 14.949 | 22 | 8.13 | | | | | | | | | | | | | | | 2 | 1.6 | | |
| V49 | WP104 | 38.422 | 14.952 | 22 | 8.13 | | | | | | | | | | | | | | | 1 | 1.1 | | |
| V50 | WP105 | 38.419 | 14.955 | 22 | 8.13 | | | | | | | | | | | | | | | 1 | 0.9 | | |
| | **2021** | | | | | | | | | | | | | | | | | | | | | | |
| BB-01 | Black Beach | | | 24 | 8.22 | 646 | 0.95 | 32.15 | | 11 | | 11 | 89 | 55 | | 514 | 1417 | | | 5 | 1.4 | | 0.03 |
| | **2019** | | | | | | | | | | | | | | | | | | | | | | |
| | **Inside Baia di Levante** | | | | | | | | | | | | | | | | | | | | | | |
| V01 | Surface 01 | 38.42 | 14.963 | 23 | 8.14 | 597 | 0.92 | 29 | BDL | 11 | BDL | 11 | BDL | 54 | BDL | 520 | BDL | 101 | BDL | 1 | 1.1 | | |
| V02 | Surface 02 | 38.418 | 14.963 | 23 | 8.13 | 599 | 0.93 | 29 | BDL | 12 | BDL | 11 | BDL | 54 | BDL | 520 | BDL | 101 | BDL | 1 | 0.9 | | |
| V03 | Surface 03 | 38.417 | 14.963 | 22.8 | 8.14 | 595 | 0.91 | 29 | BDL | 11 | BDL | 11 | BDL | 55 | BDL | 524 | BDL | 100 | BDL | 1 | 0.7 | | |
| V04 | Surface 04 | 38.415 | 14.963 | 22.7 | 8.15 | 602 | 0.93 | 29 | 2.86 | 11 | BDL | 11 | BDL | 54 | BDL | 522 | BDL | 101 | BDL | 1 | 0.6 | | |
| V05 | Surface 05 | 38.414 | 14.964 | 22.9 | 8.13 | 599 | 0.92 | 29 | BDL | 11 | BDL | 11 | BDL | 54 | BDL | 517 | 14 | 100 | BDL | 1 | 0.6 | | |
| V06 | Surface 06 | 38.413 | 14.964 | 22.6 | 8.13 | 598 | 0.91 | 29 | BDL | 12 | BDL | 11 | BDL | 55 | BDL | 531 | 18 | 101 | BDL | 1 | 0.6 | | |
| V07 | Surface 07 | 38.42 | 14.962 | 23.3 | 8.17 | 598 | 0.92 | 29 | BDL | 11 | BDL | 11 | BDL | 54 | BDL | 525 | 8 | 102 | BDL | 2 | 0.7 | | |
| V08 | Surface 08 | 38.418 | 14.962 | 23 | 8.16 | 602 | 0.92 | 29 | BDL | 11 | BDL | 11 | BDL | 57 | BDL | 525 | BDL | 101 | BDL | 1 | 0.8 | | |
| V09 | Surface 09 | 38.416 | 14.962 | 22.7 | 8.15 | 602 | 0.92 | 29 | BDL | 11 | BDL | 10 | BDL | 53 | BDL | 510 | BDL | 99 | BDL | 1 | 0.8 | | |
| V10 | Surface 10 | 38.415 | 14.962 | 22.6 | 8.15 | 617 | 0.95 | 30 | BDL | 11 | BDL | 10 | BDL | 52 | BDL | 504 | BDL | 99 | BDL | 1 | 0.7 | | |
| V11 | Surface 11 | 38.414 | 14.963 | 22.6 | 8.15 | 607 | 0.93 | 29 | BDL | 11 | BDL | 11 | BDL | 55 | BDL | 506 | BDL | 96 | BDL | 1 | 1 | | |
| V12 | Surface 12 | 38.413 | 14.963 | 23 | 7.92 | 604 | 0.93 | 29 | BDL | 11 | BDL | 11 | BDL | 54 | 10 | 516 | 52 | 98 | BDL | 1 | 0.7 | | |
| V13 | Surface 13 | 38.419 | 14.961 | 23.4 | 8.05 | 607 | 0.93 | 29 | BDL | 11 | BDL | 11 | BDL | 54 | BDL | 523 | 12 | 100 | BDL | 2 | 0.7 | | |
| V14 | Surface 14 | 38.418 | 14.961 | 22.8 | 8.15 | 608 | 0.93 | 29 | BDL | 11 | BDL | 11 | BDL | 53 | BDL | 519 | BDL | 99 | BDL | 1 | 0.6 | | |
| V15 | Surface 15 | 38.416 | 14.961 | 23.2 | 6.78 | 608 | 0.93 | 83 | BDL | 11 | BDL | 11 | BDL | 54 | BDL | 521 | 18 | 100 | BDL | 43 | 11.3 | | |
| V16 | Surface 16 | 38.415 | 14.961 | 22.4 | 8.1 | 612 | 0.94 | 82 | BDL | 11 | BDL | 10 | BDL | 54 | BDL | 503 | BDL | 96 | BDL | 2 | 0.7 | | |

# 4. Hg in the hydrothermal fluids and gases in Baia di Levante, Vulcano, Italy

Appendix 1. Surface water samples from in and outside of Baia di Levante, Vulcano. Updated with missing Bambino bottom water data

| Sample Number | Sample Description | Lat. | Long. | °C | pH | Cl | Br | SO4 | As | Ca | Fe | K | Li | Mg | Mn | Na | Si | Sr | H2S | THg | Hg_diss | Volatile | Sed. |
|---|---|---|---|---|---|---|---|---|---|---|---|---|---|---|---|---|---|---|---|---|---|---|---|
| | | | | | | mM | mM | mM | uM | mM | uM | mM | uM | mM | uM | mM | uM | uM | uM | pM | pM | pM | nmol/g |
| V17 | Surface 17 | 38.414 | 14.961 | 22.6 | 8.13 | 608 | 0.93 | 82 | BDL | 11 | BDL | 11 | BDL | 52 | BDL | 503 | BDL | 96 | BDL | 1 | 0.7 | | |
| V18 | Surface 18 | 38.419 | 14.96 | 23.1 | 8.13 | 606 | 0.93 | 82 | BDL | 11 | BDL | 11 | BDL | 53 | BDL | 511 | 9 | 98 | BDL | 2 | 0.8 | | |
| V19 | Surface 19 | 38.418 | 14.96 | 23 | 7.94 | 608 | 0.96 | 82 | 5.01 | 11 | BDL | 11 | BDL | 54 | BDL | 518 | 9 | 99 | BDL | 2 | 1.3 | | |
| V20 | Surface 20 | 38.418 | 14.96 | 24.9 | 5.63 | 608 | 0.94 | 82 | BDL | 11 | BDL | 11 | BDL | 52 | BDL | 511 | 148 | 99 | 188 | 131 | 56.3 | | |
| V21 | Surface 21 | 38.417 | 14.96 | 25.7 | 6.31 | 611 | 0.94 | 82 | BDL | 12 | BDL | 11 | BDL | 54 | BDL | 526 | 99 | 100 | BDL | 13 | 11 | | |
| V22 | Surface 22 | 38.416 | 14.96 | 27.2 | 5.97 | 603 | 0.92 | 82 | BDL | 11 | 14 | 11 | BDL | 54 | BDL | 518 | 158 | 98 | 17 | 186 | 104.7 | | |
| V34 | V15: 0 m | 38.416 | 14.961 | | 7.52 | 608 | 0.93 | 29 | BDL | 11 | BDL | 11 | BDL | 54 | BDL | 515 | 18 | 100 | BDL | 71 | 27.9 | | |
| V33 | V15: 2.7 m | 38.416 | 14.961 | | 7.5 | 608 | 0.9 | 29 | BDL | 11 | BDL | 11 | BDL | 53 | BDL | 516 | 10 | 99 | BDL | 5 | 2.9 | | |
| V32 | V15: 5.4 m | 38.416 | 14.961 | | 6.32 | 605 | 0.93 | 29 | 2.95 | 11 | BDL | 11 | BDL | 54 | BDL | 521 | 74 | 99 | BDL | 3 | 2.1 | | |
| | 2021 | | | | | | | | | | | | | | | | | | | | | | |
| MB-01 | Mudbath-Surface 01 | 38.416 | 14.96 | 30.6 | 5.75 | 624 | 0.92 | 33.35 | BDL | 12 | 19 | 11 | 90 | 55 | 8 | 510 | 1 | 62 | | 5110 | 7.6 | | |
| MB-02 | Mudbath-Surface 02 | 38.416 | 14.96 | 28.4 | 5.99 | 632 | 0.93 | 32.03 | BDL | 11 | BDL | 11 | 91 | 56 | 6 | 515 | 42 | 9 | | 677 | 9.6 | | |
| MB-03 | Mudbath-Surface 03 | 38.416 | 14.961 | 28.5 | 6.11 | 631 | 0.93 | 31.74 | 0.41 | 11 | BDL | 11 | 93 | 57 | 1 | 527 | BDL | 1 | | 379 | 12.1 | | |
| MB-04 | Mudbath-Surface 04 | 38.416 | 14.96 | 29.4 | 6.04 | 633 | 0.93 | 31.78 | BDL | 11 | BDL | 11 | 90 | 56 | 1 | 516 | 1058 | 10 | | 164 | 29.8 | | |
| MB-05 | Mudbath-Surface 05 | 38.416 | 14.96 | 28 | 6.15 | 628 | 0.93 | 31.43 | 0.4 | 10 | BDL | 10 | 86 | 52 | 5 | 482 | 54 | 0 | | 146 | 35.7 | | |
| MB-06 | Mudbath-Surface 06 | 38.416 | 14.96 | 29.8 | 6.06 | 637 | 0.94 | 32.07 | BDL | 11 | BDL | 11 | 89 | 54 | 4 | 502 | 25 | 13 | | 351 | 33.9 | | |
| MB-07 | Mudbath-Surface 07 | 38.416 | 14.96 | 29 | 6.09 | 635 | 0.94 | 31.95 | 2.69 | 11 | BDL | 11 | 89 | 54 | 4 | 496 | 25 | | | 417 | 26.5 | | |
| MB-08 | Mudbath-Surface 08 | 38.416 | 14.96 | 28 | 6.21 | | | | | | | | | | | | | | | 107 | 24.8 | | |
| MB-09 | Mudbath-Surface 09 | 38.416 | 14.96 | 30.6 | 6.17 | 642 | 0.96 | 32.29 | BDL | 11 | BDL | 11 | 96 | 55 | 2 | 504 | 52 | 17 | | 207 | 31.4 | | |
| MB-10 | Mudbath-Surface 10 | 38.417 | 14.96 | 30 | 6.14 | 639 | 0.94 | 32.07 | BDL | 10 | BDL | 11 | 90 | 53 | 3 | 493 | 39 | 8 | | 232 | 35.1 | | |
| MB-11 | Mudbath-Surface 11 | 38.417 | 14.96 | 29.1 | 6.19 | 638 | 0.93 | 31.98 | 2.32 | 11 | BDL | 11 | 90 | 55 | 3 | 517 | | 8 | | 175 | 32.7 | | |
| MB-12 | Mudbath-Surface 12 | 38.417 | 14.96 | 30.1 | 6.18 | 635 | 0.93 | 31.89 | BDL | 11 | BDL | 11 | 89 | 56 | 1 | 519 | | 17 | | 158 | 32.9 | | |
| MB-13 | Mudbath-Surface 13 | 38.417 | 14.96 | 31 | 6.02 | 638 | 0.94 | 32.12 | BDL | 11 | BDL | 11 | 91 | 55 | 4 | 507 | | 13 | | 226 | 27.8 | | |
| MB-14 | Mudbath-Surface 14 | 38.417 | 14.96 | 29 | 6.25 | 646 | 0.95 | 32.32 | BDL | 11 | BDL | 11 | 89 | 57 | 2 | 527 | 86 | | | 120 | 31.9 | | |
| MB-15 | Mudbath-Surface 15 | 38.417 | 14.96 | 29 | 6.27 | | | | | | | | | | | | | | | 132 | 25.8 | | 2.42 |
| MB-16 | Mudbath-Surface 16 | 38.417 | 14.96 | 28.6 | 6.2 | 641 | 0.94 | 32.14 | BDL | 11 | BDL | 11 | 90 | 56 | 1 | 517 | | | | 140 | 29 | | |
| MB-17 | Mudbath-Surface 17 | 38.416 | 14.96 | 31.4 | 6.05 | 636 | 0.94 | 32.11 | BDL | 11 | BDL | 11 | 91 | 56 | 1 | 523 | 78 | 28 | | 375 | 37.5 | | |

Appendix 1. Surface water samples from in and outside of Baia di Levante, Vulcano. Updated with missing Bambino bottom water data

| Sample Number | Sample Description | Lat. | Long. | °C | pH | Cl | Br | SO4 | As | Ca | Fe | K | Li | Mg | Mn | Na | Si | Sr | H2S | THg | Hg_diss | Volatile | Sed. |
|---|---|---|---|---|---|---|---|---|---|---|---|---|---|---|---|---|---|---|---|---|---|---|---|
| | | | | | | mM | mM | mM | uM | mM | uM | mM | uM | mM | uM | mM | uM | uM | uM | pM | pM | pM | nmol/g |
| MB-18 | Mudbath-Surface 18 | 38.416 | 14.96 | 31.7 | 5.96 | 641 | 0.95 | 32.44 | 1.76 | 11 | BDL | 11 | 91 | 56 | 1 | 517 | 811 | 25 | | 382 | 48.1 | | |
| B-01 | Near Bambino-01 | 38.418 | 14.96 | 26.7 | 6.18 | 629 | 0.92 | 31.58 | BDL | 11 | BDL | 12 | 92 | 58 | | 546 | 29 | | | 44 | 8 | | |
| B-02 | Near Bambino-02 | 38.418 | 14.96 | 27 | 6.54 | 624 | 0.93 | 31.28 | BDL | 11 | BDL | 12 | 91 | 58 | | 549 | 4 | | | 30 | 8.6 | | |
| B-03 | Near Bambino-03 | 38.418 | 14.961 | 27 | 6.17 | 621 | 0.92 | 31.18 | BDL | 11 | BDL | 12 | 91 | 59 | | 550 | 33 | | | 39 | 9.1 | | |
| B-S-01 | Bambino Transect-01 | 38.418 | 14.96 | 27.7 | 6.53 | | | | | | | | | | | | | | | 46 | | | |
| B-S-02 | Bambino Transect-02 | 38.418 | 14.96 | 27.7 | 6.47 | | | | | | | | | | | | | | | 33 | | | |
| B-S-03 | Bambino Transect-03 | 38.418 | 14.96 | 27.7 | 6.49 | | | | | | | | | | | | | | | 33 | | | |
| B-S-04 | Bambino Transect-04 | 38.418 | 14.96 | 27.7 | 6.37 | | | | | | | | | | | | | | | 26 | | | |
| B-S-05 | Bambino Transect-05 | 38.418 | 14.96 | 27.7 | 6.35 | | | | | | | | | | | | | | | 101 | | | |
| B-S-06 | Bambino Transect-06 | 38.418 | 14.96 | 27.7 | 5.94 | | | | | | | | | | | | | | | 92 | | | |
| B-B-02 | Bambino Transect Bottom-02 | 38.418 | 14.96 | 27.7 | 6.51 | | | | | | | | | | | | | | | 45 | | | |
| B-B-03 | Bambino Transect Bottom-03 | 38.418 | 14.96 | 27.7 | 6.48 | | | | | | | | | | | | | | | 43 | | | |
| B-B-05 | Bambino Transect Bottom-05 | 38.418 | 14.96 | 27.7 | 6.1 | | | | | | | | | | | | | | | 55 | | | |
| B-B-06 | Bambino Transect Bottom-06 | 38.418 | 14.96 | 89.7 | 5.97 | | | | | | | | | | | | | | | 61 | | 7.27 | |

# 4. Hg in the hydrothermal fluids and gases in Baia di Levante, Vulcano, Italy

Appendix 2. Point source samples from in and outside of Baia di Levante, Vulcano.

| Sample Number | Sample Description | Latitude | Longitude | °C | pH | Cl | Br | SO4 | As | Ca | Fe | K | Li | Mg | Mn | Na | Si | Sr | $H_2S$ | THg | $Hg_{diss}$ | Sed. |
|---|---|---|---|---|---|---|---|---|---|---|---|---|---|---|---|---|---|---|---|---|---|---|
| | | | | | | mM | mM | mM | µM | mM | mM | mM | µM | mM | µM | µM | µM | µM | µM | pM | pM | nmol/g |
| | **Point Sources and Porewaters** | | | | | | | | | | | | | | | | | | | | | |
| 2019 | **Bambino** | | | | | | | | | | | | | | | | | | | | | |
| V51 | Low Tide | 38.4176 | 14.96 | 100.1 | | | | | | | | | | | | | | | | | | |
| V52 | High Tide | 38.4176 | 14.96 | 100.1 | | | | | | | | | | | | | | | | | | |
| 2021 | | | | | | | | | | | | | | | | | | | | | | |
| B-B-06 | Bambino | 38.4176 | 14.96 | 89.7 | 5.97 | | | | | | | | | | | | | | | 61 | | |
| B-Bowl | Bambino Bowl | | | 100 | 5.79 | 624 | 0.91 | 31 | BDL | 11 | BDL | 12 | 91 | 58 | BDL | 541 | 193 | BDL | BDL | 342 | 16 | 49.52 |
| B-MB | Mini-Bambino | 38.4177 | 14.9599 | 84 | | | | | | | | | | | | | | | | | | |
| | **White Patch** | | | | | | | | | | | | | | | | | | | | | |
| V29 | White Patch 10 cm | 38.4163 | 14.9613 | 54 | 5.52 | 521 | 0.8 | 85 | BDL | 14 | 0 | 13 | 0 | 49 | 33 | 447 | 3949 | 74 | 990 | 276 | | 7 |
| V37 | White Patch T Map: Seagrass | 38.4163 | 14.9613 | 21.4 | 7.7 | 610 | 0.94 | 29 | BDL | 11 | 19 | 11 | 0 | 54 | 0 | 523 | 146 | 100 | 0 | 186 | | 3.7 |
| V38 | White Patch T Map: Sand | 38.4163 | 14.9613 | 22.7 | 6.26 | 603 | 0.93 | 29 | BDL | 12 | 336 | 11 | 0 | 54 | 10 | 518 | 728 | 94 | 34 | 226 | | 5.5 |
| V39 | White Patch T Map: White | 38.4163 | 14.9613 | 36 | 5.28 | 528 | 0.81 | 32 | BDL | 14 | 0 | 12 | 0 | 51 | 32 | 458 | 3659 | 79 | 1675 | 325 | | 0 |
| V40 | White Patch T Map: Sand, Bubbling | 38.4163 | 14.9613 | 22.2 | 5.09 | 608 | 0.93 | 30 | BDL | 11 | 0 | 11 | 0 | 54 | 0 | 524 | 437 | 101 | 2045 | 7 | | 1.7 |
| V41 | White Patch T Map: White Patchy | 38.4163 | 14.9613 | 22 | 5.18 | 549 | 0.84 | 32 | 3.9 | 14 | 0 | 12 | 0 | 51 | 32 | 459 | 3578 | 80 | 1333 | 56 | | 5.6 |
| | **Subaerial and Tidal Sites** | | | | | | | | | | | | | | | | | | | | | |
| 2019 | **Baia di Levante** | | | | | | | | | | | | | | | | | | | | | |
| V27 | Mudbath | | | | 6.03 | 550 | 0.83 | 82 | 3.3 | 15 | 333 | 13 | | 51 | 63 | 466 | 1970 | 107 | 0 | 5 | | 3.3 |
| V30 | Subaerial low-Cl | 38.4175 | 14.9592 | 27.3 | 5.55 | 582 | 0.87 | 95 | BDL | 15 | 4836 | 14 | 0 | 53 | 66 | 495 | 1729 | 19 | 0 | 132 | | 16.8 |
| V25 | Tidal Cave | 38.4162 | 14.9604 | 46.6 | 2.46 | 494 | 0.76 | 93 | BDL | 15 | 1069 | 11 | 0 | 47 | 49 | 428 | 4827 | 44 | 226 | 536 | | 8.7 |
| V42 | Shore Sample | 38.4165 | 14.9602 | 99.4 | 5.82 | 529 | 0.81 | 27 | BDL | 10 | 0 | 12 | 49 | 48 | 30 | 447 | 2655 | 70 | 391 | 2888 | | 235.5 |
| V43 | Rock Boulder at Mud Bath | 38.4163 | 14.9602 | 101.5 | 5.45 | | | | | | | | | | | | | | | 716 | | 272.9 |
| 2021 | | | | | | | | | | | | | | | | | | | | | | |
| F-01 | Tidal Cave | 38.4162 | 14.9604 | 53 | 2.38 | 504 | 0.73 | 44 | BDL | 13 | 1192 | 11 | 94 | 49 | 46 | 439 | BDL | 1388 | | 122 | | 59.7 |
| F-02 | Faraglione-Port-1 | 38.4157 | 14.9606 | 74.4 | 2.73 | 495 | 0.73 | 40 | 0.5 | 13 | 704 | 11 | 105 | 50 | 55 | 433 | BDL | 1575 | | 27 | | 6.5 |
| F-03 | Faraglione-Port-2 | 38.4157 | 14.9606 | 68.8 | 5.89 | 590 | 0.86 | 34 | 1.3 | 13 | | 12 | 97 | 55 | 22 | 501 | 3226 | 1034 | | 26 | | 5.5 |
| | **La Fossa Area** | | | | | | | | | | | | | | | | | | | | | |

Appendix 1. Surface water samples from in and outside of Baia di Levante, Vulcano. Updated with missing Bambino bottom water data

| Sample Number | Sample Description | Lat. | Long. | °C | pH | Cl | Br | SO4 | As | Ca | Fe | K | Li | Mg | Mn | Na | Si | Sr | H2S | THg | Hg_diss | Volatile | Sed. |
|---|---|---|---|---|---|---|---|---|---|---|---|---|---|---|---|---|---|---|---|---|---|---|---|
| | | | | | | mM | mM | mM | uM | mM | uM | mM | uM | mM | uM | mM | uM | uM | uM | pM | pM | pM | nmol/g |
| V26 | Submarine Cave | 38.4086 | 14.9742 | 48 | 6.11 | 348 | 0.52 | 79 | BDL | 13 | 235 | 12 | 0 | 39 | 71 | 301 | 2543 | 78 | BDL | 3 | 1.5 | | |
| V44 | Mushroom Stone | 38.4122 | 14.9639 | 51.9 | 2.88 | 484 | 0.68 | 59 | BDL | 16 | 471 | 18 | 160 | 74 | 864 | 378 | 3166 | 60 | 43 | 9 | 4.7 | | |
| V45 | Outcrop | 38.4122 | 14.9639 | 63 | 4.1 | 578 | 0.82 | 48 | BDL | 20 | 244 | 20 | 160 | 71 | 688 | 455 | 3062 | 82 | 34 | 8 | 0.4 | | |
| V46 | Beach | 38.4122 | 14.9639 | 46 | 4.42 | 436 | 0.64 | 40 | BDL | 14 | 0 | 16 | 158 | 51 | 282 | 363 | 3046 | 52 | BDL | 29 | 11.6 | | |

Appendix 3. Surface water concentrations of Hgdiss (pM) and calculated flux to the atmosphere assuming 10% of THg is Hg0.

| Year | Sample | Hg$_{diss}$ pM | Flux pmol/m²/hr |
|------|--------|------|------|
| 2019 | V01 | 1.1 | 0.1 |
| | V02 | 0.9 | 0.1 |
| | V03 | 0.7 | 0.1 |
| | V04 | 0.6 | 0 |
| | V05 | 0.6 | 0.1 |
| | V06 | 0.6 | 0.1 |
| | V07 | 0.7 | 0.1 |
| | V08 | 0.8 | 0.1 |
| | V09 | 0.8 | 0.1 |
| | V10 | 0.7 | 0.1 |
| | V11 | 1 | 0.1 |
| | V12 | 0.7 | 0.1 |
| | V13 | 0.7 | 0.1 |
| | V14 | 0.6 | 0.1 |
| | V15 | 11.3 | 2.1 |
| | V16 | 0.7 | 0.1 |
| | V17 | 0.7 | 0.1 |
| | V18 | 0.8 | 0.1 |
| | V19 | 1.3 | 0.2 |
| | V20 | 56.3 | 10.5 |
| | V21 | 11 | 2 |
| | V22 | 104.7 | 19.6 |
| 2021 | MB-01 | 7.6 | 1.4 |
| | MB-02 | 9.6 | 1.7 |
| | MB-03 | 12.1 | 2.2 |
| | MB-04 | 29.8 | 5.6 |
| | MB-05 | 35.7 | 6.7 |
| | MB-06 | 33.9 | 6.3 |
| | MB-07 | 26.5 | 4.9 |
| | MB-08 | 24.8 | 4.6 |
| | MB-09 | 31.4 | 5.8 |
| | MB-10 | 35.1 | 6.5 |
| | MB-11 | 32.7 | 6.1 |
| | MB-12 | 32.9 | 6.1 |
| | MB-13 | 27.8 | 5.2 |
| | MB-14 | 31.9 | 5.9 |
| | MB-15 | 25.8 | 4.8 |
| | MB-16 | 29 | 5.4 |
| | MB-17 | 37.5 | 7 |
| | MB-18 | 48.1 | 9 |
| | B-S-06* | 7.3 | 13.6 |

\* Hg0 concentration (pM)

## 5. A Marine Shallow Water Hydrothermal System as a Hg Emitter to the Local Environment of Panarea, Italy

Hannah Roberts, Thomas Pichler

Universität Bremen, Fachbereich Geowissenschaften, Geochemistry and Hydrogeology, Klagenfurter Str. 2-4, 28359 Bremen, Germany

## Abstract

The importance of marine shallow water hydrothermal systems (MSWHS) with regard to local and global Hg cycling has yet to be established. We evaluated data of mercury-(Hg)-contents in water, gas, and sediment collected from Panarea, Aeolian Arc, Italy, which hosts a variable and well-studied system. Samples were collected from June 2018, June 2019, and September 2021. Fluids were collected with porewater probes, and gases were collected into Tedlar$^©$ bags. Total Hg (THg) concentrations in the hydrothermal fluids ranged from 22 pM to 24.8 nM. Monomethyl Hg (MMHg) was below the detection limit. Total Hg in the gases (Hg$_{gas}$) ranged from 0.9 to 1899 nmol / m$^3$. Sediment THg ranged in concentration from 0.3 to 16.7 nmol / g.

The sampled hydrothermal sites included a range of depths (7 to 21 m depth), consisting of localized and distinct areas of emission (point sources) and larger areas of diffuse emission. In the main area of interest (La Calcara, LC), high concentrations of THg (> 500 pM) in porewaters were associated with low sedimentation, high temperature (> 65 °C), indicating greater and more direct hydrothermal flow. In seawater above LC, THg and 0.45 µm filtered Hg (Hg$_{diss}$) concentrations were elevated (> 14 pM THg) throughout the 20 m water column. Small changes in environmental conditions, likely redox conditions, led to large fluctuations in THg at a singular point source that were not reflected in cation or anion data. Other point sources remained stable when measured for multiple years.

The MSWHS at Panarea is a local source of Hg to the environment. Deposition occurs within the shallow subsurface, particularly for point sources with low hydrothermal flow or those that have a sediment layer overlying the point of emission to the water column. However, higher rates of flow coupled with minimal sedimentation led to large portions of Hg entering the marine environment. Scavenging and deposition near sources were significant sinks of emitted species

such as Hg for many systems. However, at the site LC the detected Hg emission led to Hg transport away from the point source and presented a potential for biological uptake. Elevations of THg throughout the 20 m water column above the LC area implies a significant local contribution of Hg, making obvious that the previously accepted model of immediate removal of Hg to sediments after its prior volcanic emission via MSWHS is an oversimplification.

# 5. A Marine Shallow Water Hydrothermal System as a Hg Emitter to the Local Environment of Panarea, Italy

## 5.1 Introduction

Mercury (Hg) is a bioaccumulating toxin. Human activities have raised concentrations of mercury within marine waters and the atmosphere above pre-industrial levels up to 230 % and 450 % respectively (Lamborg et al., 2002; Outridge et al., 2018). Natural sources to the environment, such as hydrothermal systems, are not as well constrained as their anthropogenic counterparts. For this reason, despite known close associations between Hg and hydrothermal systems, current ocean cycling models assume hydrothermal systems to have a minimal impact on the environment as far as Hg is concerned (Fitzgerald et al., 2007; Mason and Fitzgerald, 1996; Obrist et al., 2016; Outridge et al., 2018). However, these systems present unique opportunities to study the effects of prolonged Hg exposure on the local environment. In the case of marine shallow water hydrothermal systems (MSWHS), research indicates that environments become enriched in mercury in a local scale (Leal-Acosta et al., 2013; Roberts and Pichler, 2022; Roberts et al., 2021).

Hydrothermal systems transfer heat and mass through circulating water in a permeable geological formation. Seawater and meteoric water are pulled down into the subsurface, undergoing multiple subsurface processes, gaining and losing constituents dependent upon physical, geological, and chemical factors. According to Beaulieu and Szafranski (2020), a total of 184 systems are confirmed active across the globe. Of these, 43 are classified as shallow (>200 m water depth) and considered MSWHS. Hydrothermal fluids gain Hg from magmatic vapors, mineral dissolution, and leaching from unmineralized sources or host rocks (Barnes, 1973; Giggenbach, 1997; Saupe, 1990; Varekamp and Buseck, 1984). Above 150 °C, Hg is transported as a conservative element (Christenson and Mroczek, 2003; Pokrovski et al., 2013; Williams-Jones and Heinrich, 2005). At temperatures < 150 °C and dependent upon the chemistry of the systems, Hg will preferentially bind to S or Cl species (Barnes et al., 1967; Helgeson, 1969). However, in the presence of reduced S, Hg-Cl complexes are negligible (Barnes, 1979). Precipitation of Hg within a hydrothermal system generally results in the formation of mercury sulfide (HgS) (Varekamp and Buseck, 1984). In a given geothermal system with elemental mercury ($Hg_{aq}^0$) as the dominant species, the solubility of HgS is described by equation 1 (Varekamp and Buseck, 1984). Where dissolution of HgS as aqueous $Hg_{aq}^0$ is limited by increasing H$^+$, HS$^-$, and $p$O$_2$. The $p$O$_2$ of the system can be internally controlled

## 5. A Marine Shallow Water Hydrothermal System as a Hg Emitter to the Local Environment of Panarea, Italy

through an $HS^-$-$SO_4^-$ reaction (equation 2) (Spirakis, 1981; Varekamp and Buseck, 1984), with $SO_4$ contributed by circulated source water, precipitated as anhydrite ($CaSO_4$) (e.g., seawater) (Seyfried Jr and Ding, 1995).

1) $HgS + H_2O \leftrightarrow Hg^0_{aq} + HS^- + H^+ + \frac{1}{2}O_2$

2) $2H^+ + SO_4^{2-} \leftrightarrow H_2S + 2O_{2(g)}$
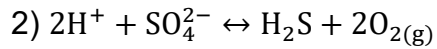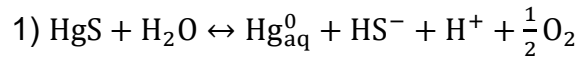
Importantly, seawater derived magnesium (Mg) in hydrothermal fluids drives low pH conditions through water-rock interactions, however this process competes with silicate hydrolysis reactions which consume generated $H^+$ (Seyfried and Mottl, 1982). Therefore, the pH of the system at any point results primarily from the balance between seawater flow and the rates of subsurface reactions. Due to the volatility of Hg, deposition of Hg ores occurs at near-surface environmental conditions (Barnes and Seward, 1997; Christenson and Mroczek, 2003; Krupp, 1988; Varekamp and Buseck, 1984). For example, extreme enrichment of Hg was observed in the top 10 m of drillings in New Zealand, with low concentrations below 10 m (Christenson and Mroczek, 2003). In the case of MSWHS, hydrothermal emissions include gases and fluids which are emitted in two different scenarios, either diffusely across wider areas (diffuse emission) or in large fluxes of fluid or gas in a discrete area (point source).

Previous models of global mercury cycles dismissed hydrothermal systems as insignificant sources compared to anthropogenic influences (Lamborg et al., 2002; Mason and Sheu, 2002). However, these systems have been shown to impact marine systems on a local scale, resulting in elevated concentrations within sediments, organisms (e.g., fish, seagrasses, mussels), and the water column (e.g., this study, Leal-Acosta et al., 2013; Leal-Acosta et al., 2010; Nakanishi et al., 1989; Prol-Ledesma et al., 2004; Roberts and Pichler, 2022; Roberts et al., 2021). Arguments against hydrothermal systems as major sources to the marine cycle assumed hydrothermally sourced Hg was removed through scavenging and sedimentation (Fitzgerald et al., 2007; Mason and Fitzgerald, 1996; Outridge et al., 2018). Indeed, the chalcophilic nature of Hg results in the formation of relatively insoluble Hg-S compounds within sediments and the water column, particularly under anoxic conditions (Christenson and Mroczek, 2003; Fitzgerald et al., 2007; Krupp, 1988). The main body of literature regarding the stability of Hg from hydrothermal deposits is primarily associated with mining and geothermal energy production

(Covelli et al., 1999; Feng et al., 2010; Nicholson, 1992) and the presence of hydrogen sulfide, often present at MSWHS, immobilizes mercury (Krupp, 1988). However, both biological and chemical transformation can lead to the dissolution of HgS as discussed in detail by Chen et al. (2017). The balance between accumulation, dissolution, and deposition generates areas of extreme enrichment with the potential for further mobilization given proper environmental changes (Konovalov et al., 2018; Lacerda et al., 2004).The environmental impact of MSWHS is therefore likely local, however there is potential to affect the environment on a larger scale through dissolution and mobilization of particle bound Hg. The dissolution of Hg-S complexes and the presence of sulfur oxidizing bacteria common to MSHWS (Giovannelli et al., 2013; Price and Giovannelli, 2017), increases the potential for transformation to methylated species and bioaccumulation.

The dominant specie of Hg within a system is important when describing the fate of Hg from the system (Christenson and Mroczek, 2003), with changes in pH and redox potential resulting in greater stability of specific species over others. Hydrothermal fluids are generally reducing and acidic, due to the reactions described previously, therefore mixing with oxygenated seawater in the shallow subsurface leads to drastic changes in the dominant Hg species within the fluid. In particular, the deposition of cinnabar (HgS) is a strong controlling mechanism preventing transport of Hg away from hydrothermal sources (Christenson and Mroczek, 2003; Roberts and Pichler, 2022; Roberts et al., 2021).

This study investigated the role of hydrothermal systems as an important natural source of mercury to the environment. Additionally, this paper serves as a bridge between previous studies to paint a larger picture of MSWHS and their influence on local environments. We argue these systems contribute mercury both directly (e.g., through mercury rich gases to the atmosphere) and indirectly (e.g., transport and dissolution of precipitated mercury particles) to the surrounding environment. Such a range for the transport of Hg is important because transport of Hg away from hydrothermal sources increases the potential for exposure to biological organisms and therefore methylation processes. Panarea was chosen as a research site based upon considerable research efforts conducted on the MSWHS, and the variety of emission types within hydrothermal fluids and gases present. As Hg is present within hydrothermal fluids and gases, both were sampled.

## 5. A Marine Shallow Water Hydrothermal System as a Hg Emitter to the Local Environment of Panarea, Italy

## 5.2 Study Site

### 5.2.1 Geological Setting

The island of Panarea belongs to the Aeolian volcanic arc with several minor islets located to the east of the main island (Fig. 5.1). The hydrothermal system has been well studied (Chiodini et al., 2006; Italiano and Nuccio, 1991; Longo et al., 2021; Price et al., 2015; Sieland, 2009; Stanulla, 2021), however investigations into the composition of fluids and gases regarding Hg are limited (Bagnato et al., 2009a; Bagnato et al., 2017). This group of formations is the remnant of an eroded volcanic complex between the Vulcano-Lipari-Salina volcanic belt. The exposed land masses are composed of volcanic rocks, whose semi-circular formation surround a 1 km shallow depression (maximum depth 30 m) with multiple locations of hydrothermal activity (Lucchi et al., 2013). A deep hydrothermal body (< 220 °C) is overlayed by two hydrothermal reservoirs (170 to 210 °C) which feed the MSWHS (Italiano and Nuccio, 1991). One reservoir beneath the island of Panarea is recharged by circulated continental waters, and the other recharged by marine waters (Fig 5.1). The emitted hydrothermal gases are mainly comprised of $CO_2$, with variable concentrations of $H_2S$, Ar, $N_2$, $CH_4$, $H_2$, He, and CO (Chiodini et al., 2006; Gugliandolo et al., 2006; Italiano and Nuccio, 1991). Fluids are near seawater values or slightly depleted in Cl and $SO_4$, but some contain enrichments of Ca, K, and $SiO_2$ (Caracausi et al., 2005; Italiano and Nuccio, 1991; Price et al., 2015). Temperatures of hydrothermally active areas can exceed 130 °C. However, the chemical compositions of the MSWHS fluids and gases at Panarea are not static (Caracausi et al., 2005; Tassi et al., 2009). Following a 2002 gas burst, multiple studies were conducted on the stability of the system (Capaccioni et al., 2005; Caracausi et al., 2005; Chiodini et al., 2006; Tassi et al., 2009). Furthermore, recent studies have linked Panarea activity to Stromboli, where increases and subsidence of gaseous activity were observed prior to larger events on Stromboli (Heinicke et al., 2009; Longo et al., 2021). Panarea is an ideal system of study, combining point sources with large emissions of gases and liquids at high temperature (< 100 °C), and large areas of diffuse emission with a thick sediment layer. Additionally, the system has been well studied, inclusive of Hg data in fluids and gases (e.g., Bagnato et al., 2017; Caracausi et al., 2005; Chiodini et al., 2006; Longo et al., 2021; Lucchi et al., 2013; Price et al., 2015; Sieland et al., 2009; Stanulla, 2021; Tassi et al., 2009).
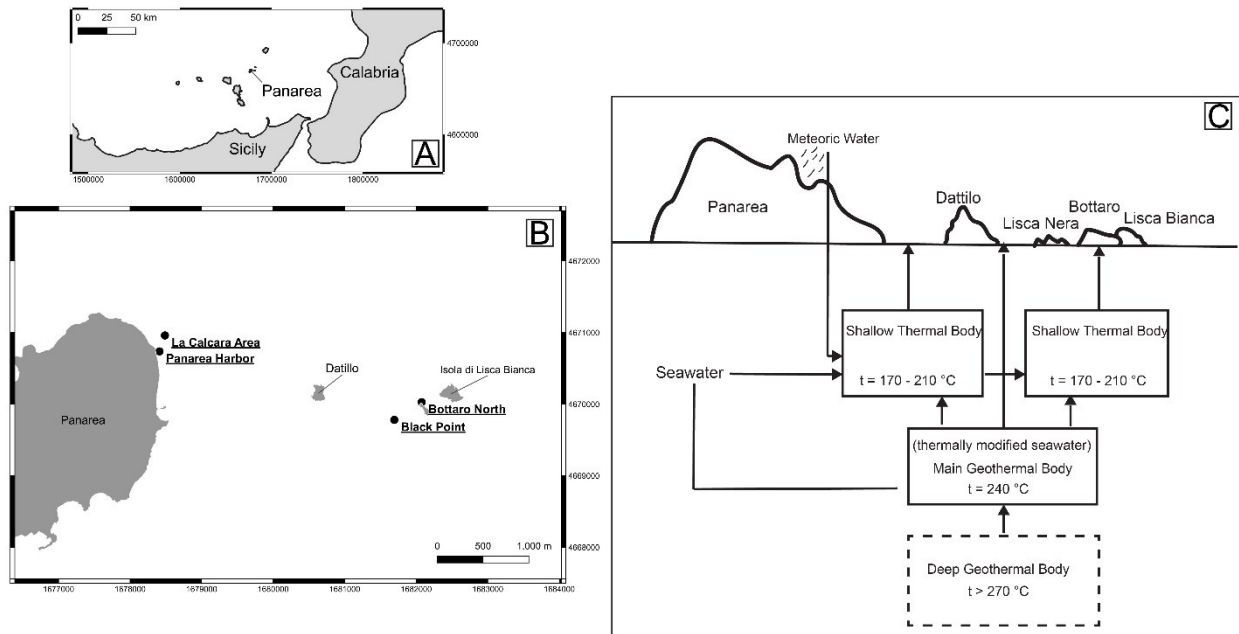
93

Figure 5.1: Map overview of the Aeolian island region (A), Panarea and major sites of interest (B), and general schematic of the Panarea hydrothermal system adapted from Italiano and Nuccio (1991). Maps A and B were generated using QGIS.

## 5.2.2 Research Area

In this study, the main area of interest was La Calcara (LC), located approximately 200 m from the northeast shore of Panarea at a water depth of approximately 20 m (Fig. 5.1). Hydrothermal activity includes diffuse emissions and multiple point sources (Fig. 5.2). Diffuse emissions were apparent across wide areas of LC with microbial white mats, metal precipitates, concentrated and wide spread bubbling, and hot (>50 °C) sands (Fig. 5.2A). Distinct lines of precipitates, changes in temperature (> 50 °C to 21 °C) or change in emission type (fluid to gas) were observed at LC (Fig 2). The primary point of interest within LC was the main point source (MPS), which largely emitted gases with some visible fluid emission from sediments (Fig. 5.2B). MPS is comprised of many small gas point sources in a small area that have been grouped into MPS. A nearby fluid point source (FPS) was also investigated and emitted only fluid. A horizontal current was noted by divers, where hydrothermal bubbles rose at an angle from the seafloor at depths shallower than 10 m.
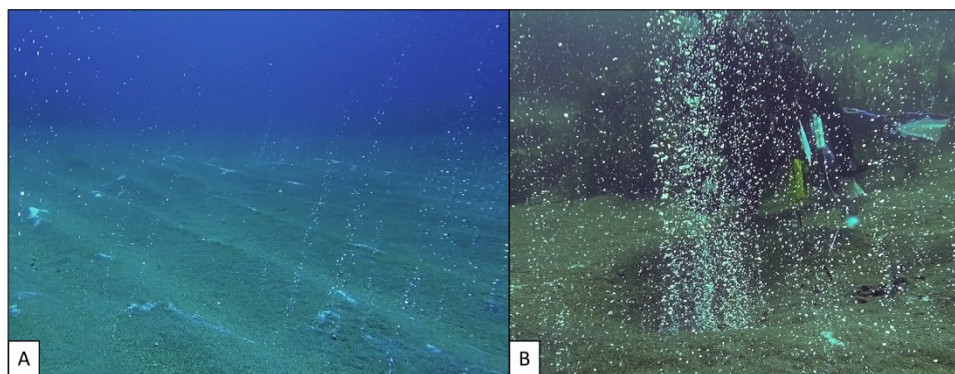
Figure 5.2: Image of emission types at LC, A) Diffuse emissions at LC with small white mat accumulations and bubbling, B) main point source (MPS) with intense bubbling with diver behind the point source.

Outside of the LC were two additional areas of interest. The first was the Panarea Harbor point source (HPS), located 50 m from shore and approximately 200 m southwest from LC. Large boulders covered the sediment-water interface, however large amounts of gas were emitted between them. The final area of interest was the islet area approximately 2.5 km from the main island of Panarea. This area included the well described gaseous point source Bottaro North (BN) and the liquid point source Black Point (BP). Within 100 m of BP, an additional liquid point source was investigated, where hot liquid flowed in front of a small boulder with a buildup of microbial white mats (BPW).

## 5.3 Methods

In June 2018, June 2019 and September 2021, a total of 40 Hg samples were collected from porewaters, the water column, and from hydrothermal point sources, along with arsenic (As), cations, and anions (Table 5.1 and 5.2). Samples were considered porewaters where sufficient sediment covered hydrothermal sources for sampling probes to pull fluid without significant seawater contamination. This was controlled through the use of temperature probes inserted into the sediment at the same point as the sample probes. Seawater contamination was considered negligible if the temperature remained stable throughout the sample retrieval process. These sites were then considered 'sedimented'. At other locations, where hydrothermal flux, water circulation, or wave action prohibited sufficient sediment accumulation, samples were considered hydrothermally altered seawater. These sites were considered 'unsedimented'. Fluid Hg samples included unfiltered (THg), 0.45 µm

Table 5.1: Sample concentrations of anions, cations, and As. Descriptors are Surf. (surface), WM (white mat), OP (orange precipitate), Degas. (degassing fluid site), B (bubbling), BrP (brown precipitate), S (sand), SB (sand bubbling), FPS (fluid point source), MPS (Main Point Source), BP (black point), LT (low tide), and HT (high tide). Descriptors with another sample in parentheses were taken next to the referenced sample (within 15 cm).

| Sample | Desc. | Depth | T | pH | ORP | Cl | Br | SO$_4$ | As | Ca | Fe | K | Li | Mg | Mn | Na | Si | Sr | H$_2$S |
|---|---|---|---|---|---|---|---|---|---|---|---|---|---|---|---|---|---|---|---|
| | | m | °C | | | mM | mM | mM | µM | mM | µM | mM | mM | mM | mM | mM | mM | µM | µM |
| **Detection Limits** | | | | | | 0.2 | 3.8 | 0.07 | 0.27 | 0.012 | 3.6 | 0.13 | 0.07 | 0.02 | 3.6 | 0.43 | 8 | 0.6 | |
| **Seawater** | | | | | | | | | | | | | | | | | | | |
| Background | Surf. | 0 | 21 | 8.16 | | 627 | 1.09 | 30.4 | BDL | 10.4 | BDL | 10.5 | BDL | 51 | BDL | 486 | 29 | 98 | |
| BP S | Surf. | 0 | | 8.1 | | 612 | 1.11 | 33.9 | BDL | 10.4 | BDL | 10.6 | BDL | 51 | BDL | 494 | 25 | 100 | |
| LC S | Surf. | 0 | | 8.24 | | 629 | 0.91 | 31.4 | BDL | 11.3 | BDL | 11.4 | 92.9 | 58 | BDL | 536 | BDL | BDL | |
| LC P-1 | Profile | 20 | | 6.31 | | 632 | 0.96 | 31.5 | BDL | 10.9 | BDL | 11.2 | 90.3 | 56 | BDL | 524 | 4914 | BDL | |
| LC P-2 | Profile | 15 | | 8.06 | | 623 | 0.92 | 31.1 | BDL | 11.0 | BDL | 11.1 | 90.2 | 57 | BDL | 532 | BDL | BDL | |
| LC P-3 | Profile | 10 | | 8.22 | | 627 | 0.93 | 31.3 | BDL | 11.8 | BDL | 11.5 | 91.5 | 58 | BDL | 545 | BDL | BDL | |
| LC P-4 | Profile | 5 | | 8.22 | | | | | | | | | | | | | | | |
| **La Calcara Active Sites** | | | | | | | | | | | | | | | | | | | |
| LC-1 | WM | 20 | 65 | 5.02 | | 589 | 0.86 | 27.5 | BDL | 8.0 | BDL | 9.7 | 88.7 | 52 | 3.6 | 467 | 340 | 339 | |
| LC-2 | OP | 21 | 37 | 5.48 | | 642 | 0.95 | 31.9 | BDL | 11.0 | 403.7 | 10.9 | 92.7 | 56 | 7.1 | 516 | BDL | 260 | |
| LC-3 | WM | 21 | 98 | 4.63 | | 534 | 0.81 | 23.2 | BDL | 6.3 | BDL | 9.6 | 88.9 | 49 | 0.5 | 447 | 216 | 454 | |
| LC-4 | Degas. | | | 5.11 | | | | | | | | | | | | | | | |
| LC-5 | WM | 20 | 79 | 5.04 | | 565 | 0.86 | 28.5 | BDL | 10.0 | BDL | 10.1 | 84.5 | 52 | 2.1 | 474 | BDL | 69 | |
| LC-6 | B | 20 | 115 | 5.55 | | 549 | 0.81 | 27.6 | BDL | 9.5 | BDL | 9.4 | 89.4 | 50 | 54.5 | 445 | BDL | 37 | |
| LC-7 | OP | 15 | 49 | 5.06 | | | | | | | | | | | | | | | |
| LC-8 | WM (LC-7) | 15 | 45 | 4.99 | | 599 | 0.86 | 27.9 | BDL | 10.8 | 56.5 | 11.0 | 98.1 | 51 | 79.6 | 491 | BDL | 436 | BDL |
| LC-9 | Near Slow B | | | 5.44 | | 623 | 0.91 | 31.0 | BDL | 11.5 | 881.3 | 11.8 | 96.5 | 57 | 23.8 | 532 | 4330 | 378 | BDL |
| LC-10 | OP | 21 | 22 | 5.95 | 121 | 613 | 0.95 | 29.5 | BDL | 11.1 | 155.41 | 10.4 | BDL | 53 | BDL | 501 | 117 | 98 | BDL |
| LC-11 | OP | 21 | 29 | 5.39 | -21 | 603 | 0.89 | 29.3 | BDL | 10.7 | 183.09 | 10.2 | BDL | 54 | BDL | 497 | 376 | 95 | 0.9 |
| LC-12 | BrP | 21 | 23 | 7.13 | -31 | 610 | 0.94 | 29.5 | BDL | 10.9 | BDL | 10.4 | BDL | 52 | BDL | 503 | 34 | 96 | BDL |
| LC-13 | WM | 21 | 33 | 5.58 | -70 | 617 | 0.95 | 29.9 | BDL | 11.3 | 121.61 | 10.8 | BDL | 53 | BDL | 516 | 221 | 99 | 33.4 |
| LC-14 | WM | 21 | 63 | 5.54 | -40 | 607 | 0.94 | 29.3 | BDL | 11.1 | 22.49 | 10.7 | BDL | 53 | BDL | 511 | 363 | 97 | 116.0 |
| LC-15 | S | 21 | 19 | 7.34 | -100 | 610 | 0.94 | 29.5 | BDL | 11.4 | BDL | 10.9 | BDL | 54 | BDL | 520 | 25 | 99 | 123.4 |
| LC-16 | BrP | 21 | 31 | 6.12 | 7 | 605 | 0.93 | 28.6 | BDL | 11.1 | 59.45 | 10.8 | BDL | 52 | 6.68 | 504 | 722 | 99 | BDL |
| LC-17 | SB | 21 | 70 | 5.84 | -38 | 536 | 0.82 | 24.9 | BDL | 8.9 | 26.31 | 8.9 | BDL | 48 | 19.17 | 443 | 1317 | 83 | 2.2 |
| FPS | FPS | 21 | 133 | 6.22 | 142 | 551 | 0.84 | 25.3 | BDL | 9.4 | BDL | 9.7 | BDL | 48 | 177.89 | 461 | 879 | 85 | BDL |
| MPS-2018 | MPS | 21 | 131 | 6.33 | | 601 | 1.14 | 29.0 | BDL | 11.7 | 0.00 | 10.5 | BDL | 49 | 0.09 | 474 | 79 | 110 | BDL |
| MPS-2019 | MPS | 21 | 133 | 5.88 | -10 | 586 | 0.90 | 27.8 | 3.35 | 13.1 | BDL | 10.4 | BDL | 53 | 160.33 | 486 | 91 | 115 | 8.8 |
| MPS-2021 | MPS | 21 | 128 | 5.13 | | 524 | 0.76 | 22.8 | BDL | 16.0 | BDL | 10.6 | 158.0 | 43 | 690.3 | 411 | BDL | 109 | BDL |

# 5. A Marine Shallow Water Hydrothermal System as a Hg Emitter to the Local Environment of Panarea, Italy

Table 5.1 (Cont.)

| Sample Name | Desc. | Depth | T | pH | ORP | Cl | Br | SO$_4$ | As | Ca | Fe | K | Li | Mg | Mn | Na | Si | Sr | H$_2$S Liq |
|---|---|---|---|---|---|---|---|---|---|---|---|---|---|---|---|---|---|---|---|
| | | m | °C | | | mM | mM | mM | µM | mM | µM | mM | mM | mM | mM | mM | mM | µM | µM |
| **Detection Limits** | | | | | | 0.2 | 3.8 | 0.07 | 0.27 | 0.012 | 3.6 | 0.13 | 0.07 | 0.02 | 3.6 | 0.43 | 8 | 0.6 | |
| **La Calcara Off Active Sites** | | | | | | | | | | | | | | | | | | | |
| LC-18 | (LC-2) | | | 5.18 | | 627 | 0.91 | 31.3 | BDL | 10.8 | BDL | 11.0 | 89.2 | 56 | -1.9 | 524 | BDL | BDL | |
| LC-19 | (LC-3) | 21 | 21 | 5.08 | | 647 | 0.96 | 32.1 | BDL | 10.6 | BDL | 10.9 | 91.5 | 55 | -0.7 | 507 | BDL | BDL | |
| LC-20 | (LC-5) | 20 | 21 | 7.36 | | 635 | 0.96 | 31.7 | BDL | 11.0 | BDL | 11.2 | 92.0 | 58 | BDL | 538 | 1181 | BDL | |
| LC-21 | (LC-2) | 21 | 21 | 6.89 | | 629 | 0.91 | 31.4 | BDL | 10.8 | BDL | 11.1 | 89.0 | 56 | -2.3 | 516 | BDL | BDL | |
| **Black Point** | | | | | | | | | | | | | | | | | | | |
| BP | BP | 23 | 131 | 2.92 | | 535 | 1.00 | 16.0 | BDL | 22.9 | BDL | 15.8 | 0.4 | 35 | 0.96 | 398 | 3032 | 236 | |
| BPW | FPS | 23 | | 4.7 | | 837 | 1.48 | 7.6 | 17.23 | 98.7 | BDL | 36.7 | 1.3 | 22 | 3.89 | 460 | 3285 | 969 | |
| **Panarea Harbor** | | | | | | | | | | | | | | | | | | | |
| PH-2018 | | | | | | | | | | | | | | | | | | | |
| PH-2019 1 | LT | 7 | 121 | | | | | | | | | | | | | | | | |
| PH-2019 2 | HT | 7 | | | | | | | | | | | | | | | | | |
| **Bottaro North** | | | | | | | | | | | | | | | | | | | |
| BN-2019 | | 9 | | | | | | | | | | | | | | | | | |
| BN-2018 | | 9 | | | | | | | | | | | | | | | | | |

Table 5.2: Sample concentrations of Hg in fluids, sediments, and gases. Concentration of $H_2S$ in the gas phase

| Sample | Desc. | THg | Hg$_{diss}$ | Sed. | Volatile Hg | Gas H2S | Hggas |
|---|---|---|---|---|---|---|---|
| | | pM | pM | nmol / g | pM | % of Gas | nmol / m3 |
| **Detection Limits** | | 0.2 | 0.2 | 0.2 (pM) | **0.25** | | 25 (pM) |
| **Seawater** | | | | | | | |
| Background | Surf. | 0.6 | | | | | |
| BP S | Surf. | 1.2 | | | | | |
| LC S | Surf. | 1.1 | 0.6 | | BDL | | |
| LC P-1 | Profile | 55 | 24 | | | | |
| LC P-2 | Profile | 14 | 2.3 | | | | |
| LC P-3 | Profile | 26 | 2.8 | | | | |
| LC P-4 | Profile | 350 | 8.2 | | | | |
| **La Calcara Active Sites** | | | | | | | |
| LC-1 | WM | 1049 | 4.5 | | | | |
| LC-2 | OP | 297 | 12 | 0.5 | | | |
| LC-3 | WM | 6251 | 141 | 11.8 | | | |
| LC-4 | Degas. | 337 | | | | | |
| LC-5 | WM | 5779 | 107 | 2.6 | | | |
| LC-6 | B | 6046 | 50 | 16.7 | | | |
| LC-7 | OP | 504 | 3.3 | 0.3 | | | |
| LC-8 | WM (LC-7) | 739 | 20 | 0.4 | | | |
| LC-9 | Near Slow B | 1325 | 4.0 | 0.3 | | | 538 |
| LC-10 | OP | 1994 | 12 | | | | |
| LC-11 | OP | 1503 | 83 | | | | |
| LC-12 | BrP | 978 | 12 | | | | |
| LC-13 | WM | 1282 | 89 | | | | |
| LC-14 | WM | 1639 | 27 | | | | |
| LC-15 | S | 1275 | 6.9 | | | | |
| LC-16 | BrP | 1371 | 5.6 | | | | |
| LC-17 | SB | 144891 | 95 | | | | |
| FPS | FPS | 26033 | 13 | | | | |
| MPS-2018 | MPS | | 126 | | | | 1899 |
| MPS-2019 | MPS | 248766 | 73 | | 1.6 | 0.1 | 1548 |
| MPS-2021 | MPS | 25554 | 61 | 15.5 | | | 1410 |
| **La Calcara Off Active Sites** | | | | | | | |
| LC-18 | (LC-2) | 547 | 12 | | | | |
| LC-19 | (LC-3) | 7470 | 21 | 0.9 | | | |
| LC-20 | (LC-5) | 6203 | 6.2 | | | | |
| LC-21 | (LC-2) | 566 | 6.6 | 0.5 | | | |
| **Black Point** | | | | | | | |
| BP | BP | 22 | 0.8 | | | | 1.8 |
| BPW | FPS | | 1.5 | | | | |
| **Panarea Harbor** | | | | | | | |
| PH-2018 | | | | | | | 1264 |
| PH-2019 1 | LT | | | | | 0.1 | 1224 |
| PH-2019 2 | HT | | | | | 0.1 | 1234 |
| **Bottaro North** | | | | | | | |
| BN-2019 | | | | | | 3.3 | 0.9 |
| BN-2018 | | | | | | | 1.1 |

filtered (Hg$_{diss}$), elemental Hg (Hg$^0$), monomethyl Hg (MMHg), and dimethylmercury (DMHg). Gaseous mercury samples (Hg$_{gas}$) were presumed to be entirely elemental Hg in the vapor phase. Surface waters (n = 2) were collected by boat using 60 mL polypropylene syringes and filtered immediately onboard through a 0.45 µm membrane. Hydrothermal fluids were collected using pore fluid samplers constructed from PTFE tubing and 10 mL pipette tips at 10 cm depth using polypropylene 60 mL syringes. Porewater temperatures were monitored at the pipette tip and deviations in temperature were not observed during sampling. This ensured that samples were not contaminated with seawater. Measurements of pH (Halo Wireless pH meter, Hanna Instruments), conductivity and ORP (Myron Ultrameter) were immediately taken in the field. The subsample for anion analysis was filtered with a 0.45 µm syringe filter, and the subsamples for elemental analysis (ICP-OES and ICP-MS) were additionally preserved with 2 % (m/v) concentrated nitric acid.

Hg speciation was completed for MPS, which included the determination of THg, Hg$_{diss}$, Hg$^0$, DMHg, and MMHg. The required sample volume was collected at the same time. The temperature at the point of sampling was constantly monitored to assess the potential of seawater contamination. A total of ten gas samples were collected for analysis of Hg$_{gas}$ (Table 1). The background surface seawater sample was collected in an area with no visible hydrothermal activity.

Total Hg samples were collected as unfiltered and filtered (0.45 µm), stored and analyzed following the USEPA (2002) protocol with a Brooks Rand CV-AFS analyzer. The acidified samples arrived from the field in the laboratory and were held at 4 °C until analysis. On the day of analysis, 40 mL sample was transferred into a 60 mL Volatile Organic Analysis (VOA) glass vial with a PTFE lined cap. 400 µL acidified bromide/bromate (1:1 mixture of 0.01 M bromide/bromate solution (Tritrisol, Merck) and 32 % hydrochloric acid (Optima grade, Fisher Scientific)) were added to the sample and left standing for at least 30 min at room temperature. The reactivity of the bromine chloride was then quenched by adding 100 µL 30 % (m/v) hydroxylamine hydrochloride solution (ReagentPlus, 99 %, Sigma-Aldrich). Elemental Hg was generated in the solution upon the addition of 200 µL 20 % (m/v) tin(II)chloride solution (Reagent grade, Alfa Aesar). Each sample was analyzed in duplicate whenever the sample volume allowed. The limit of detection for this method in our laboratory was determined to be 0.04 ng/L (n = 10). The certified reference material

ORMS-5 (elevated Hg in river water, National Research Council Canada) was used for quality control. The reference material is certified for a concentration of 26.2 ± 1.3 ng / L THg.

Sediment samples were collected from multiple sites across the LC with 60 mL sample tubes. The sediment samples were digested in 10:3 $HCl:HNO_3$ following Bloom et al. (2003) and THg was analyzed by CV-AFS. The certified reference material PACS-1 (marine sediment, National Research Council Canada), certified for a concentration of 4.57 ± 0.16 µg/g THg was used for quality control.

$Hg^0$ in the liquid phase was collected from selected samples by purging 1 L of hydrothermal fluid with Hg free nitrogen onto gold and carbo traps and analyzed by CV-AFS (Cossa et al., 2011; Lehnherr et al., 2011).

MeHg was analyzed by species-specific isotope dilution-gas chromatography-inductively coupled plasma-mass spectrometry (SSID-GC-ICP-MS) (Brombach et al., 2018). A 100 mL sample was spiked with a solution of $Me^{201}Hg$ (ISC Science, Spain) and left standing for an hour for equilibration. An optimal ratio of 4.25 for $Me^{201}Hg$ in the spike to $Me^{202}Hg$ in the sample was the aim of the spiking. Based on the assumption that 5 % of THg was present as $Me^{201}Hg$, the amount of the enriched isotopic solution was calculated for the initial spiking. An addition of 5 mL of a 1 M acetic acid – acetate buffer at pH 3.9, prepared from trace metal grade acetic acid (Fisher Scientific) and 30 M NaOH (Suprapur, Merck), was added to the sample and the pH was adjusted to 3.9 with sodium hydroxide (30 M, Suprapur, Merck). Subsequently, 1 mL propylation reagent (1 g sodium tetrapropylborate (Merseburger Spezialchemikalien, Germany) in 100 mL oxygen-free Milli-Q water was added to the sample followed by 200 µL n-hexane (Reagent Grade ACS, Riedel-de-Haen). The Hg species were extracted into the n-hexane phase by shaking for 10 min and the n-hexane phase was analyzed using a Thermo Scientific Trace 1300 GC coupled to a Thermo Scientific Element 2 ICP-MS. A cyclonic spray chamber was attached to the transfer line just before the ICP torch for wet plasma conditions giving the option of plasma tuning and monitoring with an internal Thallium standard. General settings of the GC and the ICP-MS can be found elsewhere (Brombach et al., 2015). As has been previously discussed for other systems, no measurable MeHg was observed in hydrothermal samples (Roberts and Pichler, 2022; Roberts et al., 2021) and is therefore not further reported here.

## 5. A Marine Shallow Water Hydrothermal System as a Hg Emitter to the Local Environment of Panarea, Italy

Gas samples were collected into Tedlar© bags using a custom-built glass funnel connected to Teflon tubing in combination with a standard underwater lift bag. The lift bag was attached to lead weights which enabled the calculation of the gas volume collected, i.e., the volume of gas needed to displace enough seawater to lift the bag at a given depth and lead weight. In some instances, gas point sources were located at depths too shallow to use the lead weights. In these instances, gas sample bags were filled as much as possible without damaging the sample bag. Gas samples were filtered through an alkaline solution to remove sulfur species. The sample was then trapped in 0.5 M permanganate solution in 2 N sulfuric acid and analyzed by CV-AFS as THg (Brombach and Pichler, 2019).

Anions were analyzed using a Metrohm 883 Basic IC plus instrument fitted with a 5 µL injection loop and a Metrosep A Supp5 (150 × 4.0 mm; 5 µm) column for anion separation in combination with a mobile phase consisting of 3.2 mmol/L $Na_2CO_3$ (Analytical reagent grade, Fisher Scientific) and 1.0 mmol/L $NaHCO_3$ (puriss. p.a., ≥ 99.7 %, Sigma-Aldrich). Quality control was assured with an internal laboratory standard and the artificial seawater standard IAPSO. Major cations were measured by inductively coupled plasma-optical emission spectrometry (ICP-OES) using a Perkin Elmer Optima 7300 DV instrument. Quality control was assured by using the EnviroMAT Groundwater Low (ES-L-2) and High (ES-H-2) standards and a certified seawater (CRM-SW, High Purity Standard). Trace elements were analyzed by inductively coupled plasma-mass spectrometry (ICP-MS, Element 2 Thermo Scientific). Quality control was identical to that of the ICP-OES measurements (Table 5.1).

Sulfide was analyzed with a Merck photometer following Cline (1969). A solution of dimethyl-p-phenylene-diamine is prepared with N,N-Dimethyl-1,4-phenylenediammoniumm dichloride (Analytical reagent grade, Merck) dissolved in HCl. The dimethyl-p-phenylene-diamine binds with hydrogen sulfide in solution to form leucomethylene blue. Leucomethylene blue is then oxidized by ferric iron, prepared by dissolving $FeCl_3$*6 $H_2O$ (Analytical reagent grade, Merck) in HCl, to form methylene blue.

The use of eH-pH diagrams for hydrothermal systems assists in the identification of controlling factors regarding a single species. Lines represent transitions between primary species of a given element within a sample.

101

Hydrothermal samples are typically reducing (having a negative Eh) and acidic. The measurement of Eh is simple in principle but difficult in practice. Ratios of S speciation, or hydrogen fugacity can be used in its approximation. Within this text, Eh-pH diagrams were produced using Geochemists Workbench with the Miniteq thermodynamic dataset, as previously utilized by Swanner et al. (2014).

## 5.4 Results

### 5.4.1 Seawater

Surface water concentrations of THg above Black Point (BP) and MPS were similar to the background sample (Table 5.1 and 5.2). Concentrations ranged between 14 and 350 pM in the depth profile above MPS (Fig. 5.3). $Hg_{diss}$ for all seawater samples was below 25 pM. Cation and anion concentrations within all samples were similar, except for the bottom water (20 m below water table) sample collected directly above MPS. For this sample, 4.9 M Si was observed, where background seawater was 29 mM. Within 19 m values of pH increased from MPS, from 6.31 to 8.22. Not enough sample was available to analyze cations and anions for the sample collected at 5 m depth. With the exception of the surface, all water column samples were elevated in Hg (THg and $Hg_{diss}$) compared to the background sample. In contrast to the elevated Hg, pH returned to background values 5 m from the bottom.
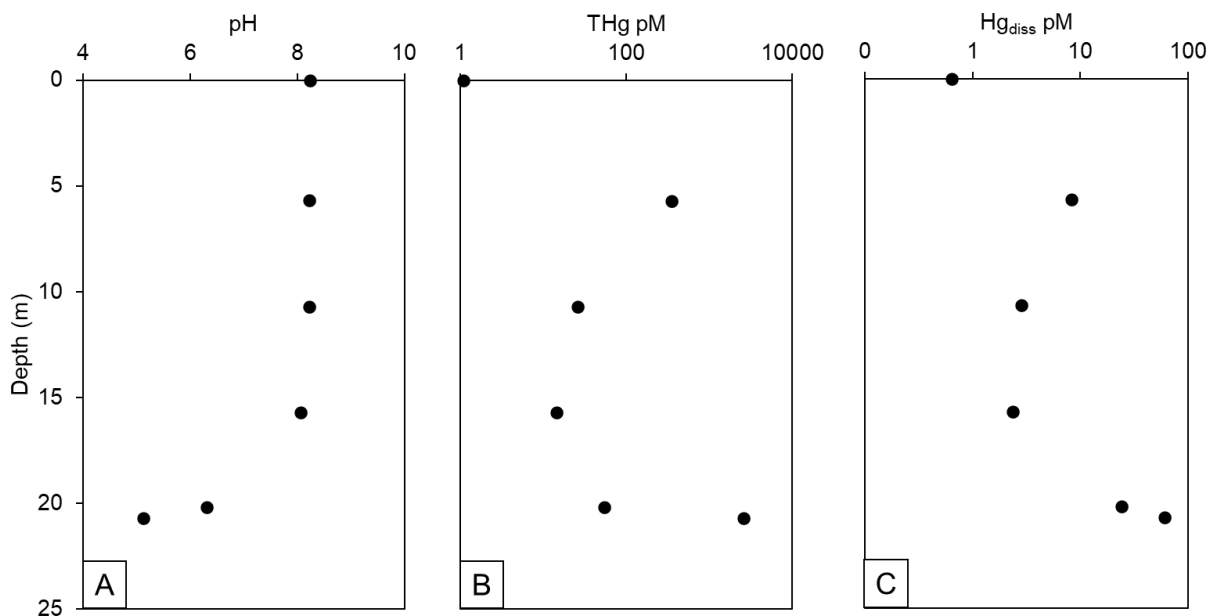


Figure 5.3: Depth profile above MPS of A) pH, B) THg pM, and C) $Hg_{diss}$ pM. Data clearly show enrichment of THg and $Hg_{diss}$ throughout the water column.

## 5.4.2 Porewaters

Porewaters collected from areas of diffuse hydrothermal emission and point sources ranged in pH-value, temperature, Sr, Si, Mn, and Fe (Table 5.1). Small deviations in major cations and anions were observed, with lower than background seawater concentrations in hydrothermally influenced samples when compared to temperature (Fig. 5.4). Concentrations of Hg within porewaters ranged between 22 pM and 248 nM THg and 0.8 to 141 pM $Hg_{diss}$. Higher concentrations of THg had a positive relationship with temperature and a negative relationship to chloride (Fig. 5.5).
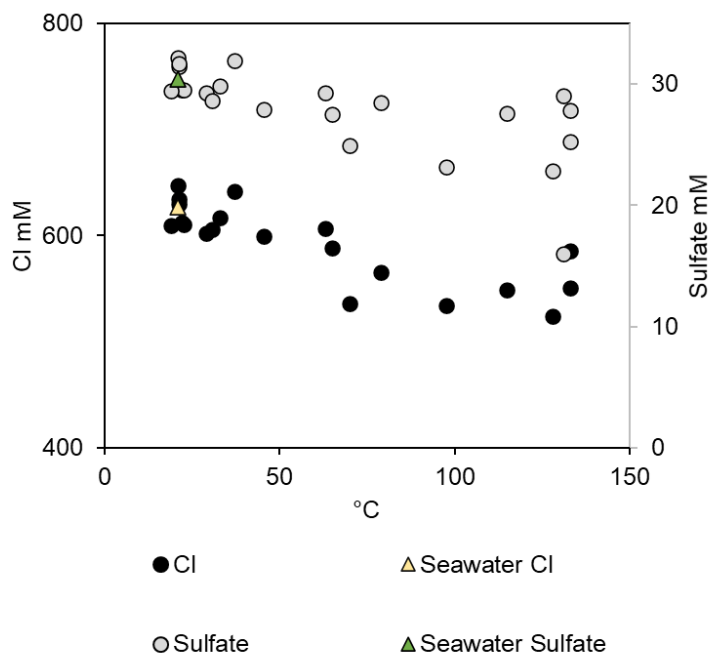


Figure 5.4: Porewater concentrations of Cl (black circle) and $SO_4$ (grey circle) with temperature compared to background seawater values (yellow triangle and green triangle respectively).
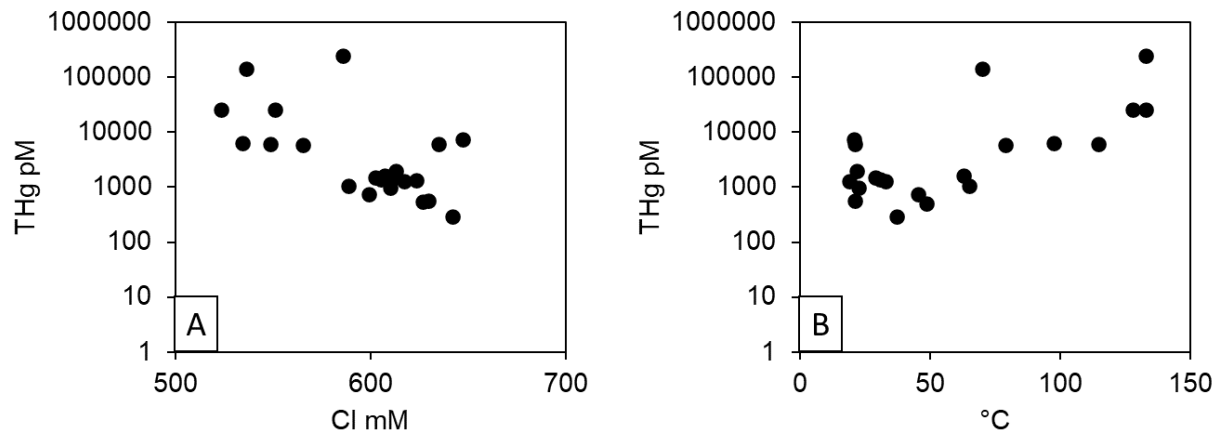
Figure 5.5: THg (pM) of LC porewaters compared to A) Cl (mM) and B) temperature (°C). THg trended negatively with Cl concentrations and positively with temperature.

### 5.4.3 Gases

Due to the complexity of gas collection sampling, data from this study were compared to those previously collected using the same techniques at other locations (Roberts and Pichler, 2022; Roberts et al., 2021). Gas concentrations of Hg ranged between 0.9 and 1899 nmol / $m^3$. Among all sampled gases sedimented point sources had low $Hg_{gas}$ concentrations, while unsedimented point sources had both high and low $Hg_{gas}$ concentrations (Fig. 5.6). Concentrations of THg within the gases at Panarea remained relatively stable in 2018, 2019, and 2021 with the exception of those at MPS (Fig. 5.7). Gas concentrations were highest at point sources with high temperatures (> 100 °C), pH between 5 and 7, and increased with porewater THg (Fig. 5.8A-D). Additionally, the highest $Hg_{gas}$ concentrations were in samples with high Mg, Ca, and K in associated fluid samples (Fig. 5.9 A-C).

# 5. A Marine Shallow Water Hydrothermal System as a Hg Emitter to the Local Environment of Panarea, Italy
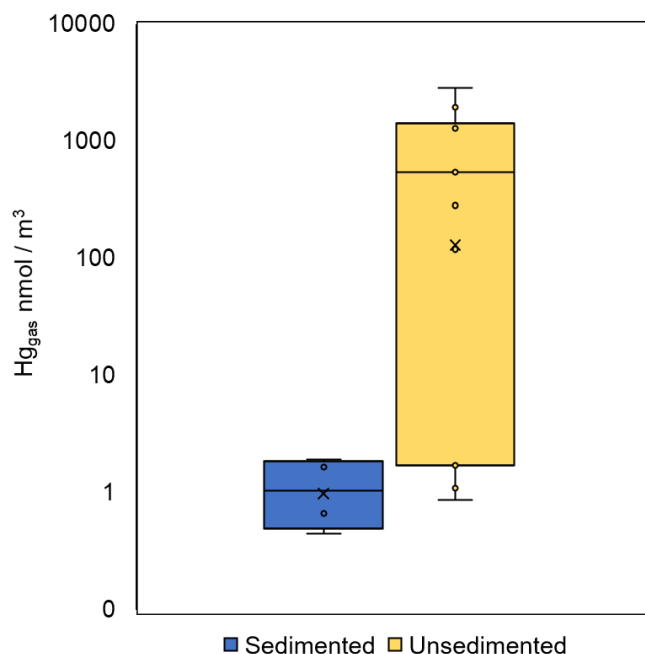


Figure 5.6: Comparison of Hg$_{gas}$ (nmol / m$^3$) sedimented (blue) versus unsedimented (yellow) gaseous point sources. Concentrations were highly variable between unsedimented point sources, however sedimented point sources were all low in Hg$_{gas}$. Samples include those collected for this study in Panarea, Italy, from Vulcano, Italy (Roberts and Pichler, 2022), and from Milos, Greece (Roberts et al., 2021).
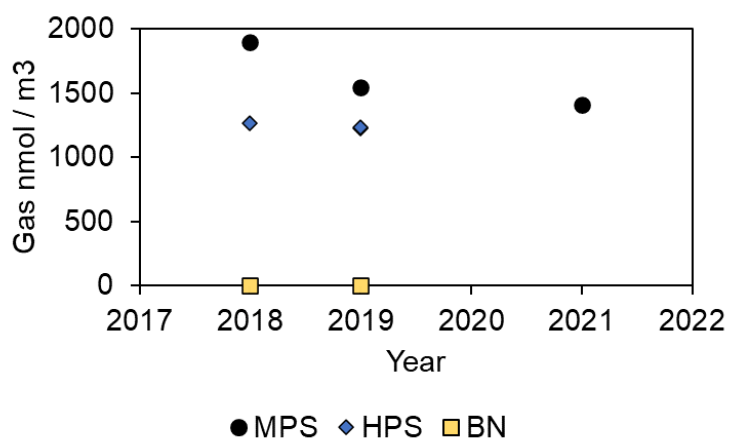


Figure 5.7: Concentrations of Hg$_{gas}$ (nmol / m$^3$) from Panarea samples collected in 2018, 2019, and 2021. MPS samples in black circles, HPS samples in blue diamonds, and BN samples in yellow squares. No variation was observed with the exception of MPS.
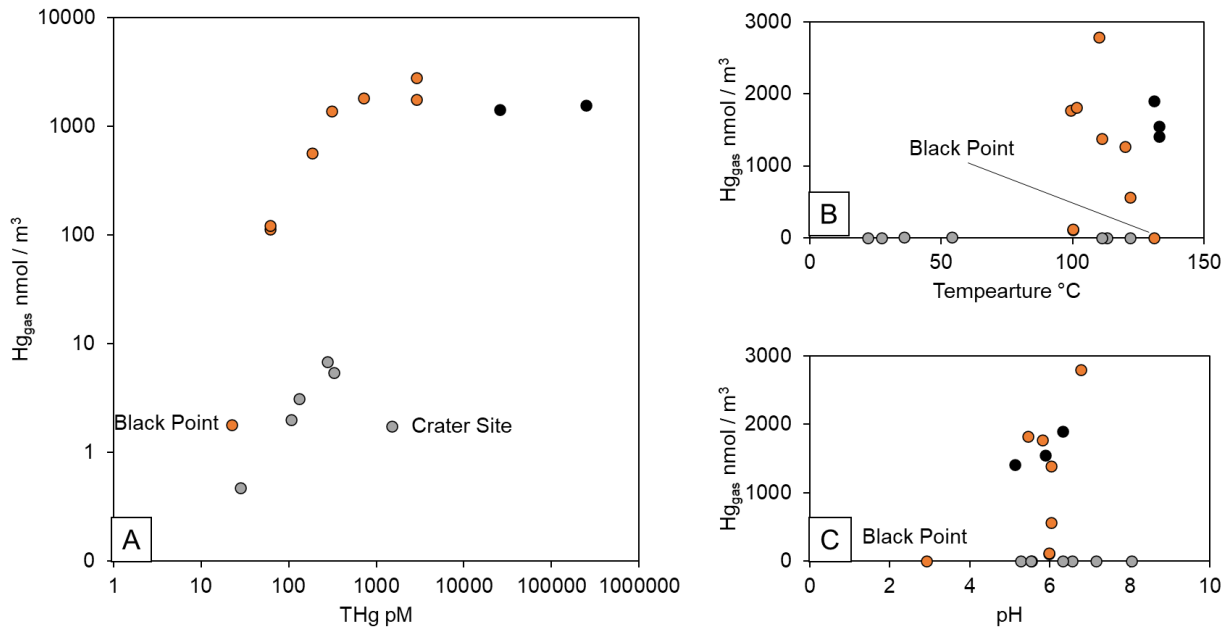
Figure 5.8: Comparisons of Hg$_{gas}$ (nmol / m$^3$) with A) THg (pM), B) temperature (°C), and C) pH. Sedimented sites are in grey, unsedimented sites are in orange, and MPS (2018, 2019, and 2021) are in black. The highest Hg$_{gas}$ concentrations were in unsedimented sites with high THg in poerwaters, with high temperature and near neutral pH. Data includes this study from Panarea, Italy, from Vulcano, Italy (Roberts and Pichler, 2022), and Milos, Greece (Roberts et al., 2021).
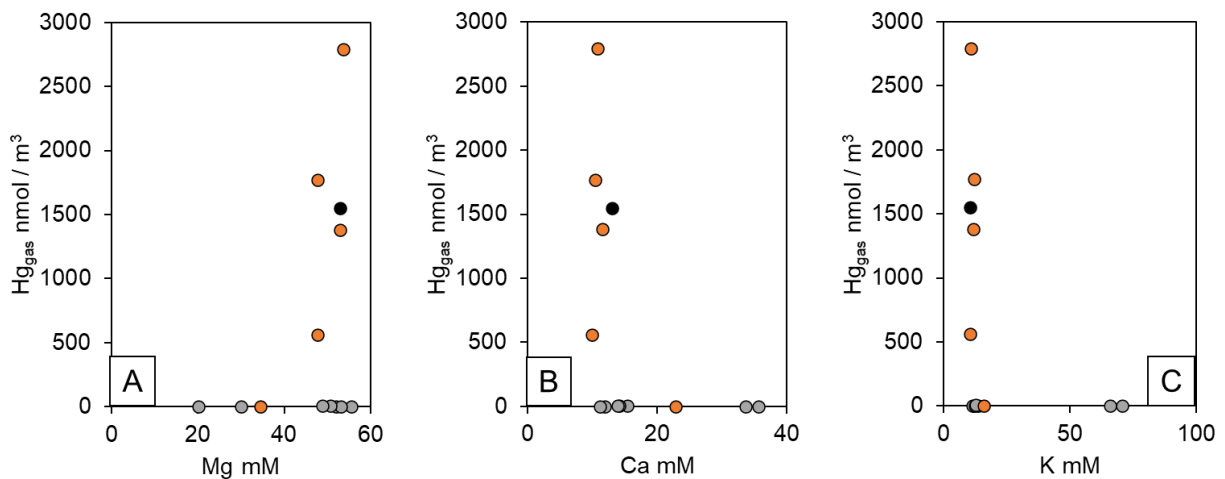


Figure 5.9: Comparisons of Hg$_{gas}$ (nmol / m$^3$) with A) Mg (mM), B) Ca (mM), and C) K (mM). Sedimented sites are in grey, unsedimented sites are in orange, and MPS (2018, 2019, and 2021) are in black. The highest Hg$_{gas}$ concentrations were in unsedimented sites with high Mg and low Ca and K in porewaters. Data includes this study from Panarea, Italy, from Vulcano, Italy (Roberts and Pichler, 2022), and Milos, Greece (Roberts et al., 2021).

## 5.4.4 Sediments

Sediments at LC ranged in THg concentration between 0.49 to 16.7 nmol / g. Concentrations were highest from high temperature sites (Fig. 5.10). Concentrations of THg within the sediments were higher with low Cl. No clear relationship was observed between sediment THg and porewater THg concentration. At two locations sediments were taken directly from an active area ("on" samples) and compared to a non-active (low temperature) area ("off" samples). At another location, white mat and orange precipitates were found directly next to one another. Concentrations were consistently higher in 'on' samples compared to 'off' samples and the white mat contained significantly more THg than the orange precipitate (Fig. 5.11). At MPS, limited sediment was present above the point source. However, one piece of cemented material was gathered and analyzed, providing a concentration of 15.5 nmol / g THg. The highest sample, 16.7 nmol / g (LC-6), was collected from a high temperature gas emission point source.
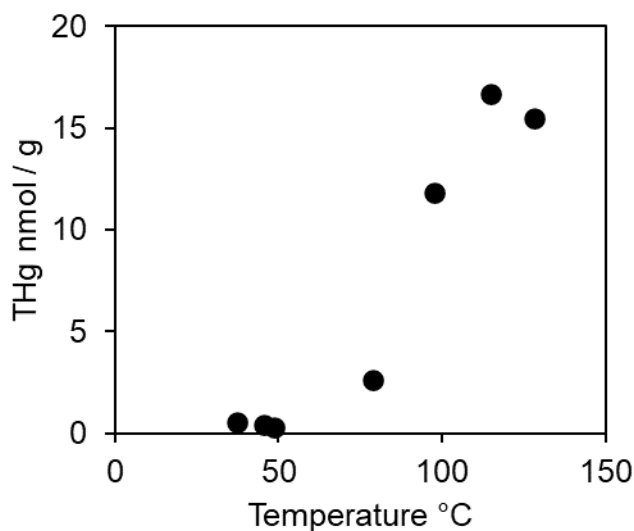


Figure 5.10: Concentration of THg (nmol / g) in the sediments of Panarea. Data clearly show increasing THg concentration with temperature.
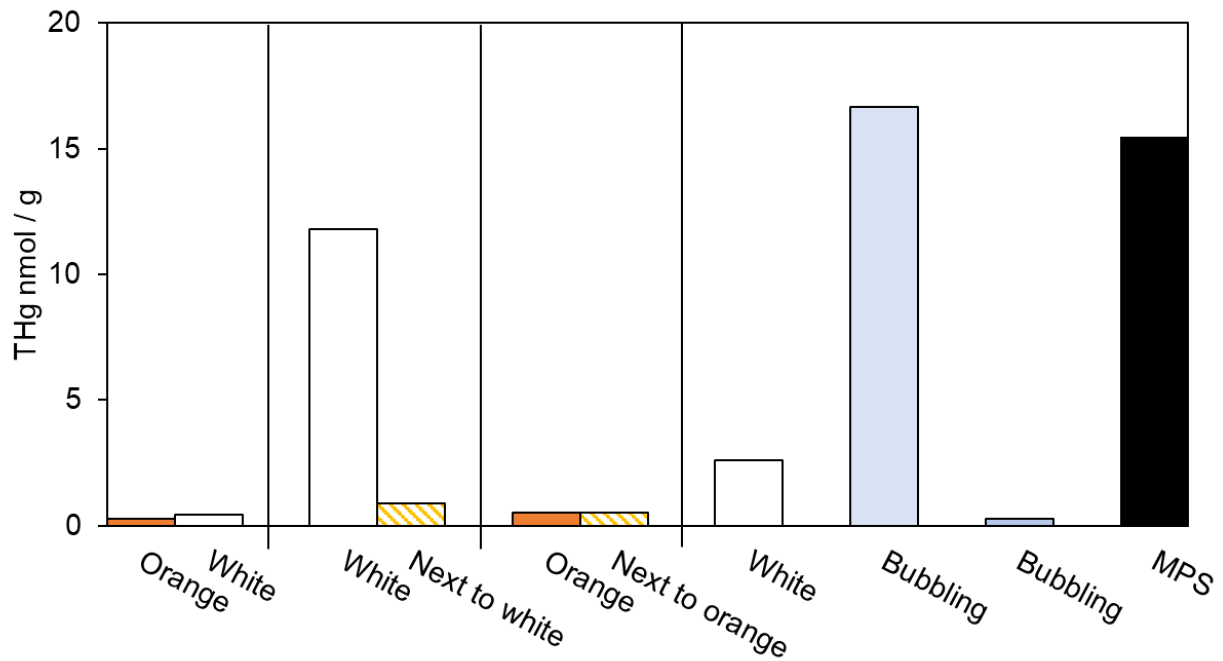
Figure 5.11: Comparison of sediment THg (nmol / g) of LC samples. Groups of samples (samples taken within 50 cm) are separated by black lines. Samples with orange precipitates are in orange, white mat areas are in white, background temperature adjacent samples are in striped yellow, bubbling samples are in grey, and MPS is in black. Areas with orange precipitates contained near background THg concentrations. White mats were highly variable in THg, and actively bubbling samples contained the highest THg, but were also variable.

## 5.5 Discussion

### 5.5.1 Hydrothermal Gases

The role of sedimentation over point sources seems to be critical to $Hg_{gas}$ (Fig. 5.6). Therefore, the following discussion was divided into sedimented and unsedimented point sources. Within the subsurface, Hg primarily travels within a vapor phase bound to S or Cl complexes (Varekamp and Buseck, 1984). Therefore, Hg is expected in the emitted gases of MSWHS. However, as has been previously established, Hg is present within gases, fluids, ores, and sediments associated with MSWHS, due to processes within the subsurface and at the point of emission (Bagnato et al., 2017; Bagnato et al., 2009b; Leal-Acosta et al., 2018; Prol-Ledesma et al., 2004; Roberts and Pichler, 2022; Roberts et al., 2021; Voudouris et al., 2021). Environmental factors at the point of emission had strong influences on concentrations of Hg within the gases of multiple MSWHS (Roberts and Pichler, 2022; Roberts et al., 2021).

# 5. A Marine Shallow Water Hydrothermal System as a Hg Emitter to the Local Environment of Panarea, Italy

### *5.5.1.1 Sedimented Gaseous Point Sources*

At sedimented sites, hydrothermal gases were likely impacted by mixing with hydrothermal fluids and seawater to a greater degree than unsedimented sites. The greatest indicator of low $Hg_{gas}$ was sufficient sediment coverage where emitted gas was consistently filtered through sediment grains and removed Hg from the gas (Fig. 5.6) (see section 5.2.2). It should be noted that relationships between sedimented samples and porewaters can be discussed more readily than unsedimented samples, as porewaters reflected mixtures of seawater, dissolved hydrothermal gas components, and hydrothermal fluids that react with the sediment (Pichler et al., 1999a; Roberts et al., 2021). Among sedimented samples, $Hg_{gas}$ showed a clear negative relationship with Cl and pH (Fig. 5.12), and samples with higher $H_2S_{gas}$ % had higher $Hg_{gas}$.

As hydrothermal gases ascend to the sediment-water interface, temperature and pressure is reduced and oxic seawater is increasingly present (Price and Giovannelli, 2017). A positive trend between $Hg_{gas}$ with $H_2S_{gas}$ is therefore expected. The greater interaction between $H_2S_{gas}$ and seawater oxidizes $H_2S$ to form $S_2O_3^-$, $SO_4^{2-}$ and $S^0$ (Pichler et al., 1999a; Wenzhofer et al., 2000). Therefore, decreased interaction and removal of gaseous species within the subsurface (e.g., increased $H_2S_{gas}$) results in greater concentrations within collected gases at the sediment-water interface (e.g., $H_2S_{gas}$ and $Hg_{gas}$). The negative trends observed between $Hg_{gas}$ and percent $Hg_{diss}$ of THg, Cl, and pH, follow the same pattern. Higher pH and Cl are indicative of greater contributions of seawater in the subsurface which lead to $Hg_{gas}$ removal from the gas phase, (see equations 1 and 2).
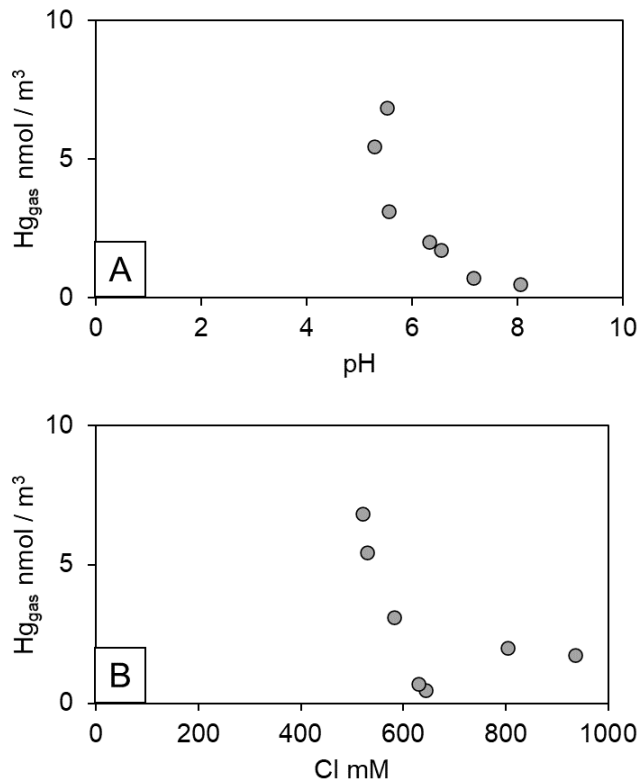
Figure 5.12: Trends of concentrations of Hg$_{gas}$ (nmol / m$^3$) from sedimented point sources with A) pH, and B) Cl (mM). Hg$_{gas}$ was highest where porewaters were most affected by rising vapor (e.g., low pH and low Cl).

### 5.5.1.2 Unsedimented Gaseous Point Sources

Before considering unsedimented point sources, it is important to discuss the relationship between Hg$_{gas}$ and porewater fluid samples. Due to the nature of these sites and the methods employed to sample them, fluid samples uncontaminated by seawater were not possible. Therefore point sources with no sedimentation reflect seawater altered by hydrothermal fluids and gases, where the primary component of the sample is seawater (Roberts et al., 2021). The flow of hydrothermal fluid from unsedimented point sources and the sampling technique used in retrieving the sample may greatly impact results. Fluid samples taken from unsedimented sites are therefore considered indicative of the impact of hydrothermal gas and fluid chemistry on seawater at the point of emission, rather than a reflection of hydrothermal fluid or subsurface reactions. Indeed, the highest gas concentrations were associated with fluid pH values between 5 and 7, with the highest gas concentration measured (2791 nmol / m$^3$) with a pH of 6.78. The composition of gases collected at Panarea, Vulcano, and Milos, were primarily $CO_2$, with varying concentrations of $H_2S$, $CH_4$, $H_2$,

Ar, He, CO, and others (Capaccioni et al., 2001; Dando et al., 1995; Italiano and Nuccio, 1991). Additionally, unsedimented $Hg_{gas}$ increased with increasing Mg (Fig. 5.9), which is associated with higher seawater content in porewaters (Khimasia et al., 2021; Roberts et al., 2021; Valsami-Jones et al., 2005). Relationships of Ca and K with Mg from unsedimented fluid samples, indicate the samples are similar to gas-rich fluids as described by Price et al. (2015) (Fig. 5.9).

Despite the contamination of samples by seawater, the relationship between $Hg_{gas}$ and THg among unsedimented point sources is informative, as higher THg indicates greater hydrothermal influence (Roberts and Pichler, 2022; Roberts et al., 2021). Higher THg was associated with higher $Hg_{gas}$ and higher $H_2S_{gas}$. The reaction of $H_2S_{gas}$ with Hg and seawater led to the formation of Hg-bearing minerals in both, sulfur rich (equation 3), and sulfur poor (equation 4) systems (Krupp, 1988). Here Hg is transported as either $HgS_2^{2-}$, a Hg sulfide complex species, or $Hg_x^0$, $Hg^0$ in the liquid or gaseous phase.

3) $HgS_2^{2-} + 2O^2 \leftrightarrow HgS + SO_4^{2-}$

4) $Hg_x^0 + H_2S + 0.5O_2 \leftrightarrow HgS + H_2O$
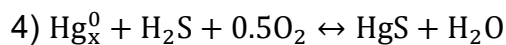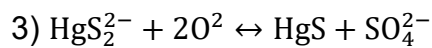
The $Hg_{gas}$ concentrations at MPS between 2018, 2019, and 2021 were below expected values given the high THg concentration in fluids assuming a relationship exists between fluid and gas concentrations. The pH of MPS provided a possible explanation. MPS was more acidic than other measured unsedimented point sources and was less reducing. While the $Hg_{gas}$ followed similar trends as other unsedimented point sources, the THg of the sample was unique. Increasing concentrations of $H_2S_{gas}$ and $H_2S_{aq}$ were associated with lower ORP values (< -100), as increasing seawater oxidizes the porewater and removes $H_2S$. The concentrations of $H_2S_{gas}$ and $H_2S_{aq}$ at MPS were low in comparison to other point sources. Greater oxidation of hydrothermal fluids and gases led to the accumulation of Hg in the fluid phase (THg), however the high temperature (> 130 °C) maintained THg in solution.

Sedimentation clearly affects $Hg_{gas}$ through removal processes or as an indication of limited flow (e.g., insufficient to expel sediment from the point of emission). The highest $Hg_{gas}$ measured between Panarea, Vulcano, or Milos were from unsedimented point sources (2791 nmol / m³), while sedimented sources did not exceed 2 nmol / m³ (Fig. 5.6). Sediments clearly show enrichment from hydrothermal point sources (this study, Roberts and Pichler, 2022; Roberts et al., 2021; Saupe,

1990; Varekamp and Buseck, 1984; Voudouris et al., 2021), which may act as adsorption for some point sources and therefore limit $Hg_{gas}$. The adsorption of $Hg^{2+}$ onto soils occurs most readily at pH values between 3 and 5 where dissolved organic matter was low, however the presence of Cl inhibited that uptake where organic matter was very low (Yin et al., 1996). The limited data available regarding oxidation of $Hg_{gas}$ to $Hg_{diss}$ or $Hg^{2+}$ from MSWHS is currently insufficient to be conclusive. However, data indicates the process to be significant to Hg cycling from MSWHS (Christenson and Mroczek, 2003; Davey and van Moort, 1986; Roberts and Pichler, 2022; Roberts et al., 2021)

### 5.5.1.3 Gas concentration outlier: Black Point

The high temperature unsedimented point source BP was an outlier with respect to gas concentration trends. BP was depleted in THg and $Hg_{gas}$ when compared to other unsedimented point sources with high temperatures (Fig. 5.8). This is particularly surprising given the formation of BP, where very "clean" (e.g., limited contamination by seawater) samples were possible for an unsedimented point source. Interestingly, previous studies have inferred Black Point as having a significant magmatic gas component which infers greater $Hg_{gas}$ (Roberts et al., 2021; Sieland et al., 2009). However, the very low pH observed at BP poses a significant deviation from other point sources. At high temperature (100 °C) and low pH (< 5), cinnabar is stable at low $H_2$ fugacity, with decreasing total reduced sulfur concentrations increasing cinnabar stability (Krupp, 1988). The Eh-pH diagram of BP fluids indicates $Hg(HS)_{2\ aq}$ as the dominant Hg species at low pH reducing fluids (Fig. 5.13). The most suitable thermodynamic data inclusive of Hg (miniteq) was used, but was also limited to 100 °C. It should be noted, however, that reports indicate oxidizing conditions at BP (Sieland et al., 2009), which would shift the primary Hg species to $Hg_{aq}$. Therefore, higher concentrations of Hg within the fluids would be anticipated, particularly given the high temperature of the point source. Additionally, a significant portion of THg would be expected as $Hg_{diss}$. However, neither of these is the case. Either significant subsurface deposition of Hg occurs, or the hydrothermal source is already depleted in Hg. Further investigations would be necessary to discuss BP in more detail, particularly with a focus on subsurface processes.

## 5. A Marine Shallow Water Hydrothermal System as a Hg Emitter to the Local Environment of Panarea, Italy
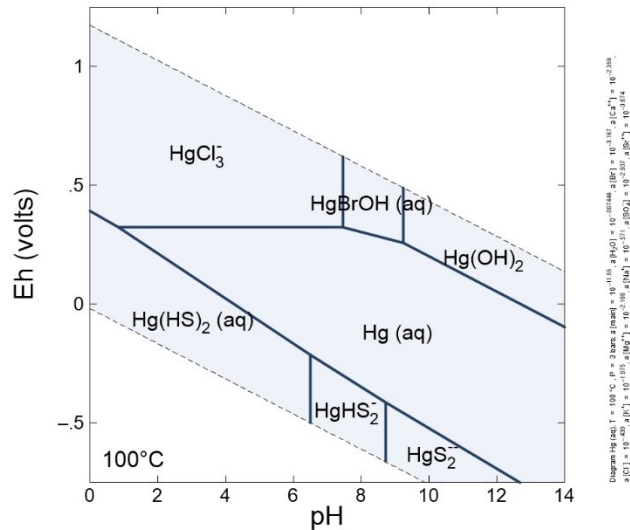


Figure 5.13: Stability diagram of Black Point fluid using calculated activities for measured analytes and the Miniteq thermodynamic data at 100 °C. Produced using Geochemists Workbench.

### 5.5.2 La Calcara

Previous research was heavily focused on the BP site. However, very high concentrations of $Hg_{gas}$ and THg were found at La Calcara. The area contained a mixture of highly active point sources and large areas of diffusive emission. At a depth of approximately 20 m, wave action was less prominent than shallower point sources (< 5 m). Due to this aspect, the stability of the area was conducive to multiple day and multiple year sampling. Therefore, the La Calcara area was selected for in-depth sampling across multiple years of study.

#### 5.5.2.1 Water column profile

The depth profile obtained over MPS emphasized the difficulty of sampling hydrothermal plumes (Fig. 5.3). The increase in Hg concentration between 15 m and 10 m depth was reflected in increases of cations and anions (Table 5.1 and 5.2). Cations and anions rapidly returned to background values away from the seafloor, whereas THg remained elevated. During sampling, divers noted a change in bubble flow direction due to a current at shallower depth. With this in mind, the high concentration of Hg at 5 m depth had two explanations. First, the sample at 5 m was taken directly in the hydrothermal plume, where deeper samples may have been taken adjacent to the rising plume. Second, a large accumulation of hydrothermally

derived Hg was present at 5 m, as has been previously speculated and discussed for other MSWHS with regard to Hg (Roberts and Pichler, 2022; Roberts et al., 2021), other metals (Pichler et al., 2019; Pichler et al., 1999b), and deep-sea systems (German et al., 1998). Additionally, a mixture of the two explanations is possible. Regardless, despite a large decrease in Hg (THg and Hg$_{diss}$) between hydrothermal fluid, bottom water (20 m), and mid-depth (15 m), Hg was elevated within all samples below the surface (0 m). In deep sea systems, Hg$_{diss}$ declined away from hydrothermal sources to background values, with warmer bottom waters accumulating Hg$_{diss}$ (Bowman et al., 2016). Within the MSWHS of Milos, active areas with high THg and Hg$_{gas}$ at point source located at 5 m depth elevated surface waters (5 to 9 pM) (Roberts et al., 2021).

The implication of a dynamic concentrated plume would affect previous studies of air-sea flux (e.g., Bagnato et al., 2017; Roberts et al., 2021), and potentially marine mercury modeling as well (e.g., Fitzgerald et al., 2007; Outridge et al., 2018). Air-sea flux calculations rely heavily upon concentration differences between the air and seawater. If samples were not collected from the actual hydrothermal plume, the differences between the air and seawater would be significantly less extreme, and therefore flux estimates would not reflect actual values. Marine mercury modeling does not generally discuss hydrothermal systems in detail. Previously, the limited data available indicated hydrothermally derived Hg to be removed from the marine system through scavenging and sedimentation (Bowman et al., 2015). However deep-sea systems differ substantially from MSWHS. Growing evidence suggests Hg remains within marine waters, impacting local environmental systems (Leal-Acosta et al., 2018; Leal-Acosta et al., 2013; Prol-Ledesma et al., 2004; Roberts and Pichler, 2022; Roberts et al., 2021).

At a minimum, MSWHS should be considered important locally. Because MSWHS do not exhibit the same visual plumes associated with deep sea black and white smoker vents, and THg remains elevated where other elements return to background values, sampling from water column plumes in shallow systems remains difficult. Therefore, significantly more data is required to properly evaluate the impact of MSWHS on local Hg cycling. In particular, attention to flow, local water currents, suspended matter, biological samples, and a high density of samples would improve constraints on MSWHS as significant points of Hg emission.

# 5. A Marine Shallow Water Hydrothermal System as a Hg Emitter to the Local Environment of Panarea, Italy

### 5.5.2.2 LC Sediments

High concentrations of Hg within sediments (> 1 nmol / g) resulted from locations of extended, concentrated flow of hydrothermal fluid. Large accumulations of Hg occurred at sampling sites with high temperature (> 80°C) white mat and main vent sites (Fig. 5.10). Where temperatures were below 80 °C, sediments were within background values of THg. Beneath the sediments of La Calcara, locations of greater hydrothermal flow occur along tube-like formations and cracks within cemented material, primarily ironhydroxides, massive sulfides, and clay minerals (Stanulla, 2021). The cementation occurs as hydrothermal fluid temperatures drop alongside decreases in pressure, and fluid mixes with oxic seawater (Barnes, 1979). These formations likely insulated hydrothermal fluid from oxygenated seawater until emission as evidenced by the high Hg concentration and high temperatures observed only at discrete locations at LC. It has long been established that rich Hg ores occur as veins (Barnes, 1979), with greater Hg content associated with deep sea hydrothermal activity, hot spring sediments, gold deposits, and shales (Table 2.1). In previous studies, high concentrations of Hg within sediments associated with hydrothermal systems is concentrated in the upper 100 m, with strong decreases with depth (Christenson and Mroczek, 2003; Davey and van Moort, 1986). Enriched zones were particularly associated with hydrothermal plumbing. Low concentrations of THg observed in this study within samples of orange precipitates (likely Fe- or Mn- oxides) is not surprising, given THg within porewaters was among the lowest of the measured samples. Under reducing conditions, the dominant chemical reaction is adsorption of $Hg^{2+}$ by inorganic sulfides leads to the precipitation of insoluble metacinnabar (Acquavita et al., 2021; Han et al., 2020; Sakamoto et al., 2020; Shen et al., 2020). $Hg^{2+}$ can form associations with organic matter, and Fe- and Mn-oxyhydroxides(Acquavita et al., 2021), however this does not appear to be the case at LC. Therefore, accumulations of THg within sediments is strongly associated with consistent Hg supply.

### 5.5.2.3 LC Porewaters

High THg (> 1,000 pM THg) within LC porewaters was largely due to subsurface flow patterns. Notably, increasing concentrations of $H_2S_{aq}$ trended with lower THg and percent $Hg_{diss}$ of THg inclusive of samples from Panarea, Vulcano, and Milos (Fig. 5.14). Sulfide ions within sediments are associated with the formation

of Hg-S complexes, particularly under anoxic conditions (Fitzgerald et al., 2007). Previously, high THg concentrations within hydrothermal fluids were associated with two main processes: higher arc-magmatic input or greater gas flux. On the island of Milos, hydrothermal fluids with high THg concentrations were associated with low Na / K ratios (Roberts et al., 2021). The high THg values were therefore associated with greater arc-magmatic input. In contrast, on the island of Vulcano higher THg concentrations in fluids were associated with greater gas flux and higher Na / K ratios (Roberts and Pichler, 2022). Similar to Vulcano, THg concentrations at LC were high for most samples, with all Na / K (g-ratio) ratios above 27. High Na / K ratios are associated with conductive cooling and lateral subsurface flow (Nicholson, 1993). However, high THg concentrations (> 1000 pM) did not clearly trend with low Cl and Mg compared to Vulcano, because little variation was observed between the samples. Rather, the near-background concentrations (e.g., Mg, $SO_4$, and Cl) indicated greater seawater contamination of hydrothermal fluids within the subsurface prior to emission. Despite this, concentrations of THg generally exceeded 1000 pM within LC porewaters and trended positively with temperature (Fig. 5B). Similarly, sediment THg also trended positively with temperature, even where samples were taken within 50 cm (see Section 5.2.2). Beneath LC sediments, lies a network of tube-like formations which directs hydrothermal fluid flow (Stanulla, 2021; Stanulla et al., 2017). Above 150 °C, Hg is transported conservatively (Christenson and Mroczek, 2003) and the deposition of Hg within hydrothermal ores is strongly associated with near-surface conditions (Barnes and Seward, 1997). Considering the high temperature (128 to 133 °C) present at MPS, THg reflected hydrothermal fluid minimally diluted by seawater prior to emission with the least deposition in the subsurface. The localized accumulation of THg in fluids and sediments was due to areas of greater, more consistent, hydrothermal flow.

## 5. A Marine Shallow Water Hydrothermal System as a Hg Emitter to the Local Environment of Panarea, Italy
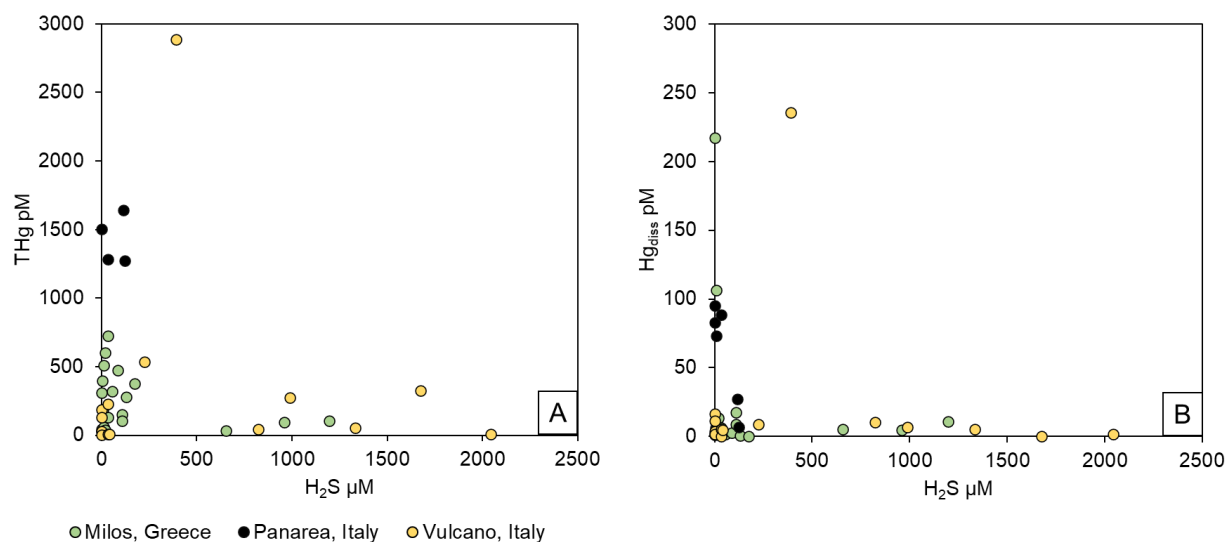


Figure 5.14: Porewater concentrations of A) THg pM, and B) $Hg_{diss}$ pM vs $H_2S$ µM from this study (black), Vulcano, Italy (yellow) (Roberts and Pichler, 2022), and Milos, Greece (green) (Roberts et al., 2021). High concentrations of $H_2S$ limited both THg and $Hg_{diss}$, while the highest THg and $Hg_{diss}$ contained low (< 250 µM) $H_2S$.

### 5.5.2.4 Variation of Hg emissions at LC

A previous study on the island of Vulcano, Italy has shown limited year to year variation in Hg concentrations within fluids and gases (Roberts and Pichler, 2022). However, MPS showed the most variation between 2018, 2019, and 2021 (Fig. 5.7). Most significantly, pH values dropped from 6.33 to 5.13, and THg decreased from 248 nM to 26 nM between 2019 and 2021. It should be noted that MPS is unsedimented, therefore variations in chemical composition are expected dependent upon seawater contamination of fluid samples. However, cation and anion concentrations were similar (Fig. 5.15). Therefore, significant differences of seawater infiltration do not account for the differences in Hg concentration. Thus, the environmental conditions determining Hg emission from MPS changed. The Panarea MSWHS is known to fluctuate, with research supporting a link between increased activity at both Panarea and nearby Stromboli (Heinicke et al., 2009; Longo et al., 2021). The increasing acidity of MPS signals a change in flow and/or subsurface reaction rates (Seyfried and Mottl, 1982). The point of emission of MSHWS represents a highly dynamic environment, particularly for point sources at high temperature. As described by Christenson and Mroczek (2003), Hg is concentrated in the upper 100 m of stratigraphic cuttings due to the nature of Hg deposition (at near surface conditions) (Barnes and Seward, 1997). Zones enriched in Hg were found to

117

correspond to narrow intervals of acid-altered silicic volcanic units, with the upper 5 to 8 m of thermal ground considered an 'ore zone'. Conditions favorable for deposition occur along a non-linear gradient, where flow and chemical reactions compete to determine Hg behavior. Where each point source is located along that gradient at a given time alters the speciation of Hg and therefore the potential for removal or emission. The instability of Hg emissions from MPS is an example of this process and highlights the importance of data inclusive of thermal water, water column (plume), and surface water concentrations.
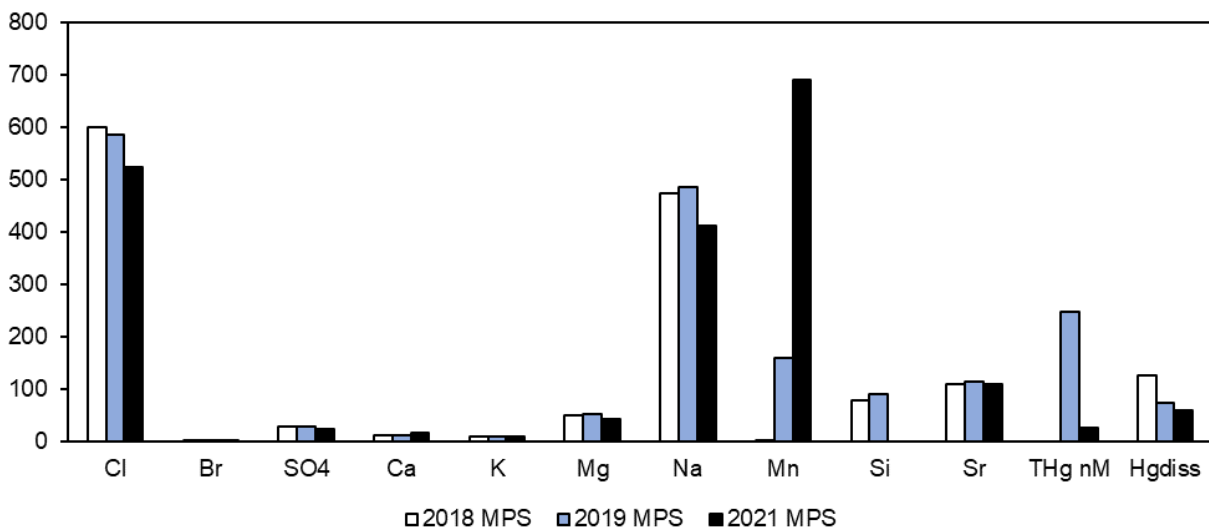


Figure 5.15: Concentrations of cations, anions, THg and Hg$_{diss}$ for MPS from 2018, 2019, and 2021. Cations and anions showed little variation between years, while Mn, THg, and Hg$_{diss}$ were highly variable. Units for cations are in mM; Mn, Si, and Sr are in µM; THg is in nM; and Hg$_{diss}$ is in pM.

### 5.5.2.5 LC as a natural source of Hg to the environment

For the LC area, Hg concentrations in porewaters were generally higher than those at the sites investigated at Vulcano and Milos (Fig. 5.14), however sediment concentrations of THg were lower. Considering the elevated THg present in the water column, transport of THg away from LC, and therefore increased potential for methylation and bioaccumulation, is greatly increased compared to sites of greater sedimentation. Regardless of the importance of MSWHS on a global scale, local environments have been shown to accumulate Hg (Leal-Acosta et al., 2018; Leal-Acosta et al., 2013; Leal-Acosta et al., 2010; Prol-Ledesma et al., 2004; Roberts and

Pichler, 2022; Roberts et al., 2021). Clearly, high concentrations of Hg are emitted to marine waters at LC, with no significant removal mechanism yet established.

## 5.6 Conclusions

Emissions of Hg are generally determined by three basic principles (Fig. 16). First, the concentration of Hg in source material (e.g., subsurface magmatic vapor) determines the limits of Hg emission from any given system. Second, direct, high temperature, high volume flow maintains the most Hg emission within gases and fluids within the subsurface. Third, sedimentation plays a crucial role in filtering Hg from gases and fluids. Methylation of Hg from MSWHS was not found to occur within these systems, however it is clear that transport of inorganic species increases the likelihood of integration into local food webs, particularly at areas such as LC.

Sedimented point sources act as filters for Hg, particularly within the emitted gases. Additionally, sediments aid oxygen circulation within the shallow subsurface which in turn results in further $Hg_{gas}$ oxidation and sedimentation (Davey and van Moort, 1986; O'Hara et al., 1994; Roberts et al., 2021). The addition of microbial white mat activity indicated a balance between three key parameters: oxygen penetration into the shallow subsurface, hydrogen sulfide production, and hydrothermal flow with a larger $H_2S$ component (Roberts et al., 2021). White mat areas provided enough $H_2S$ to sustain microbial activity and limited oxygen exposure in the shallow subsurface. The available $H_2S$ was therefore not oxidized to $SO_4$ and was more readily available to form HgS (Hsu-Kim et al., 2013).
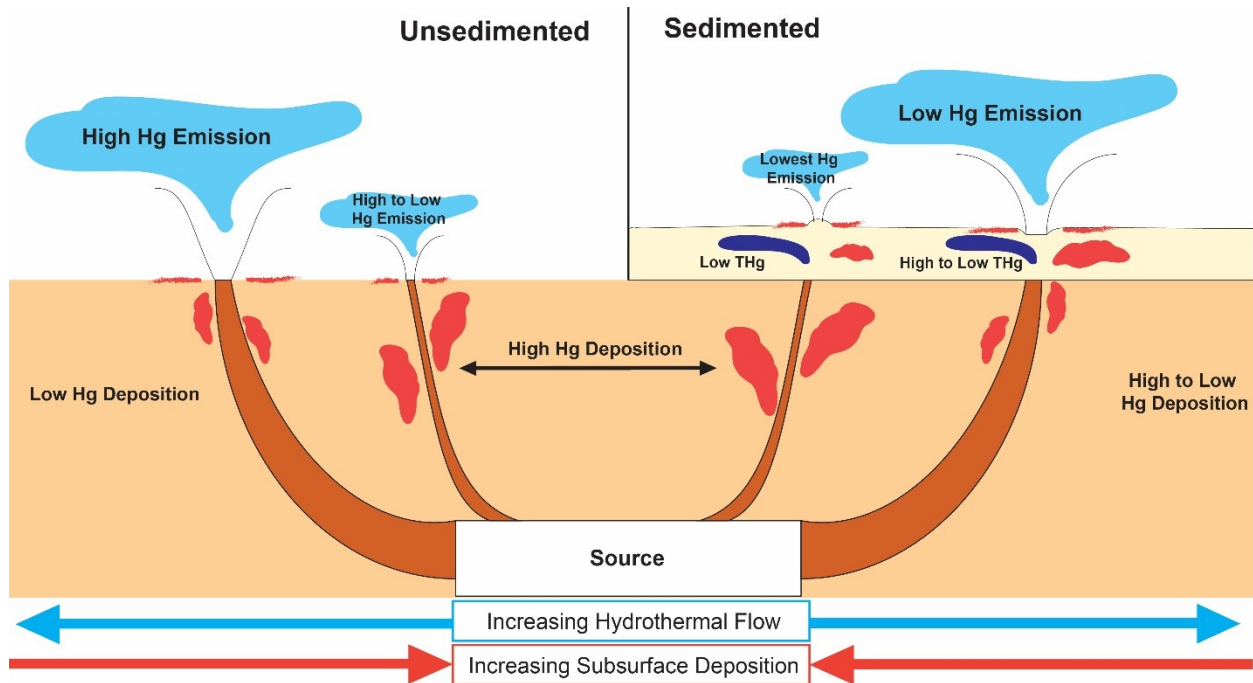
Figure 5.16: Schematic of Hg cycling at MSWHS point sources, emphasizing the importance of sedimentation and hydrothermal flow. Patches of red indicate relative importance of solid phase deposition or sedimentation. Light blue represents hydrothermal flow at the point of emission. Dark blue represents porewaters. Increasing hydrothermal fluid flow coupled with low sedimentation more frequently leads to high Hg emission within fluids and gases. Low Hg emissions are anticipated from point sources with high sedimentation and low flow.

Slower hydrothermal flow increases the potential for redox reactions, increasing oxidation and Hg removal from fluids and gases (Hsu-Kim et al., 2013; Roberts and Pichler, 2022; Roberts et al., 2021). In contrast, greater hydrothermal flow reduces the potential redox changes and can reflect faster ascension of the hydrothermal fluid and gas (Roberts and Pichler, 2022).

Between observations reported at Panarea (this study), Vulcano, Italy (Roberts and Pichler, 2022), and Milos, Greece (Roberts et al., 2021), MSWHS impact Hg cycling within the local environment. Indeed, large mercury deposits are strongly associated with hydrothermalism (Hall et al., 1997; Hernandez et al., 1999; Saupe, 1990). While the largest contributor to the global mercury cycle continues to be anthropogenic influences (Outridge et al., 2018), MSWHS are points of natural Hg emission. Dynamic interplay between environmental conditions (e.g., temperature, sedimentation, pH, hydrothermal flow) alter the fate of that emitted Hg. The role of MSWHS is therefore complex, and at a minimum of importance to the local

environment. Continued observations of MSWHS is necessary to appropriately describe the extent of this impact, with special attention to transport and the potential for biological uptake through more widespread and continuous monitoring of fluids and organisms.

## 6. Conclusions

### 6.1 Sources of Hg within hydrothermal fluids

High concentrations of Hg within hydrothermal fluids were associated with characteristics that are highly dependent upon the system (Fig. 5.14). Hydrothermal systems transport fluids through the subsurface on both a micrometer and kilometer scale. Convection pulls water from sources towards the heat source, driving alteration of the fluid and surrounding rocks under increasing pressure and temperature. Mercury, along with other metals, is transported primarily as a vapor in the subsurface, with the constituents of the heated vapor (e.g. $H_2O$, $CO_2$, $CO$, $SO_2$, etc) likely acting as ligands for metallic species. With increasing heat and buoyancy, the hydrothermal fluid begins to rise. When conditions approach those of the surface, the likelihood of Hg precipitation greatly increases, primarily within sulfur minerals.

On the island of Milos, Greece, high THg concentrations were associated with fast ascension of arc-magmatic fluid. Higher concentrations of cations and anions were therefore an indication of higher THg concentrations. In contrast, high concentrations of THg were associated with low-Cl samples on the islands of Vulcano and Panarea. These systems are dominated by a boiling aquifer, where Hg partitions strongly into the gas phase.

### 6.2 Hg concentration and speciation in hydrothermal fluids

Concentrations of THg and $Hg_{diss}$ in hydrothermal fluids was highly variable. Environmental factors and fluid flow were significant in determining Hg concentration at the point of emission. THg ranged between background seawater values (< 5 pM) to greater than 249 nM.

Primarily, Hg was bound to particulates (> 0.45 μm) with no measurable concentration of organic species present. In some areas with high gas flow, $Hg_{diss}$ was a significant (> 25 %) portion of THg. $Hg^0$ was generally a very small portion of $Hg_{diss}$. Considering the temperatures (< 133 °C) and pH (generally > 4) present at MSWHS, it is likely that precipitation began in the shallow subsurface prior to emission and continued following emission.

122

## 6. Conclusions

### 6.3 Atmospheric flux

Atmospheric flux proved to be a significant removal mechanism where hydrothermal point sources and diffuse emission were present at shallow (< 5 m) depth at both the Milos and Vulcano systems. The Vulcano system in particular exhibited the greatest potential for atmospheric flux. The high $Hg^0$ concentration from samples directly above gaseous point sources was rapidly oxidized to $Hg^{2+}$ with distance. This process increased the Hg transported away from the point source rather than evasion to the atmosphere. The extent of Hg transport in surface waters exceeded those of other hydrothermal indicators, increasing the surface area of affected water to the atmosphere.

The depletion of Hg concentrations within fluid plumes in the water column prior to reaching surface waters can be extensive. However, the environmental parameters present at emission sites play a large role. Immediately upon emission, large changes in temperature, redox conditions, and pH resulted in depletions of Hg. At depths of less than 1 m, with strong emissions, such as Panarea and Vulcano, elevated THg is observed within surface waters (< 100 pM) with over 50% in the dissolved phase in some instances.

### 6.4 Relationship of Hg with microbial white mats

Areas with white mat activity on the island of Milos did not follow relationships observed in areas without white mats. Generally, THg concentrations increased dramatically with temperatures greater than 75 °C. However, white mats did not follow this relationship. Environmental conditions conducive to white mat formation rely upon an interplay between hydrothermal fluid flow and oxygen penetration into the sediments. In non-white mat areas, higher temperatures indicated greater hydrothermal fluid flow, with source material containing high Hg concentrations. In areas with white mats, oxygen penetration into the sediment was limited, thereby inhibiting production of $SO_4$ from $H_2S$ and instead created HgS and limiting emission of Hg.

### 6.5 Hg within the gas phase

Unsedimented sites were the greatest indicator of high $Hg_{gas}$ concentrations. Sedimentation increased the potential for oxidation within the gas plume prior to emission, which oxidized the $Hg^0$ present. Unsedimented point sources were

generally above 100 nmol / m$^3$, while all measured gas samples at sedimented sites were below 10 nmol / m$^3$.

## 6.6 Concluding Remarks

This doctoral study was focused on identifying important factors for Hg emission from MSWHS from three systems (Milos, Greece; Vulcano, Italy; and Panarea, Italy). The major conclusions of this work can be summarized as follows:

- The concentration of Hg in source material (e.g., subsurface magmatic vapor) determined the limits of Hg emission.
- Removal of Hg in the shallow subsurface resulted in high variability between sampling sites independent of distance between point sources. Sedimentation appears to play a crucial role in Hg emissions, significantly affecting Hg$_{gas}$ in particular.
- Environmental parameters of the surrounding seawater significantly impacted the potential for transport of Hg species away from the localized area of the hydrothermal system.

MSWHS present unique opportunities to study a naturally occurring point of Hg emission. The nonlinear behavior, potential for biological uptake, and particle transport are all avenues of potential future research.

## Acknowledgements

Thank you to Prof. Dr. Thomas Pichler for the opportunity to complete my thesis at FB5 at the Universität Bremen. Your knowledge and wisdom were essential to my completion.

Thank you to my committee members for their support, questions, and essential feedback.

A special thank you to the working group of FB5 for all of the essential support and assistance. Dr. Kay Hamer, Dr. Cornelius Brombach, and Dr. Henning Fröllje for your knowledge in the lab and through the editing process. Dr. Andreas Kubier and Imke Gudenschwager for sharing an office with an American with strange ideas. And thank you to Laura Knigge-Stratmann, and Janin Scheplitz for their support in the lab.

Special thanks to Mina Walkiewicz, Manuel Ruben, Anant Khimasia, Athanasios Godelitsas, Mike Vichos, and Dr. Daniel Doischer for their support and knowledge in the field.

A large thank you to my husband Tom, to my family in the United States, and to my new family here in Germany, for all of their support and cheering me on from the sidelines.

# Literature

Acquavita, A., Floreani, F., Covelli, S., 2021. Occurrence and speciation of arsenic and mercury in alluvial and coastal sediments. Current Opinion in Environmental Science & Health, 22: 100272.

Alt, J.C., 1995. Subseafloor processes in mid-ocean ridge hydrothermal systems. In: Humphries, S.E., Zierenberg, R.A., Mullineaux, L.S., Thomson, R.E. (Eds.), Seafloor hydrothermal systems. American Geophysical Union, Washington, pp. 85-114.

Aubert, M., Diliberto, S., Finizola, A., Chébli, Y., 2008. Double origin of hydrothermal convective flux variations in the Fossa of Vulcano (Italy). Bulletin of Volcanology, 70(6): 743-751.

Baeyens, W., Meuleman, C., Muhaya, B., Leermakers, M., 1998. Behaviour and speciation of mercury in the Scheldt estuary (water, sediments and benthic organisms). In: Baeyens, W.F.J. (Ed.), Trace Metals in the Westerschelde Estuary: A Case-Study of a Polluted, Partially Anoxic Estuary. Springer Netherlands, Dordrecht, pp. 63-79.

Bagnato, E. et al., 2009a. Mercury concentration, speciation and budget in volcanic aquifers: Italy and Guadeloupe (Lesser Antilles). Journal of Volcanology and Geothermal Research, 179(1-2): 96-106.

Bagnato, E. et al., 2017. Hydrochemical mercury distribution and air-sea exchange over the submarine hydrothermal vents off-shore Panarea Island (Aeolian arc, Tyrrhenian Sea). Marine Chemistry, 194: 63-78.

Bagnato, E., Parello, F., Valenza, M., Caliro, S., 2009b. Mercury content and speciation in the Phlegrean Fields volcanic complex: Evidence from hydrothermal system and fumaroles. Journal of Volcanology and Geothermal Research, 187(3-4): 250-260.

Barnes, H., 1979. Solubilities of ore minerals. Geochemistry of hydrothermal ore deposits: 404-460.

Barnes, H., Romberger, S., Stemprok, M., 1967. Ore solution chemistry;[Part] 2, Solubility of HgS in sulfide solutions. Economic Geology, 62(7): 957-982.

Barnes, H., Seward, T., 1997. Geothermal Systems and Mercury Deposits Chapter 14. Geochemistry of Hydrothermal Ore Deposits, 3rd ed. Wiley.

Barnes, I., 1973. Chemical composition of naturally occurring fluids in relation to mercury deposits in part of north-central California. US Government Printing Office.

Beaulieu, S.E., Szafranski, K., 2020. InterRidge Global Database of Active Submarine Hydrothermal Vent Fields, Version 3.4.

Bowman, K.L., Hammerschmidt, C.R., Lamborg, C.H., Swarr, G., 2015. Mercury in the North Atlantic Ocean: The US GEOTRACES zonal and meridional sections. Deep-Sea Research Part Ii-Topical Studies in Oceanography, 116: 251-261.

Bowman, K.L., Hammerschmidt, C.R., Lamborg, C.H., Swarr, G.J., Agather, A.M., 2016. Distribution of mercury species across a zonal section of the eastern tropical South Pacific Ocean (US GEOTRACES GP16). Marine Chemistry, 186: 156-166.

Boyd, E.S. et al., 2009. Methylmercury enters an aquatic food web through acidophilic microbial mats in Yellowstone National Park, Wyoming. Environmental Microbiology, 11(4): 950-959.

Brombach, C.-C., Fröllje, H., Pichler, T., 2018. Speciation analysis of methylmercury via species specific isotope dilution GC-ICP-MS.

## 7. Literature

Brumsack, H.-J., 2006. The trace metal content of recent organic carbon-rich sediments: Implications for Cretaceous black shale formation. Palaeogeography, Palaeoclimatology, Palaeoecology, 232(2): 344-361.

Cabral, A.R., Lehmann, B., Kwitko, R., Costa, C.H.C., 2002. The Serra Pelada Au-Pd-Pt deposit, Carajas mineral province, northern Brazil: Reconnaissance mineralogy and chemistry of very high grade palladian gold mineralization. Economic Geology and the Bulletin of the Society of Economic Geologists, 97(5): 1127-1138.

Capaccioni, B., Tassi, F., Vaselli, O., 2001. Organic and inorganic geochemistry of low temperature gas discharges at the Baia di Levante beach, Vulcano Island, Italy. Journal of Volcanology and Geothermal Research, 108(1): 173-185.

Capaccioni, B., Tassi, F., Vaselli, O., Tedesco, D., Rossi, P.L., 2005. The November 2002 degassing event at Panarea Island (Italy): five months of geochemical monitoring. Annals of Geophysics, 48(4-5).

Caracausi, A. et al., 2005. Changes in fluid geochemistry and physico-chemical conditions of geothermal systems caused by magmatic input: The recent abrupt outgassing off the island of Panarea (Aeolian Islands, Italy). Geochimica et Cosmochimica Acta, 69(12): 3045-3059.

Chen, Y. et al., 2017. Analytical methods, formation, and dissolution of cinnabar and its impact on environmental cycle of mercury. Critical Reviews in Environmental Science and Technology, 47(24): 2415-2447.

Chiodini, G. et al., 2006. Geochemistry of the Submarine Gaseous Emissions of Panarea (Aeolian Islands, Southern Italy): Magmatic vs. Hydrothermal Origin and Implications for Volcanic Surveillance. Pure and Applied Geophysics, 163(4): 759-780.

Choe, K.-Y. et al., 2004. Sediment-water exchange of total mercury and monomethyl mercury in the San Francisco Bay-Delta. Limnology and Oceanography, 49(5): 1512-1527.

Christenson, B., Mroczek, E., 2003. Potential reaction pathways of Hg in some New Zealand hydrothermal environments. Special Publication-Society of Economic Geologists, 10: 111-132.

Cline, J.D., 1969. Spectrophotometric determination of hydrogen sulfide in natural waters 1. Limnology and Oceanography, 14(3): 454-458.

Compeau, G., Bartha, R., 1984. Methylation and demethylation of mercury under controlled redox, pH and salinity conditions. Applied and Environmental Microbiology, 48(6): 1203.

Cossa, D., Averty, B., Pirrone, N., 2009. The origin of methylmercury in open Mediterranean waters. Limnology and Oceanography, 54(3): 837-844.

Cossa, D., Martin, J.M., Takayanagi, K., Sanjuan, J., 1997. The distribution and cycling of mercury species in the western Mediterranean. Deep-Sea Research Part Ii-Topical Studies in Oceanography, 44(3-4): 721-740.

Covelli, S., Faganeli, J., Horvat, M., Brambati, A., 1999. Porewater Distribution and Benthic Flux Measurements of Mercury and Methylmercury in the Gulf of Trieste (Northern Adriatic Sea). Estuarine, Coastal and Shelf Science, 48(4): 415-428.

Crepo-Medina, M. et al., 2009. Adaptation of chemosynthetic microorganisms to elevated mercury concentrations in deep-sea hydrothermal vents. Limnology and Oceanography, 54(1): 41-49.

Dando, P., Stüben, D., Varnavas, S., 1999. Hydrothermalism in the Mediterranean sea. Progress in Oceanography, 44(1-3): 333-367.

Dando, P.R. et al., 2000. Hydrothermal studies in the aegean sea. Physics and Chemistry of the Earth, Part B: Hydrology, Oceans and Atmosphere, 25(1): 1-8.

Dando, P.R. et al., 1995. Gas venting rates from submarine hydrothermal areas around the island of Milos, Hellenic Volcanic Arc. Continental Shelf Research, 15(8): 913-929.

Davey, H.A., van Moort, J.C., 1986. Current mercury deposition at Ngawha Springs, New Zealand. Applied Geochemistry, 1(1): 75-93.

Drott, A., Lambertsson, L., Björn, E., Skyllberg, U., 2007. Importance of Dissolved Neutral Mercury Sulfides for Methyl Mercury Production in Contaminated Sediments. Environmental Science & Technology, 41(7): 2270-2276.

Esposito, V. et al., 2018. Exceptional discovery of a shallow-water hydrothermal site in the SW area of Basiluzzo islet (Aeolian archipelago, South Tyrrhenian Sea): An environment to preserve. PLoS One, 13(1): e0190710.

Feng, X.B. et al., 2010. Tracing Mercury Contamination Sources in Sediments Using Mercury Isotope Compositions. Environmental Science & Technology, 44(9): 3363-3368.

Fimreite, N., 1974. Mercury Contamination of Aquatic Birds in Northwestern Ontario. The Journal of Wildlife Management, 38(1): 120-131.

Fitzgerald, W.F., Lamborg, C.H., 2004. Geochemistry of mercury in the environment. In: Lollar, B.S. (Ed.), Environmental Geochemistry. Treatise on Geochemistry. Elsevier Ltd., pp. 107-148.

Fitzgerald, W.F., Lamborg, C.H., Hammerschmidt, C.R., 2007. Marine biogeochemical cycling of mercury. Chemical Reviews, 107(2): 641-662.

German, C.R., Richards, K.J., Rudnicki, M.D., Lam, M.M., Charlou, J.L., 1998. Topographic control of a dispersing hydrothermal plume. Earth and Planetary Science Letters, 156(3): 267-273.

Giggenbach, W.F., 1997. The origin and evolution of fluids in magmatic-hydrothermal systems. In: Barnes, H.L. (Ed.), Geochemistry of hydrothermal ore deposits. Wiley, New York, pp. 737-796.

Giovannelli, D., d'Errico, G., Manini, E., Yakimov, M., Vetriani, C., 2013. Diversity and phylogenetic analyses of bacteria from a shallow-water hydrothermal vent in Milos island (Greece). Frontiers in Microbiology, 4.

Gomez-Saez, G.V. et al., 2015. Interaction between iron and dissolved organic matter in a marine shallow hydrothermal system off Dominica Island (Lesser Antilles). Marine Chemistry, 177, Part 4: 677-686.

Gugliandolo, C., Italiano, F., Maugeri, T., 2006. The submarine hydrothermal system of Panarea (Southern Italy): biogeochemical processes at the thermal fluids-sea bottom interface. Annals of Geophysics, 49(2-3).

Gustin, M.S. et al., 1999. Nevada STORMS project: Measurement of mercury emissions from naturally enriched surfaces. Journal of Geophysical Research: Atmospheres, 104(D17): 21831-21844.

Hall, C.M. et al., 1997. Dating of alteration episodes related to mercury mineralization in the Almaden district, Spain. Earth and Planetary Science Letters, 148(1-2): 287-298.

Han, Y.-S. et al., 2020. Effect of FeS on mercury behavior in mercury-contaminated stream sediment: A case study of Pohang Gumu Creek in South Korea. Journal of Hazardous Materials, 393: 122373.

Harada, M., 1995. Minamata disease: methylmercury poisoning in Japan caused by environmental pollution. Critical reviews in toxicology, 25(1): 1-24.

Heinicke, J. et al., 2009. Evidence of tectonic control on active arc volcanism: The Panarea-Stromboli tectonic link inferred by submarine hydrothermal vents monitoring (Aeolian arc, Italy). Geophysical Research Letters, 36(4).

## 7. Literature

Helgeson, H.C., 1969. Thermodynamics of hydrothermal systems at elevated temperatures and pressures. American journal of science, 267(7): 729-804.

Hernandez, A. et al., 1999. The Almaden mercury mining district, Spain. Mineralium Deposita, 34(5-6): 539-548.

Hsu-Kim, H., Kucharzyk, K.H., Zhang, T., Deshusses, M.A., 2013. Mechanisms Regulating Mercury Bioavailability for Methylating Microorganisms in the Aquatic Environment: A Critical Review. Environmental Science & Technology, 47(6): 2441-2456.

Italiano, F., Nuccio, P.M., 1991. Geochemical investigations of submarine volcanic exhalations to the east of Panarea, Aeolian Islands, Italy. Journal of Volcanology and Geothermal Research, 46(1): 125-141.

Jannasch, H.W., Mottl, M.J., 1985. Geomicrobiology of Deep-Sea Hydrothermal Vents. Science, 229(4715): 717.

Kádár, E., Costa, V., Segonzac, M., 2007. Trophic influences of metal accumulation in natural pollution laboratories at deep-sea hydrothermal vents of the Mid-Atlantic Ridge. Science of The Total Environment, 373(2): 464-472.

Khimasia, A., Renshaw, C., Price, R.E., Pichler, T., 2021. Hydrothermal flux and porewater geochemistry in Paleochori Bay, Milos, Greece. Chemical Geology(Under Review).

King, J.K., Kostka, J.E., Frischer, M.E., Saunders, F.M., 2000. Sulfate-reducing bacteria methylate mercury at variable rates in pure culture and in marine sediments. Appl. Environ. Microbiol., 66(6): 2430-2437.

King, S.A. et al., 2006. Mercury in water and biomass of microbial communities in hot springs of Yellowstone National Park, USA. Applied Geochemistry, 21(11): 1868-1879.

Konovalov, Y.I., Luchsheva, L., Kurnosov, V., 2018. First Data about Mercury in Modern Hydrothermal Process in the Ocean, Juan de Fuca Ridge, Doklady Earth Sciences. Springer, pp. 575-579.

Krupp, R., 1988. Physicochemical aspects of mercury metallogenesis. Chemical Geology, 69(3): 345-356.

Kürzinger, V., 2019. Determination and Differentiation of the Hydrothermal Precipitates of Panarea, Italy. FOG-Freiberg Online Geoscience(54).

Lacerda, L.D., de Souza, M., Ribeiro, M.G., 2004. The effects of land use change on mercury distribution in soils of Alta Floresta, Southern Amazon. Environmental Pollution, 129(2): 247-255.

Lamborg, C.H., Damm, K.L.V., Fitzgerald, W.F., Hammerschmidt, C.R., Zierenberg, R., 2006. Mercury and monomethylmercury in fluids from Sea Cliff submarine hydrothermal field, Gorda Ridge. Geophysical Research Letters, 33(17).

Lamborg, C.H., Fitzgerald, W.F., Graustein, W.C., Turekian, K.K., 2000. An examination of the atmospheric chemistry of mercury using 210Pb and 7Be. Journal of Atmospheric Chemistry, 36(3): 325-338.

Lamborg, C.H., Fitzgerald, W.F., O'Donnell, J., Torgersen, T., 2002. A non-steady-state compartmental model of global-scale mercury biogeochemistry with interhemispheric atmospheric gradients. Geochimica et Cosmochimica Acta, 66(7): 1105-1118.

Laurier, F.J.G., Mason, R.P., Gill, G.A., Whalin, L., 2004. Mercury distributions in the North Pacific Ocean—20 years of observations. Marine Chemistry, 90(1): 3-19.

Leal-Acosta, M.L. et al., 2018. Intertidal geothermal hot springs as a source of trace elements to the coastal zone: A case study from Bahia Concepcion, Gulf of California. Marine Pollution Bulletin, 128: 51-64.

Leal-Acosta, M.L., Shumilin, E., Mirlean, N., Delgadillo-Hinojosa, F., Sánchez-Rodríguez, I., 2013. The impact of marine shallow-water hydrothermal venting on arsenic and mercury accumulation by seaweed Sargassum sinicola in Concepcion Bay, Gulf of California. Environmental Science: Processes & Impacts, 15(2): 470-477.

Leal-Acosta, M.L., Shumilin, E., Mirlean, N., Sapozhnikov, D., Gordeev, V., 2010. Arsenic and mercury contamination of sediments of geothermal springs, mangrove lagoon and the Santispac bight, Bahia Concepcion, Baja California peninsula. Bull Environ Contam Toxicol, 85(6): 609-13.

Lin, Y.-S. et al., 2020. Biogeochemistry and dynamics of particulate organic matter in a shallow-water hydrothermal field (Kueishantao Islet, NE Taiwan). Marine Geology: 106121.

Longo, M. et al., 2021. Hydro-acoustic signals from the Panarea shallow hydrothermal field: new inferences of a direct link with Stromboli. Geological Society, London, Special Publications, 519.

Loppi, S., 1996. Lichens as bioindicators of geothermal air pollution in central Italy. Bryologist, 99(1): 41-48.

Loredo, J., Luque Cabal, C., Garcia Iglesias, J., 1988. Conditions of formation of mercury deposits from the Cantabrian Zone (Spain). Bulletin de minéralogie, 111(3): 393-400.

Lucchi, F., Tranne, C.A., Peccerillo, A., Keller, J., Rossi, P.L., 2013. Chapter 12 Geological history of the Panarea volcanic group (eastern Aeolian archipelago). Geological Society, London, Memoirs, 37(1): 351.

Marowsky, G., Wedepohl, K., 1971. General trends in the behavior of Cd, Hg, Tl and Bi in some major rock forming processes. Geochimica et Cosmochimica Acta, 35(12): 1255-1267.

Mason, R., 2001. The Bioaccumulation of Mercury, Methylmercury and Other Toxic Elements into Pelagic and Benthic Organisms. Coastal and Estuarine Risk Assessment, CRC/Lewis Publ.

Mason, R., Fitzgerald, W., 1996. Sources, sinks and biogeochemical cycling of mercury in the ocean, Global and regional mercury cycles: sources, fluxes and mass balances. Springer, pp. 249-272.

Mason, R.P., Reinfelder, J.R., Morel, F.M., 1996. Uptake, toxicity, and trophic transfer of mercury in a coastal diatom. Environmental Science & Technology, 30(6): 1835-1845.

Mason, R.P., Sheu, G.R., 2002. Role of the ocean in the global mercury cycle. Global Biogeochemical Cycles, 16(4): 1093.

Nakanishi, H., Ukita, M., Sekine, M., Murakami, S., 1989. Mercury pollution in Tokuyama bay. Hydrobiologia, 176(1): 197-211.

Nicholson, K., 1992. Environmental-Impact of Geothermal Resources - Examples from New-Zealand. Renewable Energy : Technology and the Environment, Vols 1-5: 2895-2899.

Nicholson, K., 1993. Geothermal Fluids Chemistry & Exploration Technique Springer Verlag. Inc. Berlin.

O'Hara, S.C.M. et al., 1994. Gas seep induced interstitial water circulation: observations and environmental implications. Continental Shelf Research, 15(8): 931-948.

Obrist, D. et al., 2016. A synthesis of terrestrial mercury in the western United States: Spatial distribution defined by land cover and plant productivity. Science of the Total Environment, 568: 522-535.

Outridge, P.M., Mason, R.P., Wang, F., Guerrero, S., Heimburger-Boavida, L.E., 2018. Updated Global and Oceanic Mercury Budgets for the United Nations Global Mercury Assessment 2018. Environmental Science & Technology, 52(20): 11466-11477.

# 7. Literature

Pichler, T. et al., 2019. Suitability of the shallow water hydrothermal system at Ambitle Island (Papua New Guinea) to study the effect of high pCO2 on coral reefs. Marine Pollution Bulletin, 138: 148-158.

Pichler, T., Giggenbach, W.F., McInnes, B.I.A., Buhl, D., Duck, B., 1999a. Fe-sulfide formation due to seawater-gas-sediment interaction in a shallow water hydrothermal system at Lihir Island, Papua New Guinea. Economic Geology, 94: 281-288.

Pichler, T., Veizer, J., Hall, G.E.M., 1999b. The chemical composition of shallow-water hydrothermal fluids in Tutum Bay, Ambitle Island, Papua New Guinea and their effect on ambient seawater. Marine Chemistry, 64(3): 229-252.

Pokrovski, G.S., Borisova, A.Y., Bychkov, A.Y., 2013. Speciation and transport of metals and metalloids in geological vapors. Reviews in Mineralogy and Geochemistry, 76(1): 165-218.

Price, R.E., Giovannelli, D., 2017. A review of the geochemistry and microbiology of marine shallow-water hyrothermal vents. Reference Module in Earth Systems and Environmental Sciences.

Price, R.E. et al., 2015. Subsurface hydrothermal processes and the bioenergetics of chemolithoautotrophy at the shallow-sea vents off Panarea Island (Italy). Chemical Geology, 407-408: 21-45.

Price, R.E. et al., 2013. Archaeal and bacterial diversity in an arsenic-rich shallow-sea hydrothermal system undergoing phase separation. Frontiers in Microbiology, 4(158): 1-19.

Prol-Ledesma, R.M., Canet, C., Torres-Vera, M.A., Forrest, M.J., Armienta, M.A., 2004. Vent fluid chemistry in Bahia Concepcion coastal submarine hydrothermal system, Baja California Sur, Mexico. Journal of Volcanology and Geothermal Research, 137: 311-328.

Roberts, H., Pichler, T., 2022. Hg in the Hydrothermal Fluids and Gases in Baia di Levante, Vulcano, Italy. Marine Chemistry, 244.

Roberts, H., Price, R., Brombach, C.-C., Pichler, T., 2021. Mercury in the hydrothermal fluids and gases in Paleochori Bay, Milos, Greece. Marine Chemistry, 233: 103984.

Ruelas-Inzunza, J., Soto, L.A., Paez-Osuna, F., 2003. Heavy-metal accumulation in the hydrothermal vent clam Vesicomya gigas from Guaymas basin, Gulf of California. Deep-Sea Research Part I-Oceanographic Research Papers, 50(6): 757-761.

Sakamoto, M. et al., 2020. Mercury speciation in preserved historical sludge: Potential risk from sludge contained within reclaimed land of Minamata Bay, Japan. Environmental Research, 180: 108668.

Saupe, F., 1990. Geology of the Almadén mercury deposit, province of Ciudad Real, Spain. Economic Geology, 85(3): 482-510.

Schluter, K., 2000. Review: evaporation of mercury from soils. An integration and synthesis of current knowledge. Environmental Geology, 39(3-4): 249-271.

Seyfried Jr, W., Ding, K., 1995. Phase equilibria in subseafloor hydrothermal systems: A review of the role of redox, temperature, pH and dissolved Cl on the chemistry of hot spring fluids at mid-ocean ridges. Seafloor Hydrothermal Systems: Physical, Chemical, Biological, and Geological Interactions, 91: 248-272.

Seyfried, W.E., Mottl, M.J., 1982. Hydrothermal alteration of basalt by seawater under seawater-dominated conditions. Geochimica et Cosmochimica Acta, 46(6): 985-1002.

Shen, J. et al., 2020. Sedimentary host phases of mercury (Hg) and implications for use of Hg as a volcanic proxy. Earth and Planetary Science Letters, 543: 116333.

Sherman, L.S. et al., 2009. Mercury isotopic composition of hydrothermal systems in the Yellowstone Plateau volcanic field and Guaymas Basin sea-floor rift. Earth and Planetary Science Letters, 279(1-2): 86-96.

Siegler, R.W., Nierenberg, D.W., Hickey, W.F., 1999. Fatal poisoning from liquid dimethylmercury: a neuropathologic study. Human pathology, 30(6): 720-723.

Sieland, R., 2009. Chemical and isotopic investigations of submarine hydrothermal fluid discharges from Panarea, Aeolian Islands, Italy, Citeseer.

Sieland, R., Steinbrückner, D., Hamel, M., Merkel, B., Schipek, M., 2009. Geochemical investigations and gas quantification of submarine fluid discharges in the hydrothermal system of Panarea (Aeolian Islands, Italy), 1st International workshop research in shallow marine and fresh water systems, pp. 87.

Slowey, A.J., 2010. Rate of formation and dissolution of mercury sulfide nanoparticles: The dual role of natural organic matter. Geochimica et Cosmochimica Acta, 74(16): 4693-4708.

Spirakis, C.S., 1981. The possible role of sulfate reduction kinetics in the formation of hydrothermal uranium deposits. Economic Geology, 76(8): 2236-2239.

Stanulla, R., 2021. Geological and mineralogical investigation of hydrothermal fluid discharge features at the sea bottom of Panarea, Italy.

Stanulla, R. et al., 2017. Structural and mineralogical study of active and inactive hydrothermal fluid discharges in Panarea, Italy. Environmental Earth Sciences, 76(11): 1-26.

Swanner, E.D. et al., 2014. Cobalt and marine redox evolution. Earth and Planetary Science Letters, 390: 253-263.

Tang, Y.Y., Bi, X.W., Yin, R.S., Feng, X.B., Hu, R.Z., 2017. Concentrations and isotopic variability of mercury in sulfide minerals from the Jinding Zn-Pb deposit, Southwest China. Ore Geology Reviews, 90: 958-969.

Tassi, F. et al., 2009. Low-pH waters discharging from submarine vents at Panarea Island (Aeolian Islands, southern Italy) after the 2002 gas blast: Origin of hydrothermal fluids and implications for volcanic surveillance. Applied Geochemistry, 24(2): 246-254.

Turekian, K.K., Wedepohl, K.H., 1961. Distribution of the elements in some major units of the earth's crust. Geological society of America bulletin, 72(2): 175-192.

Valsami-Jones, E. et al., 2005. The geochemistry of fluids from an active shallow submarine hydrothermal system: Milos island, Hellenic Volcanic Arc. Journal of Volcanology and Geothermal Research, 148(1-2): 130-151.

Varekamp, J.C., Buseck, P.R., 1984. The speciation of mercury in hydrothermal systems, with applications to ore deposition. Geochimica et Cosmochimica Acta, 48(1): 177-185.

Voudouris, P. et al., 2021. Arsenian Pyrite and Cinnabar from Active Submarine Nearshore Vents, Paleochori Bay, Milos Island, Greece. Minerals, 11(1).

Waples, J.S., Nagy, K.L., Aiken, G.R., Ryan, J.N., 2005. Dissolution of cinnabar (HgS) in the presence of natural organic matter. Geochimica et Cosmochimica Acta, 69(6): 1575-1588.

Wedepohl, K.H., 1995. The composition of the continental crust. Geochimica et cosmochimica Acta, 59(7): 1217-1232.

Wenzhofer, F., Holby, O., Glud, R.N., Nielsen, H.K., Gundersen, J.K., 2000. In situ microsensor studies of a shallow water hydrothermal vent at Milos, Greece. Marine Chemistry, 69: 43-54.

## 7. Literature

Williams-Jones, A.E., Heinrich, C.A., 2005. 100th Anniversary special paper: vapor transport of metals and the formation of magmatic-hydrothermal ore deposits. Economic Geology, 100(7): 1287-1312.

Wu, J., Wells, M.L., Rember, R., 2011. Dissolved iron anomaly in the deep tropical–subtropical Pacific: Evidence for long-range transport of hydrothermal iron. Geochimica et Cosmochimica Acta, 75(2): 460-468.

Yin, Y., Allen, H.E., Li, Y., Huang, C.P., Sanders, P.F., 1996. Adsorption of Mercury(II) by Soil: Effects of pH, Chloride, and Organic Matter. Journal of Environmental Quality, 25(4): 837-844.